Longitudinal grey-box model identification of a tailless flapping-wing MAV based on free-flight data

J.B.W. Nijboer

Delft University of Technology

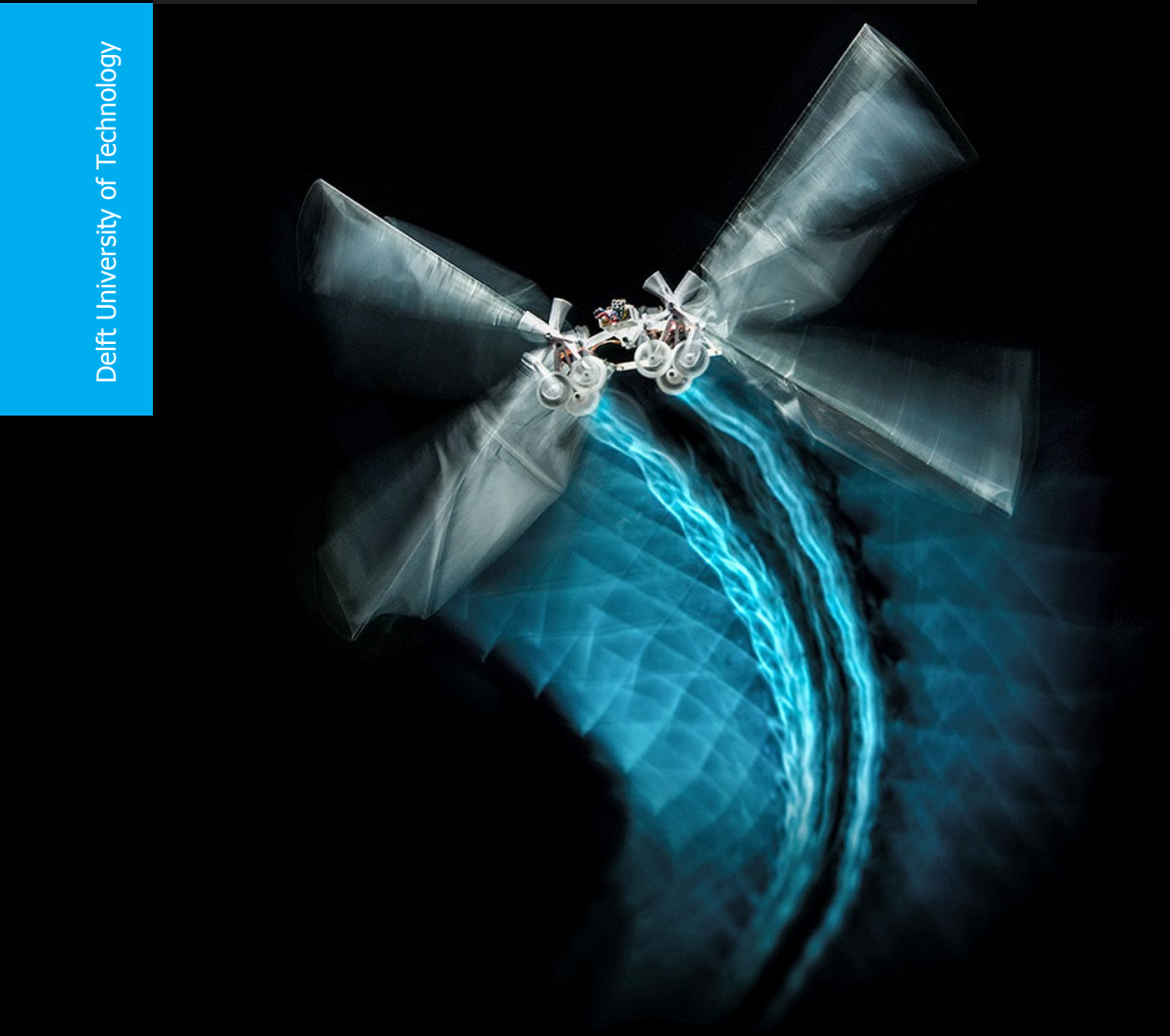

TU Delft Delft University of Technology

Challenge the future

Longitudinal grey-box model identification of a tailless flapping-wing MAV based on free-flight data

by

J.B.W. Nijboer

to obtain the degree of Master of Science,
at the Delft University of Technology,
to be defended publicly on Tuesday the 9^{th} of April, 2019 at 13:00.

Student number:	4311892	
Printed:	March 26, 2019	
Thesis committee:	Prof. Dr. G. C. H. E. de Croon	TU Delft, committee chairman
	Dr.ir. C. C. de Visser	TU Delft, daily supervisor
	Drs.ing. M. Karasek	TU Delft, daily supervisor

An electronic version of this thesis is available at http://repository.tudelft.nl.

Cover page image is retrieved from http://science.sciencemag.org/

TU Delft Delft University of Technology

Introduction

In recent times research and development on Flapping Wing Micro Aerial Vehicles (FWMAV) has grown immensely. FWMAVs are a subcategory of UAVs, and produce lift and thrust by means of their flapping wings. FWMAVs are usually very small, light weight and agile. Compared to fixed-wing MAVs, FWMAVs can take-off and land vertically demonstrating a higher maneuverability and higher performance at low Reynolds numbers. Another subcategory of UAVs, called Rotary Wing MAVs, are also able to take-off and land vertically but, at lower efficiency and lower performance at low Reynolds numbers. At this very day the practical usage of Flapping Wing Micro Aerial Vehicles (FWMAVs) is limited. This is mainly due to a combination between the high complexity of the flapping-wing flight mechanics and manufacturing difficulties. The small scale of the on-board sensors, control mechanisms and other components cause many obstacles in the manufacturing process. In addition, the small size and capacity of the batteries used in FWMAVs limits the flight time. Still, a significant amount of research is already been done on FWMAVs. Especially tailless flapping wing MAVs, such as the DelFly Nimble (Figures 1 -2), are an interesting research topic. The fact that the DelFly Nimble is a tailless flapping wing MAV makes it inherently unstable therefore, it is stabilized and controlled by means of active rate- and attitude control on its wings actuation system. The DelFly Nimble weighs just under 29 grams and can maintain controlled flight by using its two flapping wing mechanisms individually, the displacement of its dihedral and wing root deflection. In order to maintain hover- or forward flight, the two flapping mechanisms utilize the clap-and-fling effect in order to generate thrust. This configuration makes the DelFly Nimble very agile.

The goal of this thesis is to study models used in existing FWMAVs that can potentially be used for modelling the flight dynamics of the DelFly Nimble. Based on the models of existing FWMAVs, the next step is to apply system identification techniques in order to model the flight dynamics of the DelFly Nimble. As for the DelFly Nimble, it is inherently unstable and therefore closed-loop system identification and parameter estimation techniques are required in order to model its flight dynamics.

The added value of this thesis is to provide the reader insight on what techniques are available to model FWMAVs and how the flight dynamics of the DelFly Nimble can effectively be modelled. The most appropriate modelling approach will then be applied to the DelFly Nimble, with the goal that the models must be well suited for stability analysis, simulation and controller design purposes. It is therefore required that these models are accurate and relatively simple (low-order). Based on this process, we were able to meet these demands by applying the system identification approach. Although the system identification modelling approach is commonly used for conventional aircraft and tailed (inherently stable) FWMAVs, it has not yet been applied to tailless FWMAV stabilized and controlled by a active feedback control system. In this work, we will test whether or not a system identification approach can be applied to an inherently unstable tailless FWMAV, in this case the DelFly Nimble, and additionally test if this approach leads to accurate models predicting its longitudinal flight dynamics accurately. Based on the results of this work, we can conclude that a system identification approach can effectively be applied to tailless FWMAVs resulting in both computationally efficient and accurate models, in which the models can be used for stability analysis and controller design.

This report is divided into two separate parts. Part I contains a scientific paper that includes all the research results. Lastly, Part II contains the results of the preliminary studies on the DelFly Nimble and other flapping wing MAVs. The estimated parameters of all models are presented in Appendix A, the cycle of the system identification approach is described in Appendix B and additional validation data of the forward flight models is provided in Appendix C.

Figure 1: The DelFly Nimble in forward flight

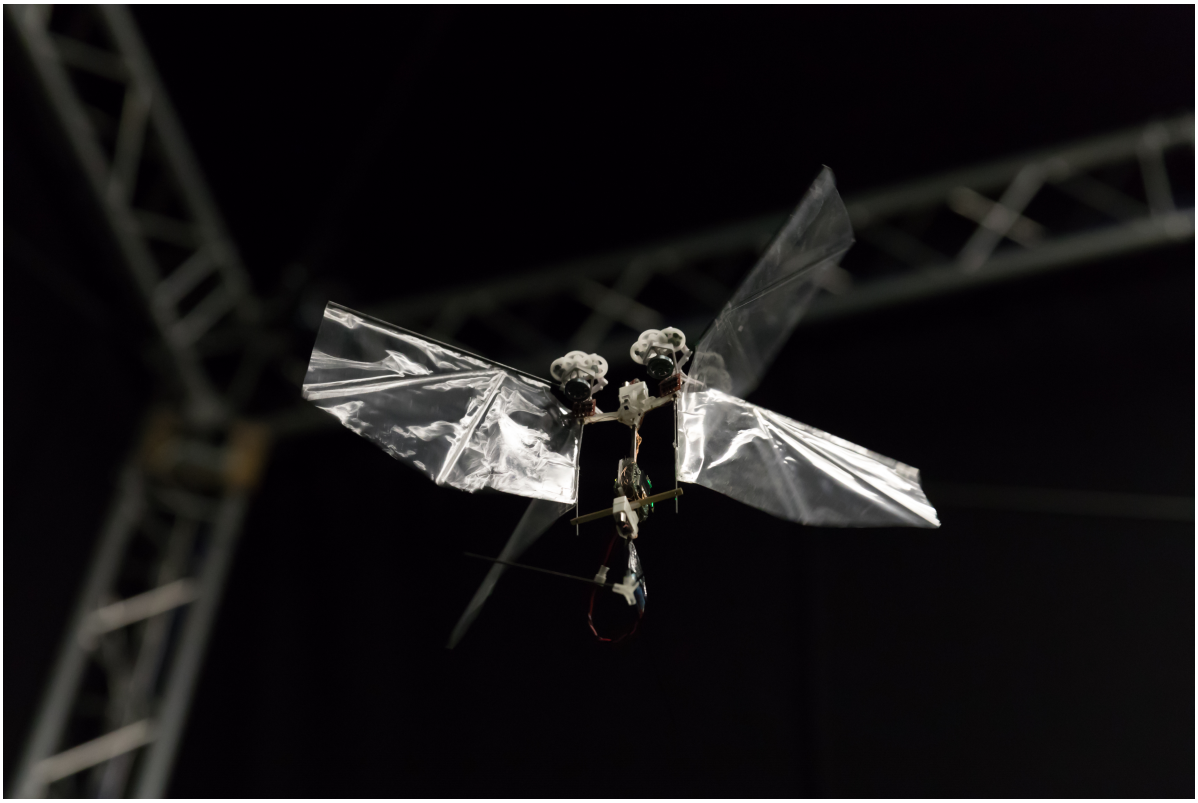

Figure 2: The DelFly Nimble in hover flight

Acronyms

AHRS	Attitude Heading Reference System
CFD	Computational Fluid Dynamics
COM	Center of Mass
EOM	Equations of Motion
FBD	Free-Body Diagram
FPS	Frames per Second
FWMAV	Flapping Wing Micro Aerial Vehicle
GLS	Generalized Least-Squares
GPS	Global Positioning System
IMU	Inertial Measurement Unit
KF	Kalman Filter
MAV	Micro Aerial Vehicle
MLE	Maximum Likelihood Estimator
NLS	Non-Linear Least-Squares
OLS	Ordinairy Least-Squares
PD	Proportional-Derivative
PSD	Power Spectrum Density
RC	Remote Controller
RMSE	Root-Mean-Square Error
UAV	Unmanned Aerial Vehicle
WLS	Weighted Least-Squares

List of Symbols

δ	Actuator output of closed-loop automatic feedback system
δ_D	Control deflection. Measured dihedral deflection [deg]
r	Reference signal of closed-loop automatic feedback system
e	Error signal of closed-loop automatic feedback system
u	Controller output signal of closed-loop automatic feedback system
y	Output system
y_m	Measured output system
x, y, z	Position [m]
q_0, q_1, q_2, q_3	Attitude quaternions
p	Roll rate
q	Pitch rate
r	Yaw rate
$\dot{p}$	Roll acceleration
$\dot{q}$	Pitch acceleration
$\dot{p}$	Yaw acceleration
a_x	Linear acceleration in x-direction
a_y	Linear acceleration in y-direction
a_z	Linear acceleration in z-direction
θ_{sp}	Pitch attitude angle set-point
f_{flap}	Flapping frequency [Hz]
θ_{ref}	Pitch angle reference
$\dot{\theta}_{ref}$	Pitch rate reference
θ_m	Measured pitch angle
$\dot{\theta}_m$	Measured pitch rate
K_d	Rate feedback gain
K_p	Attitude feedback gain
$\dot{x}_t$	Derivative of x at time t
X	Measured aerodynamic force in x-direction [N]
Y	Measured aerodynamic force in y-direction [N]
Z	Measured aerodynamic force in z-direction [N]
L	Measured aerodynamic moment around the x-axis [Nm]
M	Measured aerodynamic moment around the y-axis [Nm]
N	Measured aerodynamic moment around the z-axis [Nm]
m	Mass [kg]
g	Gravitational acceleration [m/s2]
u	Velocity along the body x-axis [m/s]
v	Velocity along the body y-axis [m/s]
w	Velocity along the body z-axis [m/s]
$\dot{u}$	Acceleration along the body x-axis [m/s2]
$\dot{v}$	Acceleration along the body y-axis [m/s2]
$\dot{w}$	Acceleration along the body z-axis [m/s2]
θ	Pitch angle
θ_0	Trimmed pitch angle
ϕ	Roll angle
ψ	Yaw angle
α	Angle of attack
I_{yy}	Moments of inertia of a 3D body
X_q, X_u, X_w, X_{δ_D}	Longitudinal-directional derivatives
Z_q, Z_u, Z_w, Z_{δ_D},Z_0, Z_{qu}	Longitudinal-directional derivatives
Z_{w^2}, Z_{u^2}, $Z_{\delta_D w}$, $Z_{\delta_D q}$, Z_{q^2}	Longitudinal-directional derivatives

M_q, M_u, M_w, M_{δ_D}	Longitudinal-directional derivatives
Δ	Perturbation of corresponding variable
$b_{\dot{q}}, b_{\dot{u}}, b_{\dot{w}}, b_{\dot{\theta}}$	Bias terms of the grey-box state-space system
$\mathbf{X}$	Regression matrix
$\mathbf{z}$	Vector of measured output OLS estimator
$\boldsymbol{\theta}$	Vector containing model parameters
$\hat{\theta}$	Vector with the best estimators for $\boldsymbol{\theta}$
$\boldsymbol{\epsilon}$	Model residuals vector
$J(\boldsymbol{\theta})$	Cost function J as a function of the vector containing model parameters
σ	Standard deviation
R^2	Coefficient of determination (goodness of fit)

Contents

List of Figures

List of Tables

I

Paper

Longitudinal Grey-Box Model Identification of a Tailless Flapping Wing MAV Based on Free-Flight Data

J.B.W. NIJBOER* Delft University of Technology

M. KARASEK† Delft University of Technology

S.F. ARMANINI‡ Imperial College London

C.C. DE VISSER§ Delft University of Technology

Abstract

Tailless flapping wing micro aerial vehicles (FMWAV) are known for their light weight and agility. However, given the fact that these FWMAVs have been recently developed, their flight dynamics have not yet been fully explained. In this paper we will develop local time-averaged longitudinal grey-box models based on closed-loop system identification techniques, where free-flight experimental data, obtained from the DelFly Nimble, is used to estimate and validate the local grey-box models. With these models we can take the first steps towards fully understanding the flight dynamics of tailless FWMAVs. The consequence of the tailless configuration is inherent instability and therefore tailless FWMAVs are generally more complex, compared to its tailed counterpart, and require a active feedback control system. The active feedback control system introduces additional challenges to the system identification process since it follows that feedback control works against the objectives of system identification. Dynamic effects that play a major role when studying the dynamic behaviour of FWMAVs are the sub-flap and the flap cycle-averaged effects. However, in this paper, we are only interested in modelling the flap cycle-averaged (time-averaged) effects of the DelFly Nimble. Based on this approach, grey-box models were estimated and validated for airspeeds near hover condition 0 m/s, up to 1.0 m/s forward flight. Despite the complexity of the system, we were able to obtain low-order local models that are both efficient and accurate (R^2 values up to 0.92) to predict the flight dynamic behaviour of the DelFly Nimble and can therefore be used for stability analysis, simulation and control design.

I. INTRODUCTION

UNmanned aerial vehicles have proven to be very valuable for both the civil- and military sectors. Their ever growing demand also motivated designers to explore more unconventional implementations [1, 2]. A good example of a unconventional unmanned aerial vehicle is the, biologically inspired, Flapping Wing Micro Aerial Vehicle (FWMAV). FWMAVs are typically very lightweight and capable of performing rapid manoeuvres, meaning that they are very agile both at hover- and high speed conditions [3, 4, 5, 6]. Especially tailless FMWAVs stand out for their high agility compared to tailed FWMAVs. The cost of using a tailless FMWAV is inherent instability. Tailless flapping wing MAVs are inherently unstable and require an active feedback control system that will control the actuators of the platform in order to stabilize the system [7, 8]. Examples of succesful FWMAV are the Nano Hummingbird, the bio-inspired Colibri and the KUBeetle [5, 9, 10, 11]. Due to the fact that FWMAVs have very useful properties, such as their small size, light weight and high agility, it is expected that the demand for these particular vehicles will grow in the near future. Given these properties, a useful application is surveillance within buildings where high manoeuvrability is essential.

Attempts were made to study the flapping-wing aerodynamics in which simplified aerodynamic models of flapping flight are used. Since FWMAVs operate in an region where the Reynolds numbers are low, they are characterized by unsteady aerodynamics [12, 13, 14]. Computational Fluid Dynamics (CFD), used to model these unsteady aerodynamics, are generally very complex and require a great amount of computation power and are usually unsuitable for control system design applications and dynamics simulation [15].

Another popular modelling approach is the use of Quasi-steady models, in combination with coefficients determined from analytical formulas and/or experimental data [16, 17, 18].

An attractive modelling approach is the use of low-order dynamic models which are based on the Equations of Motion (EOM) of a conventional rigid body aircraft [8, 19, 20, 21, 22, 23]. The EOM are then linearised around the trimmed condition and then used for the modelling process. These simple low-order dynamic models are computationally efficient and particularly useful for stability analyses and

*MSc Graduate Student, Faculty of Aerospace Engineering, Department of Control & Simulation, jorgen.nijboer@gmail.com

†Post-doctoral Researcher, Faculty of Aerospace Engineering, Department of Control & Simulation, matejkarasek@gmail.com

‡Research Associate, Faculty of Engineering, Department of Aeronautics, s.armanini@imperial.ac.uk

§Assistant Professor, Faculty of Aerospace Engineering, Department of Control & Simulation, c.c.devisser@tudelft.nl

control system design and simulation. In addition, some models make use of the cycle-averaged dynamics or flap cycle-averaged dynamics. During this process one analyzes the average dynamics of one wing beat, instead of analysing at a sub-flap cycle level [20].

In recent times aircraft system identification techniques have been applied to identify grey-box models based on flight-data obtained from optical tracking devices. These models have proven to be sufficiently accurate for control system design and simulation purposes [19]. Modelling work performed on other tailless FWMAVs are scarce. Still some work has been done on tailless FWMAVs, such as the work by A Roshanbin et al which used a simple linear model that captures the longitudinal pitch dynamics, and the parameters in the model are estimated using pendulum experiments [10]. In addition, a minimal longitudinal dynamic model of a tailless FWMAV, the DelFly Nimble, has recently been developed [24]. The DelFly Nimble is a bio-inspired tailless FWMAV developed at Delft University of Technology (Figure 1). In the study by K.M. Kajak et al, developed a longitudinal model where the unknown parameters (lengths and aerodynamic damping coefficients) were identified based on optimization routines in order to minimize the sum of the squares of the residuals between the simulation output and free-flight OptiTrack-recorded data. The parameters of the non-linear model were then optimized in order to achieve the best possible match between the simulation and recorded free-flight data. However, this paper still includes valuable information that can potentially be used to better understand the flight dynamic behaviour of the DelFly Nimble and help the development of new models.

Although the system identification approach is commonly used for conventional aircraft and tailed (inherently stable) FWMAVs, it has not yet been applied to tailless FWMAV stabilized and controlled by a active feedback control system. In this work, we will test whether or not a system identification technique can be applied to an inherently unstable tailless FWMAV, in this case the DelFly Nimble, and additionally test if this technique leads to accurate grey-box models predicting its longitudinal flight dynamics accurately. Another goal is that these models must be well suited for stability analysis, simulation and control design purposes therefore, it is required that these models are accurate and relatively simple. Relating to the latter point, computational efficiency is escpecially important for models used onboard (due to the low computational power of the on-board computer). It was found in other studies that, applying system identification techniques meet these demands within a specific flight region [19, 20].

Like other tailless FWMAVs, the DelFly Nimble is inherently unstable and therefore, in order to maintain controlled flight, it is stabilized and controlled by means of active rate- and attitude feedback control on its wings actuation system. This inherent instability brings additional challenges when applying system identification techniques in order to model the flight dynamics of the system. First of all the possibility of performing flight test experiments in open-loop is practically impossible when using the DelFly Nimble therefore, these experiments must be performed in closed-loop (when the feedback control system is active). In addition, repeatability of the flight experiments must be maintained in order to make sure the same test conditions are reproduced every flight experiment. Flight experiments of the DelFly Nimble were performed in closed-loop free-flight condition where it was difficult to maintain repeatability, especially when performing these flight experiments manually. In order to improve repeatability we adopted the use of automated manoeuvres. These automated manoeuvres were activated at the moment the DelFly Nimble was situated in the desired flight condition.

The second challenge lies in acquiring informative data during flight experiments. In the context of this paper, informative data is defined as free-flight data suitable for analysing and modelling FWMAVs. Using OptiTrack sensors, sufficiently accurate and informative data was obtained from the DelFly Nimble during free-flight experiments. However, the challenge was to perform manoeuvres that excite the natural motion of the Nimble as much as possible within the practical boundaries of the flight tests. When performing flight tests for dynamic modelling, the goal is to excite the natural motion of the system at hand as much as possible. However, this natural motion is damped and eliminated by the active feedback system of the DelFly Nimble and negatively impacts the informativeness of the data. Therefore, when flight tests are performed, the feedback control gains of the DelFly Nimble were reduced as much as possible. In this paper we tested whether reducing the control feedback gains, has the desired effect on ensuring accurate and informative data for system identification can be obtained.

As preciously mentioned, the dynamic- and aerodynamic characteristics of FWMAV are very complex and challenging to model, especially for tailless FWMAV. In this paper it is shown that simple, accurate and computational efficient models are able to capture the complex flight dynamics of the DelFly Nimble in the longitudinal plane.

Although models of the Nimble have been developed in a previous study [24], this study focusses on identifying linear models using a more structured aircraft system identification approach, where the estimated parameters are longitudinal-directional derivatives (stability- and control derivatives). These derivatives effectively provide information regarding how much change occurs in the aerodynamic- forces and moments acting on the DelFly Nimble when there is a small change in states and control surfaces deflection. As a result, the stability of the DelFly Nimble can be readily analysed using these estimated control- and stability derivatives. However, the estimated parameters in the previous study does not provide information regarding the stability of the Nimble. Furthermore, the advantage of using linear models is that they are computationally efficient and can therefore be used on-board.

In this work, we will introduce the use of cycle-averaged flapping dynamics in order to model the flight dynamic behaviour of the DelFly Nimble. The result will be the development of low-order grey-box models that are able to accurately describe the FWMAVs time-averaged behaviour in flight conditions varying from hover- (0.0 m/s) up to forward flight (1.0 m/s) conditions. In addition, the chosen grey-box models are computationally efficient, can be used for simulation and stability analysis, provide insight into the flight dynamics of the DelFly Nimble and serve as a tool for the development of new advanced controllers. The models will be estimated and validated using free-flight data obtained from optical tracking devices. Based on the results of this work, we can conclude that system identification techniques can

effectively be applied to tailless FWMAVs resulting in both computationally efficient and accurate models.
This paper is divided into five sections. In **section II** the working principles of the DelFly Nimble will be briefly discussed together with the experiment set-up. **Section III** explains the origin of the models used for the modelling process. In **section IV** the applied estimation techniques for estimating the unknown parameters in the chosen model structure will be considered. **Section V** focusses on the modelling results of the chosen model structure. And lastly, **section VI** will include a discussion regarding the conclusions of this research and recommendations will be provided for follow-up studies.

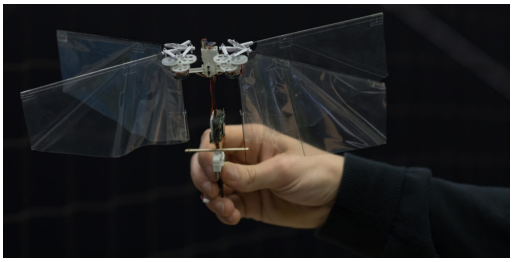

Figure 1: *The DelFly Nimble*

II. Experiment Set-up

In this work, longitudinal grey-box model identification was performed on the DelFly Nimble (Figure 2). The DelFy Nimble is a bio-inspired tailless FWMAV developed at the faculty of Aerospace Engineering of the Delft University of Technology [3]. With a wingspan of only 33 cm (from the left wing to the right wing), the DelFly Nimble is a fairly small platform weighing just under 29 grams (Figure 2). The left and right flapping mechanisms generate the thrust depending on the flapping frequency and are indicated by the red arrows/vectors in Figure **2. A**. The higher the flapping frequency, the higher the produced thrust. The platform includes two servos for yaw- and pitch control. The first servo controls the yaw of the platform by changing the vector of the two wings on opposite side (Figure **2. E, H**). Pitch control is accomplished by changing the dihedral of the flapping-wing mechanisms, thereby changing the orientation of the thrust vectors with respect to the center of mass (Figure **2. F, I**). As a result, a pitch torque will be produced which rotates the platform in order to establish forward flight (Figure **2. C**). Roll control is accomplished by differential control of right wing-pair and left wing-pair (Figure **2. G, J**). Since the thrust is linearly proportional to the flapping frequency, increasing the flapping frequency of one wing and reducing the flapping frequency of the other will generate a differential thrust and therefore causes the platform to roll enabling sideways flight (Figure **2. D**).

The system (DeFly Nimble) will be identified using the most commonly used system identification approach, such as the one described by Vladislav Klein & Eugene A. Morelli [25]. The complete system identification cycle typically includes the set-up and automated execution of the flight test experiments (manoeuvres), measuring the system states and data composition, reconstruction of the aerodynamic-forces and moments, the model structure selection and definition, the parameter estimation routine and finally evaluation and validation of the modelling results.
Performing system identification on a inherently unstable FWMAV, that is stabilized by an automatic feedback control system, is difficult. The objective of performing flight tests (manoeuvres) is to excite the natural dynamics of the FWMAV as much as possible. However, when performing these flight tests, the feedback system sees the executed manoeuvres as a disturbance and will move the control surfaces/servos in a way that mutes the natural dynamic response of the FWMAV [25]. Still system identification techniques can be applied to inherently unstable FWMAVs stabilized by an automatic feedback control system, simply by reducing the feedback control gains as much as possible [25]. There is only one requirement. In order for the system identification process to work it is important that both the output y and the input δ of the *system* in **Block-diagram 1** can be measured [25]. If measuring δ can not be realised, then one must use the techniques and methods described by L.Ljung [26] which is considered to be a very difficult process. During this research, both δ and y were measured, therefore making it possible to apply a standard system identification cycle, e.g. as described by Klein and Morelli [25]. Markers mounted on the flapping-mechanisms of the DelFly Nimble, together with the recorded on-board servo position, made it possible to measure the dihedral angle which was used as input (δ_D). This section will additionally explain how in-flight data was obtained **(Subsection i)**, the controller architecture of the Nimble **(Subsection ii)**,, the coordinate frame system used for system identification **(Subsection iii)**, the flight tests that are required and performed for exciting the natural dynamics of the DelFly Nimble **(Subsection iv)**, and how the in-flight data is processed **(Subsection v)**.

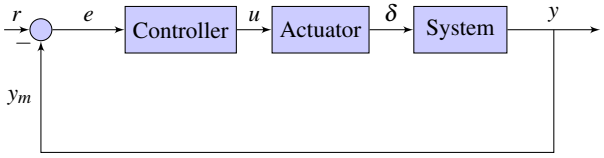

Block-diagram 1: *Basic closed-loop automatic feedback control system.*

i. In-Flight Data Acquisition

In order to obtain in-flight data for system identification, use was made of the OptiTrack - Motion Capture System. The OptiTrack system is installed in the 10m x 10m x 7m flight testing facility of the Delft University of Technology, called the CyberZoo. The 12 Prime 17W OptiTrack cameras in the CyberZoo are able to measure both the position and orientation of a body fitted with reflective markers very accurately at a rate up to 360 Hz. During the in-flight data acquisition phase of the DelFly Nimble data was captured at a rate of 200 FPS (Hz). A total of six reflective markers, made from 20mm styrofoam balls covered with reflective material, were mounted on the DelFly Nimble in order to determine the position, orientation and dihedral deflection (δ_D) of the DelFly Nimble's body in the Opti-Track environment. In addition to the Opti-Track measurements, on-board measurements were

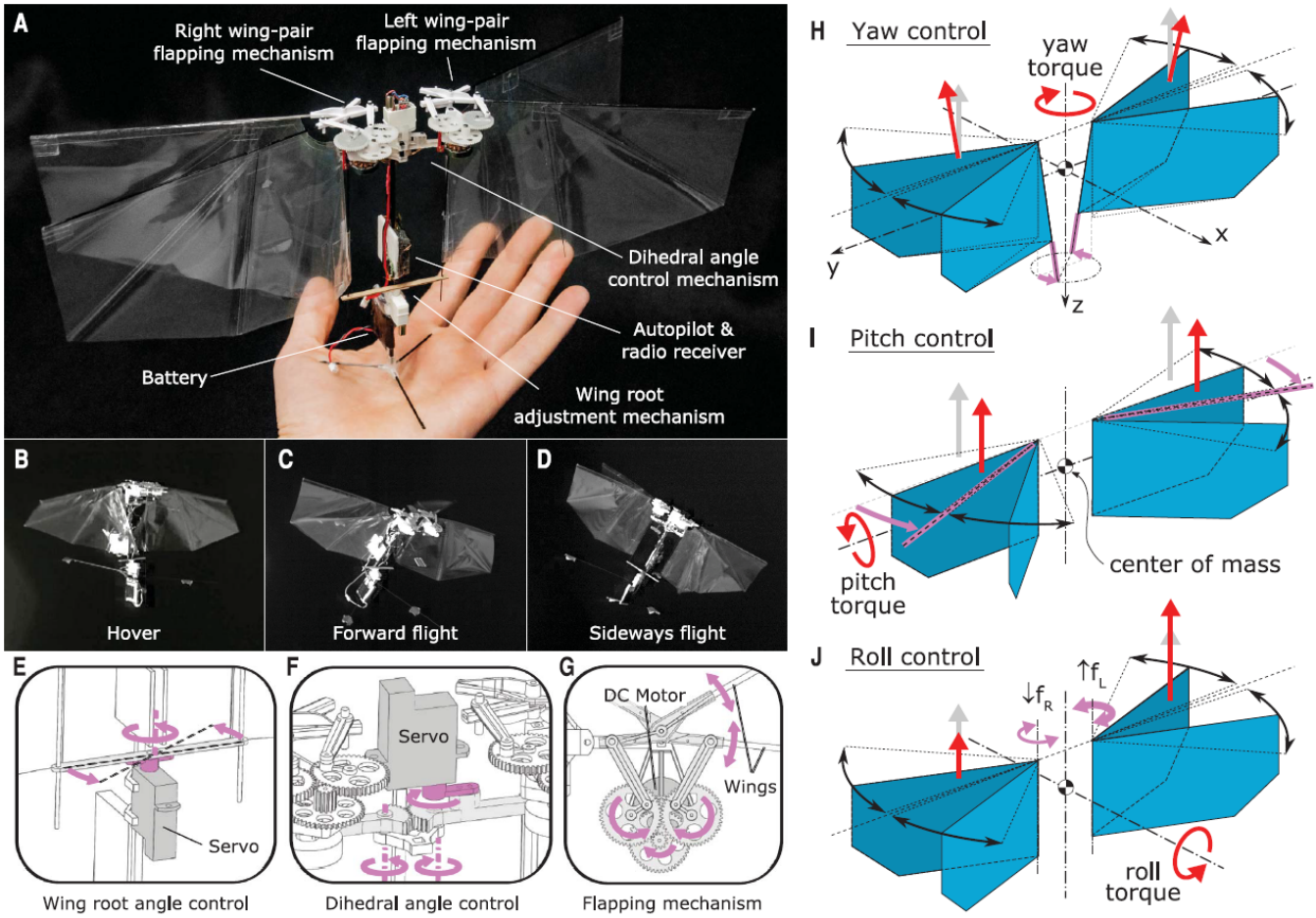

Figure 2: *The DelFly Nimble is controlled by its two flapping mechanisms and control servos. Source: [3]*

obtained from the 1.5 g Lisa MXS autopilot. Radio control set point, controller outputs and servo positions were recorded on a micro-SD card at a rate of approximately 100 Hz. Refer to Table 1 for an overview of all the data obtained and by which data acquisition system they are provided.

Type sensor	Measurements obtained
OptiTrack	Position (x,y,z)
	Attitude quaternions (q_0, q_1, q_2, q_3)
	Control deflections (δ_D)
IMU AHRS	Angular velocities (p,q,r)
	Linear accelerations (a_x, a_y, a_z)
On-board extra	Flap frequency (f_{flap})
	Set-point (θ_{sp})
	Dihedral command (cmd_{pitch})
	Servo feedback ($dihedral_{feedback}$)

Table 1: *Data provided by data acquisition systems during flight tests.*

ii. Controller Architecture

The DelFly Nimble is stabilized by a fixed-gain parallel feedback controller for attitude and rate feedback [3]. A Command filter, which is a low-pass filter with a cut-off frequency of 15 (HZ), was added to the controller in order to reduce noise that is generated by vibrations of the fuselage (as a result of the un-synchronyzed flapping mechanisms) and improves delays introduced to the control loop [3]. The pilot provides an attitude set-point sent via the remote controller (RC). The reference generator will then generate both the reference- attitude and rate. The controller architecture can be found in Figure 3.

iii. Coordinate Frame Definition

The frame used for system identification is defined as follows: The body x-axis is pointing forward, the body y-axis is pointing to the right and the body z-axis is pointing downward (refer to Figure **2. H**). In addition, the positive inertial x-axis and z-axis are pointing forward and downward, respectively (Figure 4). This coordinate frame is used

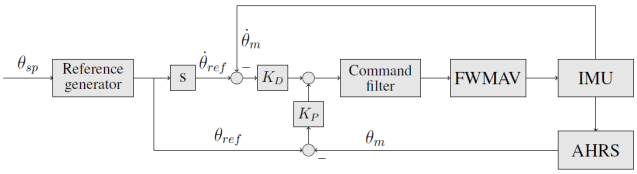

Figure 3: *Controller architecture. The setpoint is denoted by subscript **sp**, reference by **ref** and measurement by **m**. Source: [24]*

in order to prevent singularity issues when manoeuvres for system identification in hover and forward flight are performed. Note that the X_{body} axis in Figure **4** coincides with the X-axis in Figure **2. H**. The same holds for the Z-axis.

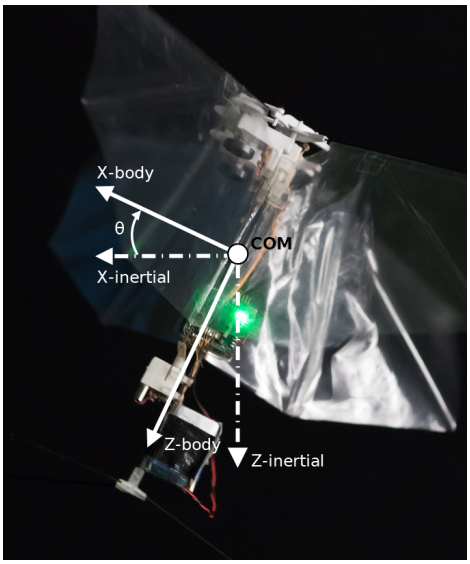

Figure 4: *Longitudinal free body diagram of the DelFly Nimble. Positive angles for θ are defined by clockwise rotation.*

iv. Flight Tests Required for System Identification

Important factors that affect the quality of the modelling- and system identification process are data acquisition and data processing. However, the flight tests, which includes the input signal applied to the system to be identified, are especially important since these signals need to be applied such that the natural dynamics of the system are excited. The goal is to obtain useful and informative data for modelling and system identification purposes in the range of interest. The chosen input design is based on existing theory on input design, the constraints associated with the experiment set-up (the dimensions of the CyberZoo for example), and partly based on the system used for the experiments. For input design it is typical to use priori knowledge of the system at hand to some extent. However, in the case of the DelFly Nimble, little a priori knowledge of the system dynamics is available. Another approach is to use a frequency sweep input, where as many frequencies as possible are excited. The problem with using a frequency sweep input is the duration of the manoeuvre. Frequency sweep inputs typically take a lot of time to perform when trying to cover a wide range of frequencies. Due to the long duration time, the limited space available in the CyberZoo will therefore hinder the flight-tests. In order to find a compromise between execution time and frequency coverage a Doublet multi-step input was applied. In this research we apply Doublet multi-step inputs based on previous studies on FWMAVs. Although Doublet inputs cover a less wider range of frequency than frequency sweep inputs, it is advantageous to use doublets due to the limited space required and the fact that it is more likely that FWMAV will remain in its initial steady flight condition since the manoeuvre is symmetrical. Especially when using linearised model structures it is important to remain inside the trimmed condition. Previous studies on modelling the dynamics of FWMAVs proved that using Doublets provided adequate excitation [19, 27]. In an effort to model the longitudinal dynamics of the Nimble we applied doublet inputs to the pitch command in closed-loop. Since the feedback gains mute the natural dynamic response of the vehicle we weakened the original feedback gains of the Nimble. Based on previous studies on the DelFly Nimble [24] we were able to gain insight into the dynamic response of the Nimble with changing feedback gains and adjusted the gain settings accordingly (Table 2).

Original gains	**Adjusted gains for system identification**
$K_P = 1.6250$	$K_P = 2.0833$
$K_D = 0.20832$	$K_D = 0.0500$

Table 2: *The adjust gain settings were used for system identification flight tests.*

Automated manoeuvres were performed to ensure repeatability and consistency during each flight test. These automated manoeuvres were tuned in (a) input duration, (b) input amplitude and (c) input type (selection of actuators) in order to improve the excitation of the natural dynamic response of the system. When the automated manoeuvre is activated it will send a Doublet attitude reference set-point (θ_{sp}) to the reference generator as seen in Figure 3. As a result, the DeFly Nimble will perform a Doublet manoeuvre in closed-loop. Figure 5 shows an example of a typical automated manoeuvre performed for system identification, where the *Set-Point* is θ_{sp} and the *Measured Dihedral* δ_D is the input that goes directly into the FWMAV.

v. Data Acquisition and Processing

The OptiTrack system was selected as the primary data acquisition system to derive all the states required for system identification, instead of using data from the IMU. Other studies have proven that OptiTrack-data based system identification will lead to sufficiently accurate models [19, 28]. On the other hand, the main advantage of using IMU sensor readings is the higher resolution (approximately 512 Hz) compared to OptiTrack (360 Hz). This higher resolution is only important when accurate analysis is required at a sub flap-cycle time scale. For the case of the DelFly Nimble, on-board data, such as the motor speed, could

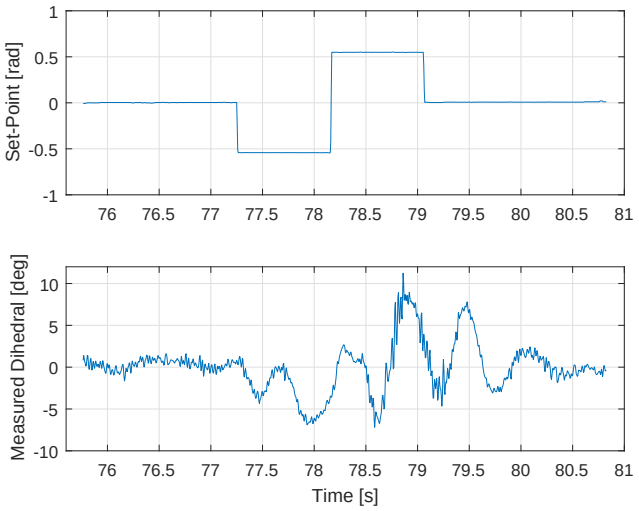

Figure 5: *Typical set-point θ_{sp} signal send to the reference generator, including the corresponding measured dihedral δ_D used for model identification of the DelFly Nimble.*

be recorded on a sd-card with a rate of approximately 100 Hz [24] and IMU data at a rate of 500 Hz. However, for the purpose of modelling the flight dynamics of the DelFly Nimble, the refresh rate of 360 Hz of the OptiTrack system is more than adequate for accurate analysis on a flight dynamics time scale [19].

Based on previous studies, a third order zero-phase Butterworth filter was used to filter the raw data [20]. First the data was filtered using a cutoff frequency of 50 Hz to remove the noise. The reason for this cutoff frequency is based on the fact that from free-flight data it becomes more difficult to distinguish the fourth flapping harmonic from the noise (Figure 6). Based on the assumption that the body and flapping dynamics are unrelated, meaning they are decoupled, we averaged out the data over a flap cycle in order to remove the time-varying effect. There are some discussions ongoing suggesting that it is not always justified to cancel out the time-varying effects however, it is the most common and accepted approach when modelling the dynamics of FWMAVs [19, 22]. The Power Spectrum Density (PSD) plot of the raw acceleration measured in z-direction, referring to Figure 6, clearly displays four peaks. The first represents mainly the flapping frequency, which is around 16 Hz, and the second peak is the second flapping harmonic (32 Hz and thus twice the flapping frequency) both of which contain the time-varying effects. Filtering the data below these frequencies will remove the time-varying effects. In this research, but also typically used in other researches [19, 24], a cut-off frequency of 5 Hz was used to filter out the time-varying effects, and thereby making sure only the body dynamics are preserved in the data.

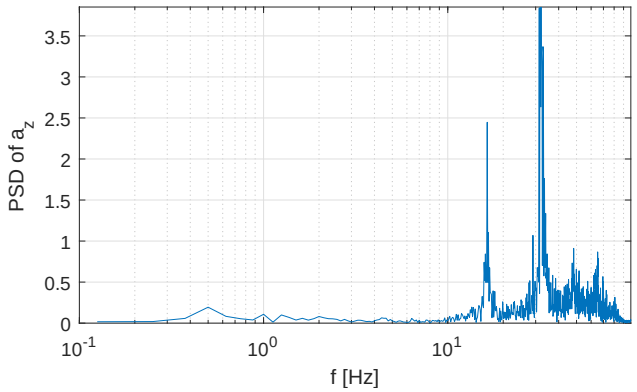

Figure 6: *Power spectrum density (PSD) of the acceleration in z-direction a_z derived from OptiTrack data.*

The OptiTrack system only provides information regarding the position and orientation of the FWMAV. However, in order to derive other states essential for system identification, such as velocity and pitch rate, we must use appropriate differentiation schemes to derive these states as accurately as possible. Based on the study by J.V.A.V. Caetano et al [28], who studied the effects of numerical differentiation on free-flight data obtained for a FWMAV, we concluded that a three point central difference (Equation 1) was best suited for numerical differentiation, as it reduces error amplification significantly compared to other methods and will not result into time lags or significant smoothing. All states where then derived from the position- and orientation data by applying Equation 1.

$$\dot{x}_t = \frac{x_{t+1} - x_{t-1}}{2\Delta t} \tag{1}$$

III. Model Structure Determination and Definition

At present there are few models and flight data available, both physically- and non-physically derived, that describe the dynamics of FWMAVs. In order to model the dynamics of the DelFly nimble a grey-box system identification approach was used based on research by S.F. Armanini et al [19]. Since little knowledge on the dynamics of FWMAVs is available, grey-box identification allows for available a priori knowledge of the system dynamics to be included in the model structure, maintaining a connection to the physics of the system. In combination with some a priori knowledge on the dynamics of the system, measured data can then be fitted to the grey-box model structure. The result will be an accurate model validated with real data, and still maintaining a connection to the physics of the system being modelled.

The time-averaged dynamics of the DelFly Nimble are based on the equations of motion (EOM) of a conventional fixed-wing rigid-body aircraft (Equations 2a-2c).

Aerodynamic force equations:

$$\begin{aligned} X &= m(\dot{u} + gsin(\theta) - rv + qw) \\ Y &= m(\dot{v} - gcos(\theta)sin(\phi) - pw + ru) \\ Z &= m(\dot{w} - gcos(\theta)sin(\phi) - qu + pv) \end{aligned} \tag{2a}$$

Aerodynamic moment equations:

$$\begin{aligned} L &= \dot{p}I_{xx} + qr(I_{zz} - I_{yy}) - (pq + \dot{r})I_{xz} \\ M &= \dot{q}I_{yy} + rp(I_{xx} - I_{zz}) - (p^2 + r^2)I_{xz} \\ N &= \dot{r}I_{zz} + pq(I_{yy} - I_{xx}) - (qr + \dot{p})I_{xz} \end{aligned} \tag{2b}$$

Kinematic equations:

$$\begin{aligned} \dot{\phi} &= p + qsin(\phi)tan(\theta) + rcos(\phi)tan(\theta) \\ \dot{\theta} &= qcos(\phi) - rsin(\phi) \\ \dot{\psi} &= q\frac{sin(\phi)}{cos(\theta)} + r\frac{sin(\phi)}{cos(\theta)} \end{aligned} \tag{2c}$$

Although the DelFly Nimble does not resemble an conventional aircraft, previous studies have shown that these EOM can describe the motion of some flapping-wing flyers [28, 29, 30, 31]. In addition, we do not know the dynamics of the DelFly Nimble very well yet therefore, the use of standard aircraft EOM is a logical first step. The EOM (Equations 2a-2c) are then linearised around a certain trimmed condition and decoupled only to include the longitudinal terms. The non-linear fixed-wing rigid-body EOM of a conventional aircraft were linearised around a forward flight condition of the Nimble. In the derivation process the small perturbations assumptions were taken into account along with the pitch attitude, forward body- and vertical body velocity, which are assumed to be non-zero for large pitch attitudes.
The next step is to assume a linear model structure for the aerodynamic forces and moments incorporated in the EOM. Model structures mostly used in fixed wing aircraft are linear-in-the-parameter models and are favoured since non-linear structures increase the complexity of the estimation process [25, 32]. Several studies on different flapping-wing flyers have shown shown that linear model structures represent the time-averaged flight dynamics fairly accurately in slow forward flight [19, 23, 28, 31]. For each longitudinal aerodynamic- force and moment a linear model structure was defined consisting of only measurable and physically plausible states (Equations 3-5), where Δ denotes the deviation from the trimmed condition. During all the system identification manoeuvres it is assumed that the Nimble flies symmetrically, meaning that the only terms affecting the aerodynamic- forces and moments in trimmed condition is the weight of the Nimble. Therefore the weight terms are included in Equation 3-4.

$$X = X_q\Delta q + X_u\Delta u + X_w\Delta w + X_{\delta_D}\Delta\delta_D + mgsin(\theta_0) \tag{3}$$

$$Z = Z_q\Delta q + Z_u\Delta u + Z_w\Delta w + Z_{\delta_D}\Delta\delta_D - mgcos(\theta_0) \tag{4}$$

$$M = M_q\Delta q + M_u\Delta u + M_w\Delta w + M_{\delta_D}\Delta\delta_D \tag{5}$$

Based on the assumption made earlier, all the states and aerodynamic-forces and moments are cycle-averaged (time-averaged), including the control surface deflection δ_D such that vibrations (due to the flapping mechanism) in the measurements are not given as input into the model. Cycle-averaged means that, for example, the thrust generated by the flapping frequency is constant over one flapping cycle.

The linear models (Equations 3-5) were then substituted into the linearised EOM (Equations 6-9) which resulted in the grey-box model of the DelFly Nimble describing its longitudinal time-averaged dynamics (Equation 10).

$$\Delta\dot{q} = \frac{M}{I_{yy}} \tag{6}$$

$$\Delta\dot{u} = \frac{X}{m} - gsin(\theta_0) - gcos(\theta_0)\Delta\theta - \Delta q w_0 \tag{7}$$

$$\Delta\dot{w} = \frac{Z}{m} + gcos(\theta_0) - gsin(\theta_0)\Delta\theta + \Delta q u_0 \tag{8}$$

$$\Delta\dot{\theta} = \Delta q \tag{9}$$

$$\begin{bmatrix} \Delta\dot{q} \\ \Delta\dot{u} \\ \Delta\dot{w} \\ \Delta\dot{\theta} \end{bmatrix} = \begin{bmatrix} \frac{M_q}{I_{yy}} & \frac{M_u}{I_{yy}} & \frac{M_w}{I_{yy}} & 0 \\ \frac{X_q}{m} - w_0 & \frac{X_u}{m} & \frac{X_w}{m} & -gcos(\theta_0) \\ \frac{Z_q}{m} + u_0 & \frac{Z_u}{m} & \frac{Z_w}{m} & -gsin(\theta_0) \\ 1 & 0 & 0 & 0 \end{bmatrix} \begin{bmatrix} \Delta q \\ \Delta u \\ \Delta w \\ \Delta\theta \end{bmatrix} + \begin{bmatrix} \frac{M_{\delta_D}}{I_{yy}} \\ \frac{X_{\delta_D}}{m} \\ \frac{Z_{\delta_D}}{m} \\ 0 \end{bmatrix} \begin{bmatrix} \Delta\delta_D \end{bmatrix} \tag{10}$$

The next step is to estimate the unknown parameters in the grey-box model. For example, the second equation consists of the unknown parameters X_q, X_u, X_w and X_{δ_D}. Note that for the state-space matrix we also included bias terms in the model. The purpose of these bias terms is to simply receive anything that is not captured in the rest of the model. In the next section we will look at the parameter estimation techniques in order to estimate the unknown parameters of equations 3-5.

IV. Parameter Estimation

In this paper an Ordinary Least Squares (OLS) estimator was used to estimate the unknown parameters in the linear equations 3-5. The working principle of an OLS estimator is minimising the difference between the measurements (obtained from the OptiTrack system) and the output determined by the model. In the case of an OLS estimator, the assumption is made that at each time point the output measurements z is a linear combination of regressor matrix X multiplied by the model parameters θ, where X contains all the regressors, plus an unknown equation error ε. So, in relation to equation (10), the measurements that represent z are given in the vector $[\Delta\dot{q} \quad \Delta\dot{u} \quad \Delta\dot{w} \quad \Delta\dot{\theta}]^T$. In equation form this becomes (Equation 11):

$$z = X\theta + \varepsilon, \tag{11}$$

where it is assumed that ε is zero-mean Guassian white noise. The best estimator for θ is obtained by minimizing the sum of squared difference between the measurements and model (Equation 12):

$$J(\theta) = \frac{1}{2}(z - X\theta)^T(z - X\theta) \tag{12}$$

The next step in finding the parameter estimate $\hat{\theta}$ is by minimizing Equation 12:

$$\frac{\partial J}{\partial \theta} = -X^T z + X^T X \hat{\theta} = 0 \tag{13}$$

Rearranging Equation 13 gives the formula for the OLS estimator:

$$\hat{\theta} = (X^T X)^{-1} X^T z \tag{14}$$

Based on the equations in the grey-box model (Eq. 10), we selected the following states and inputs for estimating the longitudinal time-averaged dynamics of the DelFly Nimble:

$$x = \begin{bmatrix} \Delta q & \Delta u & \Delta w & \Delta\theta \end{bmatrix}, \quad u = \Delta\delta_D \tag{15}$$

Taking Equation 5 as an example for the parameter estimation of the aerodynamic moment M, with the regressor matrix X containing a total number of n measurements;

$$\hat{\theta} = (X^T X)^{-1} X^T z = \begin{bmatrix} \hat{M}_q \\ \hat{M}_u \\ \hat{M}_w \\ \hat{M}_{\delta_D} \\ \hat{b}_{\dot{q}} \end{bmatrix} \tag{16}$$

where $\hat{b}_{\dot{q}}$ is the estimated bias parameter which receives all that is not captured by the model, and the regressor matrix X is defined as;

$$X = \begin{bmatrix} \Delta q(1) & \Delta u(1) & \Delta w(1) & \Delta\theta(1) & \Delta\delta_D(1) \\ \Delta q(2) & \Delta u(2) & \Delta w(2) & \Delta\theta(2) & \Delta\delta_D(2) \\ \vdots & \vdots & \vdots & \vdots & \vdots \\ \Delta q(n) & \Delta u(n) & \Delta w(n) & \Delta\theta(n) & \Delta\delta_D(n) \end{bmatrix} \tag{17}$$

V. Modelling Results

The results of the modelling process will be presented in four sections. In **section i** the results of the hover model will be covered. Furthermore, in **section ii** the performance of the estimated hover model will be validated in closed-loop. **Section iii** will be dedicated to the results of the models in forward flight conditions and in **section iv** adjusted model structures were tested.

The prediction capability of an identified model must be validated on data that is not used in the identification process. Therefore, for estimation of the parameters in equations (3-5) and validation of the estimated model, two different datasets were used. The estimation-datasets were used for parameter estimation purposes and the validation-datasets were used to validate the estimated models. The estimation manoeuvres used for the system identification process consist of doublets in pitch, as discussed in Experiment Set-Up section (Figure 5). For the validation process a different manoeuvre was used, namely a single-input in pitch, for the purpose of strengthening the validation of the estimated model.

Param.	$\hat{\theta}$	$\lvert\hat{\sigma}\rvert$	$100\lvert\hat{\sigma}/\hat{\theta}\rvert$
X_q	0.0041	1.2033e-03	1.6045
X_u	-0.1011	4.3542e-03	0.5698
X_w	0.0089	6.8437e-03	9.0203
X_{δ_D}	0.7218	4.0767e-02	0.3727
Z_q	-0.0056	2.0858e-04	5.0846
Z_u	0.0196	7.5479e-04	0.7459
Z_w	-0.0059	1.1863e-03	13.3852
Z_{δ_D}	0.2982	7.0668e-03	0.9784
M_q	-0.0019	9.8107e-06	6.8274
M_u	0.0194	3.5501e-05	7.1146
M_w	-0.0019	5.5799e-05	37.3612
M_{δ_D}	0.2782	3.3238e-04	4.3765

Table 3: *Estimated parameters $\hat{\theta}$, corresponding estimated standard deviation $\hat{\sigma}$ and the estimated standard deviation of each parameter in relation to its magnitude* $100\lvert\hat{\sigma}/\hat{\theta}\rvert$.

i. Results of Modelling Process Hover Condition

A total of four datasets were used to identify the time-averaged longitudinal hover model, where each datasets contained around six system identification manoeuvres. Table 3 displays the estimated parameters of the hover model including the corresponding standard deviations for one of the datasets used in this example (dataset #1). The estimated time-averaged longitudinal hover model was open-loop validated by calculating the output of the equations in the state-space matrix (Eq. 10) using the measured states and measured dihedral as input.

The estimated standard deviation of each parameter in relation to its magnitude (Table 3), show good results (below 10% except for Z_w and M_w), indicating a satisfactory estimation process. In addition, correlation between all the estimated parameters also show show no issues, suggesting that all are parameters are estimated separately. Figures (7a-7b) display the estimated aerodynamic forces and moments and outputs of the state-space model.

Both models estimating the aerodynamic- force X and moment M show very good results in terms of goodness of fit (R^2) and output correlation (Table 4-5). However, the model estimating the aerodynamic force Z was found to be ineffective. This inaccuracy is directly reflected in the output $\dot{w}$ which can be seen in Figure 7b. The reason for this may be lack of excitation of the Z-dynamics or deficiencies in the model structure (Equation 4). A analysis of the residuals for the aerodynamic force Z also shows that some deterministic components remain in the data (Figure 8), which might be due to a deficiency in the model structure [25]. Attempts were made to improve the Z force model by more aggressive excitation in the Z force, but this did not improved the model. The validation plots (Figures 7c-7d) again show good results in terms of the predictive capability of the longitudinal models in a similar flight regime, except for the aerodynamic force Z and corresponding state-space output $\dot{w}$.

Based on the discussion made earlier, additional excitation of the Z did not result in a better model and it is most likely that some other

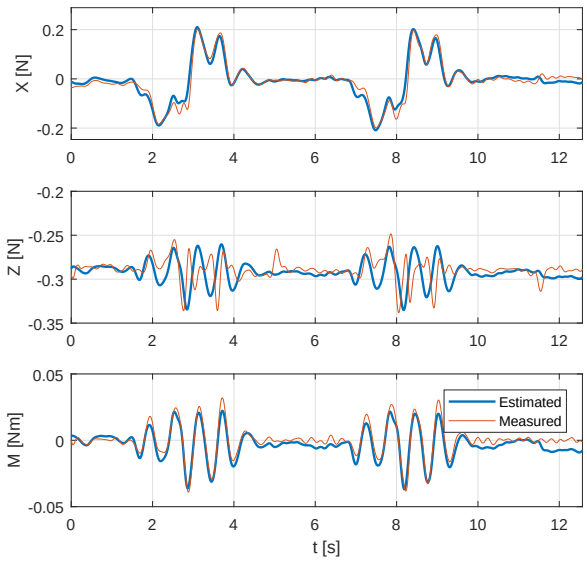

(a) *Estimation aerodynamic- forces and moment. Measured- and model-estimated output values of the aerodynamic- forces and moment.*

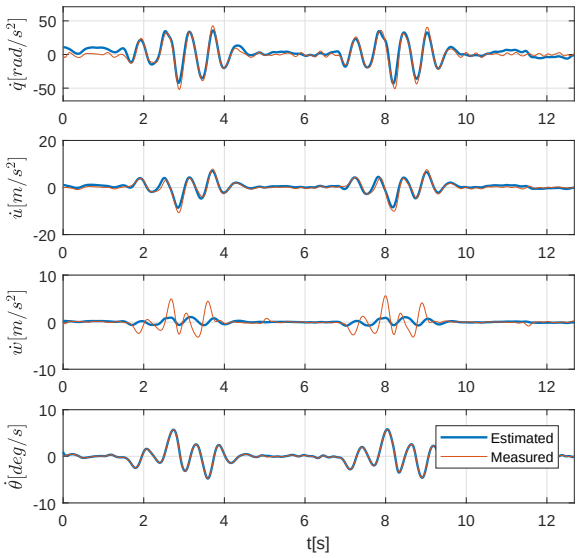

(b) *Estimation of the time-averaged longitudinal hover model. Measured- and model-estimated output values of the state-space model.*

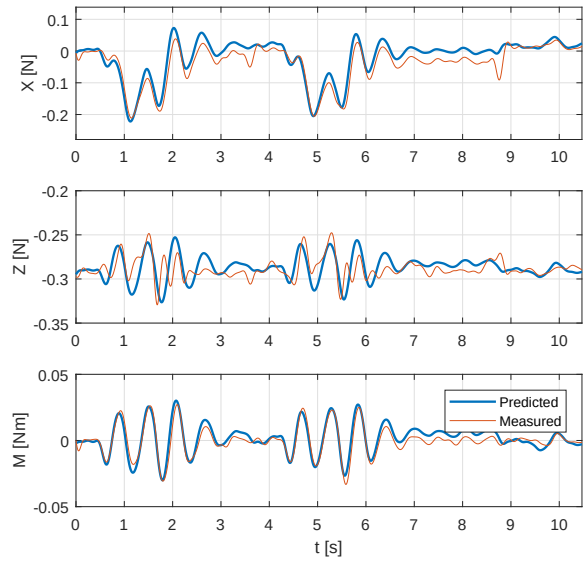

(c) *Validation aerodynamic- forces and moment. Measured- and model-predicted output values of the aerodynamic- forces and moment.*

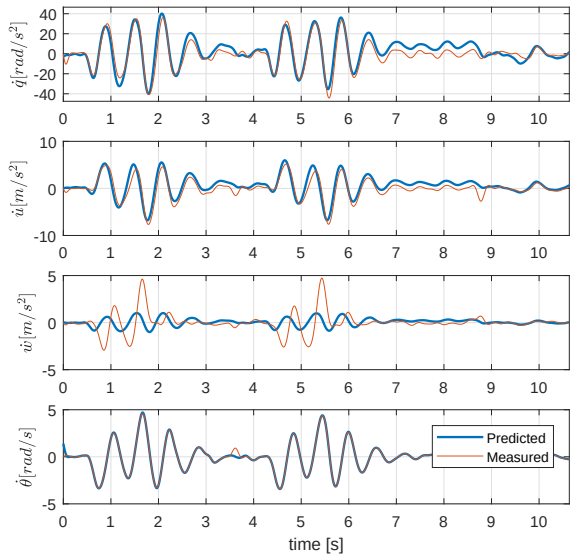

(d) *Validation of the time-averaged longitudinal hover model. Measured- and model-predicted output values of the state-space model.*

Figure 7: *Open-loop Estimation **(a-b)** and Validation **(c-d)** results for the time-averaged longitidinal model*

Match *estimation* data with measured data			
Output Variable	Output Correlation	R2	RMSE (% of measurement range)
X	0.97	0.92	5.93%
Z	0.13	-0.95	20.49%
M	0.97	0.89	5.90%
$\dot{q}$	0.97	0.94	4.44%
$\dot{u}$	0.97	0.93	3.94%
$\dot{w}$	0.30	0.09	15.31%
$\dot{\theta}$	0.99	0.99	0.63%

Table 4: *Estimation metrics of the longitudinal model of Figure (7a-7b).*

Match *validation* data with measured data			
Output Variable	Output Correlation	R2	RMSE (% of measurement range)
X	0.95	0.77	11.16%
Z	0.48	-0.40	14.29%
M	0.94	0.81	6.90%
$\dot{q}$	0.94	0.81	6.90%
$\dot{u}$	0.93	0.73	7.95%
$\dot{w}$	-0.06	-0.19	13.75%
$\dot{\theta}$	0.99	0.99	1.37%

Table 5: *Validation metrics of the longitudinal model of Figure (7c-7d).*

parameters must be included in the linear model structure of the Z force. In **section iv** we will study the improvements that can be made in relation to the original model (Equation 4).

For the linear hover model a total of four datasets were generated, where each dataset contains at least five system identification manoeuvres all of which recorded in the same flight condition. In an ideal situation the estimated linear models should be the same regardless of the dataset used. However, in practice this is impossible to achieve due to imperfections in the measurements and/or slight differences between the system identification manoeuvres, and slight changes in the flight conditions. Since the linear hover model is only valid in a particular flight condition and differences in manoeuvres and measurement imperfections affect the estimated model, it is interesting to know if the different datasets impact the estimated linear model. A comparison between the models is displayed in Figure 9 from which we can conclude that the differences between the estimated models is very small, and will therefore not affect the estimated linear model in that particular flight condition. All the estimated models are unstable which confirms the inherently unstable nature of the DelFly Nimble. Table 6 displays the eigenvalues of the estimated longitudinal model represented by one unstable oscillatory mode and two stable aperiodic modes. This model and its corresponding pole configuration corresponds with the theoretical model from M. Karásek, and that the modes qualitatively correspond to those found in many insect studies [7, 33].

Since the parameters have a physical meaning, it is possible to evaluate their physical plausibility. For example, the value of the parameter M_q (Table 3) is negative indicating the Nimble's pitch rate damping is stable which is also confirmed in the models from Karásek [7, 33]. Also the negative value for X_u matches the results of the models. The estimated value of another important parameter M_u is positive. The positive sign of the estimated parameter does not correspond to the sign estimated by M. Karásek. However, in this study M. Karásek used a non-airspace body-fixed frames. This means that a positive M_u in this paper has the same effect as negative M_u in the study of M. Karásek [7].

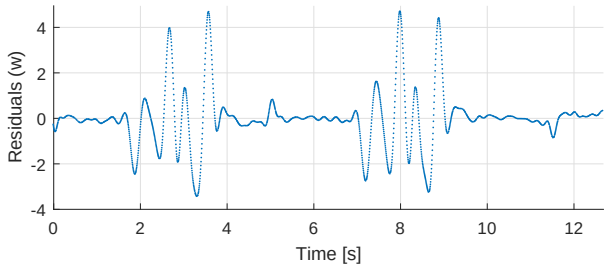

Figure 8: *Residuals of the aerodynamic force Z model.*

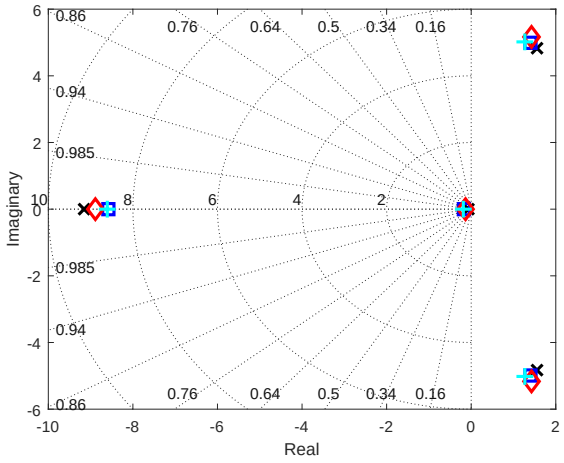

Figure 9: *Pole locations hover model using 4 datasets, where each dataset contains at least 5 system identification manoeuvres. Dataset #1 (used in the examples), Dataset #2, Dataset #3 and Dataset #4*

Eigenvalues
-8.8875
$1.4262 + 5.1659$i
$1.2668 - 5.1659$i
-0.1343

Table 6: *Eigenvalues of the estimated longitudinal hover model obtained from dataset #1.*

ii. Results of Closed-Loop Modelling

Given the fact that the DelFly Nimble is inherently unstable, active stabilization is necessary in order to guarantee stable and controlled flight. Like other tailless FWMAVs, the DelFly Nimble relies on feedback on the body rates and attitude [24]. In order to validate the estimated time-averaged longitudinal hover model in closed-loop, an exact copy of the controller architecture of the DelFly Nimble (Figure 3) was implemented in Simulink. With this Simulink model we were able to obtain both closed-loop estimation- and validation data.
In a previous study on the DelFly Nimble it was found that the dihedral angle (used as input for the longitudinal hover model) was affected by the velocity u [24] causing an error between the commanded and measured dihedral angle. The cause of this error was probably due to mechanical- play or elasticity of the dihedral actuator mechanism. In order to obtain a good estimation of the 'actual' dihedral deflection, a correction factor was introduced and added to the measured dihedral position. The same correction factor was also used in the Simulink model used in this study.
Figures (10a-10b) display the estimated output of the estimated longitudinal model in closed-loop. Both the estimated and predicted outputs match the measured data effectively, except for the state w. The estimation and validation metrics, such as goodness of fit (R2) and output correlation, are reported in Table 7 and Table 8, respectively. The performance of the estimated hover model using the original gains (fast gains; Kp = 1.6250 and Kd = 0.2083) is also accurately predicting the flight dynamics of the DelFly Nimble, as show in Figure 11, except for the state w.

Match *estimation* data with measured data			
Output Variable	Output Correlation	R2	RMSE (% of measurement range)
q	0.93	0.87	6.20%
u	0.97	0.90	7.09%
w	0.78	0.42	19.59%
θ	0.96	0.87	7.39%

Table 7: *Closed-loop estimation metrics of the longitudinal model of Figure 10a.*

Match *validation* data with measured data			
Output Variable	Output Correlation	R2	RMSE (% of measurement range)
q	0.93	0.88	5.51%
u	0.97	0.90	8.44%
w	0.42	0.08	23.11%
θ	0.97	0.78	11.23%

Table 8: *Closed-loop validation metrics of the longitudinal model of Figure 10b.*

iii. Results of the Modelling Process in Forward Flight Condition

The DelFly Nimble typically operates in both hover- and forward flight conditions, depending on the desired mission. It is therefore essential to know how the DelFly Nimble operates and behaves, not only in hover condition, but also in forward flight conditions. In this section the goal is to identify and analyse the behaviour of the estimated linear time-averaged longitudinal models in forward flight condition ranging from 0.5$\pm$0.05 m/s, to 0.75$\pm$0.05 m/s, up to 1.0$\pm$0.05 m/s. In order to estimate the linear time-averaged longitudinal model in forward flight conditions, and record informative data in that particular forward flight condition, the DelFly Nimble was first stabilized in its particular forward flight trimmed condition. At the instance when the DelFly Nimble was in the planned forward flight trimmed condition, the system identification manoeuvre was performed.
However, the process of achieving these steady trimmed conditions proved to be very difficult when using slow feedback gains. This issue was solved by using slightly faster gains which did not affect the informativeness of the data.
A total of 18 datasets were recorded containing over 90 system identification flight tests (manoeuvres) ranging from 0.5$\pm$0.05 m/s up to 1.0$\pm$0.05 m/s forward flight condition. The performance of the forward flight condition models is reported in Table 9.

Output var.	**Output correlation**	**RMSE (%)**
$\dot{q}$	0.96 ± 0.010	$4.11 \pm 0.4\%$
$\dot{u}$	0.92 ± 0.015	$6.12 \pm 0.5\%$
$\dot{w}$	0.86 ± 0.220	$7.01 \pm 5.06\%$
$\dot{\theta}$	0.99 ± 0.010	$1.15 \pm 0.2\%$

Table 9: *Performance of the forward flight models, where the average output correlation is displayed $\pm$ the standard deviation over all the datasets (same as for the RMSE).*

The performance metrics of the forward speed models indicate a successful estimation process and are in the same order of magnitude as obtained from the hover model. Also it is noticed that the values of the output correlation of the output variable $\dot{w}$ increased dramatically from 0.78 in hover, to 0.92 in forward flight condition (1.0 m/s), and the RMSE (%) decreased significantly. This is also clearly visible in the plots displaying the estimated and measured output variable $\dot{w}$ at different flight speeds (Figure 12), where the top plot indicates the 0.0 m/s trimmed condition, the 1st plot below the top indicates the 0.5 m/s condition, the 2nd plot below the top displays the 0.75 m/s condition, and the bottom plot indicates the 1.0 m/s trimmed condition. Based on this we can conclude that the original model is able to better capture the $\dot{w}$-dynamics with increasing forward speed and that the Nimble more resembles a conventional aircraft when in forward flight (only when including the time-averaged effects). However, it is also possible that the dynamics in Z-force are better excited with increasing forward speed.

In order to provide an idea of how the system dynamics of the DelFly Nimble change with respect to increasing forward speed (from 0.0- to 1.0 m/s), the pole locations of all the models obtained in over 90 flight

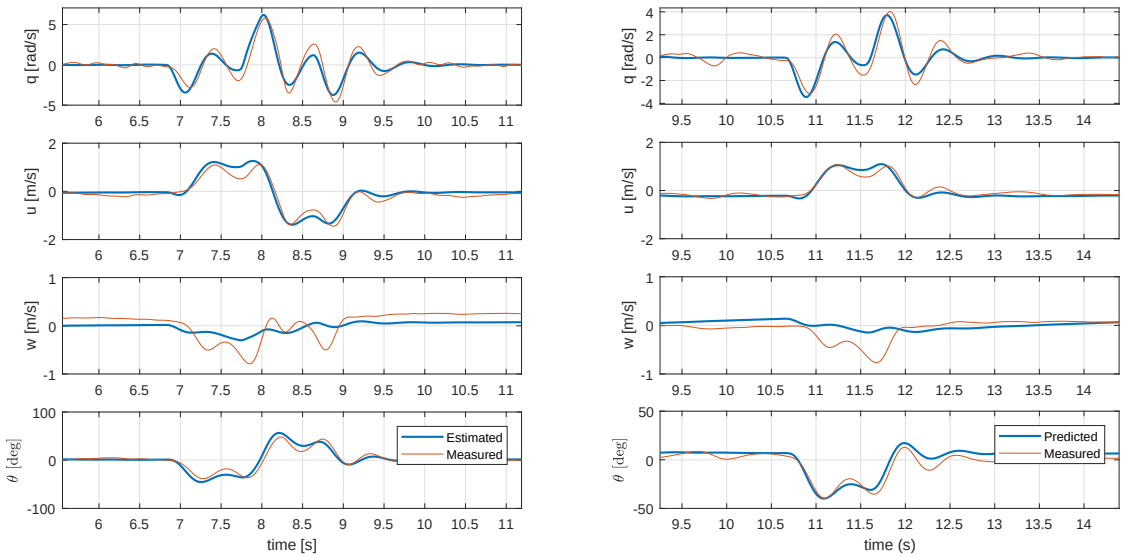

(a) *Estimation of the states. Measured- and model estimated output of the states in closed-loop.*

(b) *Validation of the states. Measured- and model predicted output of the states in closed-loop.*

Figure 10: *Estimated and Predicted output of the estimated time-averaged longitudinal hover model in closed-loop.*

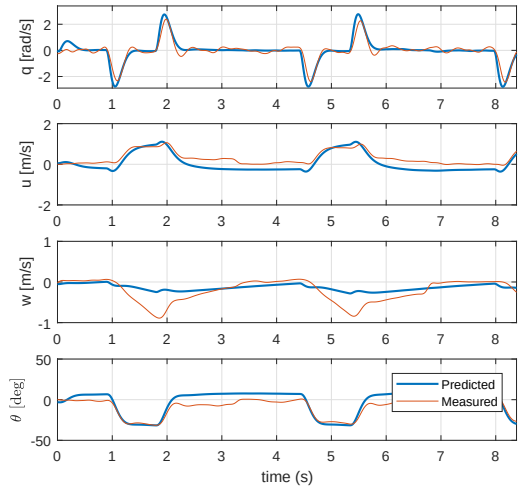

Figure 11: *Measured and predicted states in closed-loop using fast gain settings.*

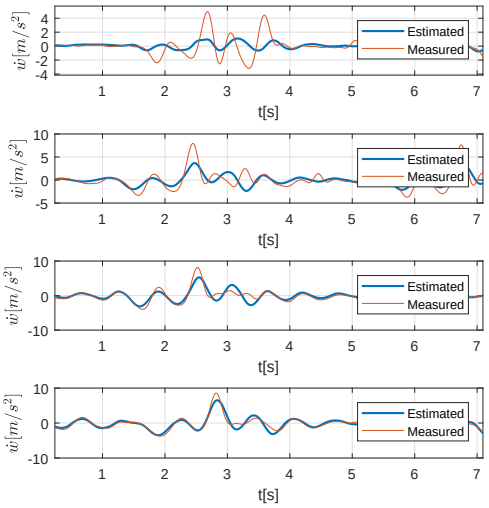

Figure 12: *Estimated and Measured ẇ. Top plot: 0.0 m/s, one below top plot: 0.5 , two below top plot: 0.75 m/s and bottom plot: 1.0 m/s flight condition.*

tests, were plotted in one pole-zero map (Figure 13), where the black crosses (**X**) represent the pole locations of the hover model, and the red crosses (**X**) the 1.0 m/s forward flight condition. As observed in the pole-zero map, with increasing velocity, the one oscillatory pole shifts to lower frequencies and the left most aperiodic pole (fast pole) increases in stability by shifting to more negative values (approx. -8.5 to -11).

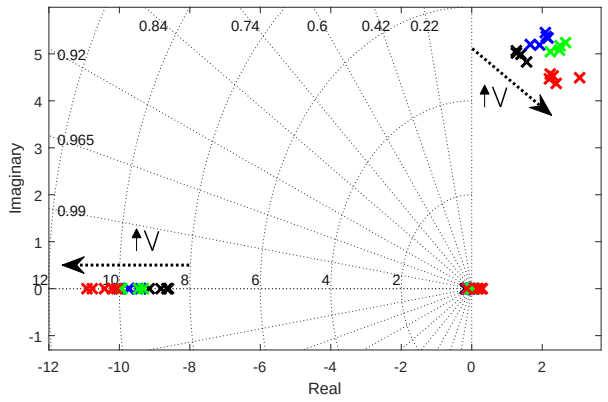

Figure 13: *Pole locations of model with increasing speed V. The hover model trimmed at 0.0 m/s indicated by **X**, the model trimmed at 0.5 m/s indicated by **X**, the model trimmed at 0.75 m/s indicated by **X**, and the model trimmed at 1.0 m/s indicated by **X** of the linear time-averaged longitudinal model.*

iv. Improvements on the Linear Model Structure for the Aerodynamic Force Z

Although the models of X and M show very accurate results, both in hover and forward flight conditions, the model describing the dynamics of the Z force can be greatly improved, especially in and near the hover flight condition. Based on previous discussions on deficiencies in the existing model structure (Equation 4), it was found that a considerable amount of dynamics was insufficiently captured by the model, and it is most likely that there are nonlinear dependencies present in and near the hover flight condition. In order to test if this indeed the case, the model structure of the aerodynamic force Z (Equation 4) was re-evaluated and updated to include nonlinear terms in the regressors. As a result of doing this, it is no longer possible to use the state-space representation used of the original model because of the nonlinear terms used in the updated models. In this particular example nonlinear regressor terms, such as qu, w^2 and u^2, were selected from a pool of regressors and included in the model, in which the regressor terms were selected based on engineering judgement, and only low-order ($<$ second order) terms were considered to keep the model plausible and avoid over-fitting. In this section we will analyse the model estimated output ($Z_{estimated}$) of three different models (Equations 18-20), compared to the measured aerodynamic force ($Z_{measured}$).
The three model structures, consisting of selected variables (and corresponding regressors), are presented in the following equations (18-20):

$$\begin{aligned} Z_{model1} = Z_0 + Z_{qu}\Delta(qu) + Z_{\delta_D}\Delta\delta_D + Z_{w^2}\Delta w^2 + Z_{u^2}\Delta u^2 \\ + Z_{\delta_D w}\Delta(\delta_D w) + Z_{\delta_D q}\Delta(\delta_D q) + Z_{q^2}\Delta q^2 \end{aligned} \tag{18}$$

$$Z_{model2} = Z_0 + Z_{qu}\Delta(qu) + Z_{\delta_D}\Delta\delta_D + Z_{w^2}\Delta w^2 + Z_{u^2}\Delta u^2 \tag{19}$$

$$Z_{model3} = Z_0 + Z_{qu}\Delta(qu) \tag{20}$$

The results of the estimation routine are provided in Figure (14) where the estimated output of the adjusted models are compared to the original model. Model $f(qu)$ (Equation 20) already captures some of the dynamics. Yet great improvements are made when using a model that is a function of $f(qu, \delta_D, w^2, u^2)$ (Equation 19), although it is not completely confirmed if this model can be physically interpreted. Since the w-dynamics are not accurately explained by the linear terms in the original model, we used quadratic terms in the adjusted model, which are still real states and sometimes used in aerodynamic models. The randomly selected variables in model Z_{model3} (Equation 20) provides the best results in terms of goodness of fit but, using too many linear and nonlinear terms probably leads to over-fitting. The corresponding metrics of the adjusted models are provided in Figure (15) indicating that the adjusted models, which include nonlinear terms, greatly improved the effectiveness of the estimation. Validation data is provided in Appendix (D). Although the adjusted models are characterized by much better RMSE (%)-, output correlation- and R2 values, compared to the original model, it remains to be answered whether or not the estimated parameters of the adjusted models are physically plausible. In addition, by applying powerful model structure determination techniques, such as Stepwise Regression, one is in a position to more effectively select regressors (terms), from a pool of candidate regressors, that most influence aerodynamic- forces and moments [25, 32]. Such a study should be considered in future work since it has the potential of providing a better understanding of the Nimble's dynamic behaviour.

VI. Conclusions and Recommendations

In this paper we presented linear time-averaged longitudinal models in hover- and forward flight (up to 1.0±0.05 m/s) conditions for a tailless FWMAV, named the DelFly Nimble, obtained by means of a data-driven system identification approach. Both models, describing the aerodynamic- force X and moment M, in hover- and forward flight conditions captured the actual dynamic behaviour of the DelFly Nimble very accurately, with values of R^2 up to 0.90 and 0.85, respectively (Appendix C). These simple and accurate models can therefore be used for dynamic simulation, advanced controller development and stability analysis. In addition, we have shown that a closed-loop system identification approach can be applied effectively to tailless FWMAVs which leads to accurate models.
Initial results obtained from the model describing the aerodynamic force Z were found to be inadequate in capturing the dynamic behaviour of the Nimble at, and near, hover flight conditions. In an attempt to improve this model, we constructed new model structures containing nonlinear terms. The results of this study showed a considerable improvement, given that the adjusted model, for example $f(qu, \delta_D, w^2, u^2)$ (Equation 19), increased the output correlation by a factor of more than 6. Still some (nonlinear) dynamics were not captured by the models used in this paper, probably due to deficiencies in the model structures or a lack of excitation. However it was proven that, when including nonlinear terms in the model, a larger fraction of the dynamics could be modelled.
In section **V.iv** we have additionally shown that adjusting the model structure can significantly improve the model accuracy, thereby suggesting that the use of stepwise regression techniques could lead to more

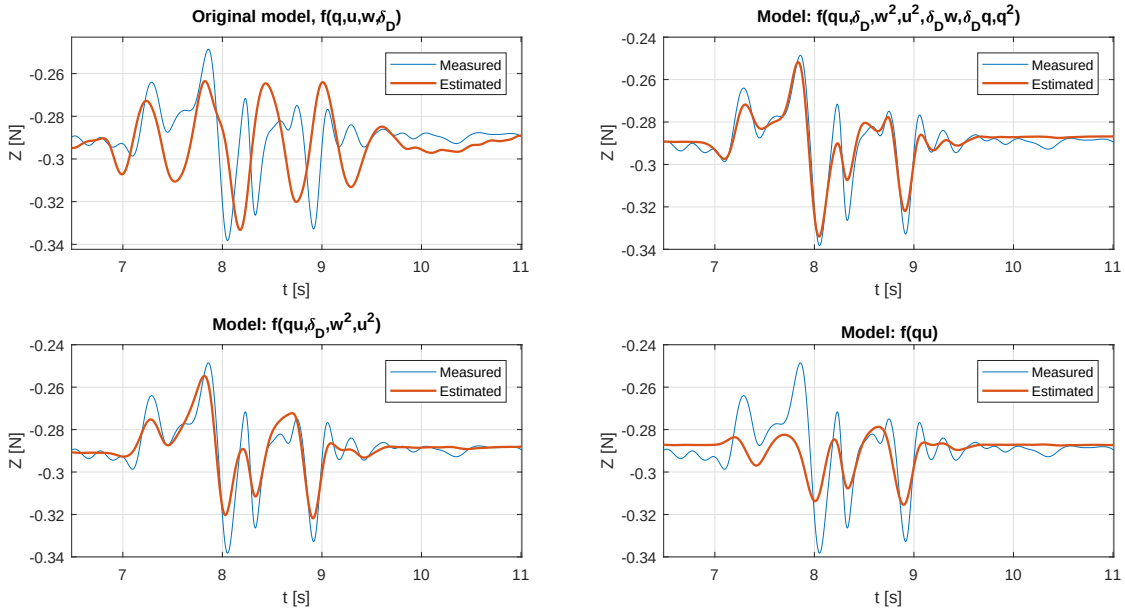

Figure 14: *Adjusted models containing nonlinear parameters. The output of model $f(qu, \delta_D, w^2, u^2, \delta_D w, \delta_D q, q^2)$ was estimated using Equation:18, model $f(qu, \delta_D, w^2, u^2)$ using Equation:19, and model $f(qu)$ using Equation: 20.*

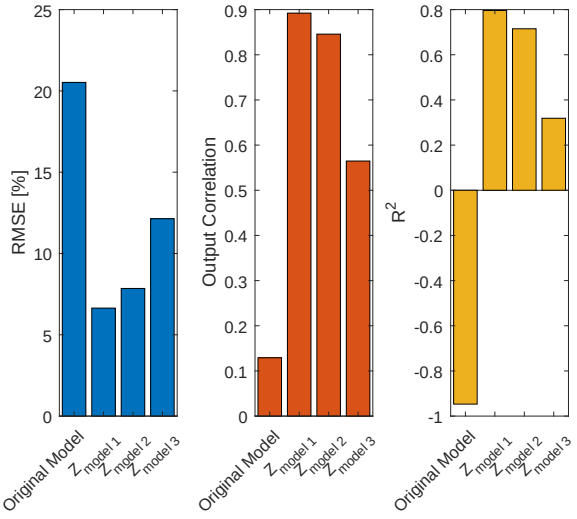

Figure 15: *The metrics of the adjusted model and the three adjusted models.*

effective models. Studies on applying stepwise regression techniques, can be considered very valuable in helping us better understand the dynamics of tailless FWMAVs and the DelFly Nimble.

The models estimated in this paper are all linear local models. These local models are therefore only valid in a particular flight region. In order to obtain a single model that is valid for the entire flight envelope of the DelFly Nimble, future research should look into the use of global modelling techniques in order to obtain a single model which is made up from all the local models identified in this paper [19].

Although the developed models in this work achieved a high accuracy, some dynamic effects remain to be modelled. For example, the time-varying dynamics (flapping dynamics), longitudinal models valid in fast forward flight conditions (> 1.0 m/s) and models describing the lateral dynamics of the Nimble, are some of the subjects that should be looked into in future research.

References

[1] U. . P. O. Tony Murfin, Contributing Editor, *UAV Report: Growth trends and opportunities for 2019*, 2018 (2019-02-17), https://www.gpsworld.com/uav-report-growth-trends-opportunities-for-2019/.

[2] R. Levick, *Drone Industry Just Beginning To Take Off*, 2018 (2019-02-17), https://www.forbes.com/sites/richardlevick/2018/05/15/drone-industry-just-beginning-to-take-off/.

[3] M. Karásek, F. T. Muijres, C. De Wagter, B. D. Remes, and G. C. de Croon, "A tailless aerial robotic flapper reveals that flies use torque coupling in rapid banked turns," *Science*, vol. 361, no. 6407, pp. 1089–1094, 2018.

[4] G. De Croon, K. De Clercq, R. Ruijsink, B. Remes, and C. De Wagter, "Design, aerodynamics, and vision-based con-

trol of the delfly," *International Journal of Micro Air Vehicles*, vol. 1, no. 2, pp. 71–97, 2009.

[5] M. Keennon, K. Klingebiel, and H. Won, "Development of the nano hummingbird: A tailless flapping wing micro air vehicle," in *50th AIAA aerospace sciences meeting including the new horizons forum and aerospace exposition*, 2012, p. 588.

[6] R. J. Wood, "The first takeoff of a biologically inspired at-scale robotic insect," *IEEE transactions on robotics*, vol. 24, no. 2, pp. 341–347, 2008.

[7] M. Karasek, "Robotic hummingbird: Design of a control mechanism for a hovering flapping wing micro air vehicle," *Université libre de Bruxelles*, 2014.

[8] I. Faruque and J. S. Humbert, "Dipteran insect flight dynamics. part 1 longitudinal motion about hover," *Journal of theoretical biology*, vol. 264, no. 2, pp. 538–552, 2010.

[9] P. Chirarattananon, K. Y. Ma, and R. J. Wood, "Perching with a robotic insect using adaptive tracking control and iterative learning control," *The International Journal of Robotics Research*, vol. 35, no. 10, pp. 1185–1206, 2016.

[10] A. Roshanbin, H. Altartouri, M. Karásek, and A. Preumont, "Colibri: A hovering flapping twin-wing robot," *International Journal of Micro Air Vehicles*, vol. 9, no. 4, pp. 270–282, 2017.

[11] H. V. Phan, T. Kang, and H. C. Park, "Design and stable flight of a 21 g insect-like tailless flapping wing micro air vehicle with angular rates feedback control," *Bioinspiration & biomimetics*, vol. 12, no. 3, p. 036006, 2017.

[12] W. Shyy, Y. Lian, J. Tang, D. Viieru, and H. Liu, *Aerodynamics of low Reynolds number flyers*. Cambridge University Press, 2007, vol. 22.

[13] R. Ramamurti and W. C. Sandberg, "A three-dimensional computational study of the aerodynamic mechanisms of insect flight," *Journal of experimental biology*, vol. 205, no. 10, pp. 1507–1518, 2002.

[14] S. A. Ansari, R. Żbikowski, and K. Knowles, "Non-linear unsteady aerodynamic model for insect-like flapping wings in the hover. part 2: implementation and validation," *Proceedings of the Institution of Mechanical Engineers, Part G: Journal of Aerospace Engineering*, vol. 220, no. 3, pp. 169–186, 2006.

[15] X. Deng, L. Schenato, W. C. Wu, and S. S. Sastry, "Flapping flight for biomimetic robotic insects: Part i-system modeling," *IEEE Transactions on Robotics*, vol. 22, no. 4, pp. 776–788, 2006.

[16] G. J. Berman and Z. J. Wang, "Energy-minimizing kinematics in hovering insect flight," *Journal of Fluid Mechanics*, vol. 582, pp. 153–168, 2007.

[17] D. Sigthorsson, M. Oppenheimer, and D. Doman, "Flapping wing micro air vehicle aerodynamic modeling including flapping and rigid body velocity," in *50th AIAA Aerospace Sciences Meeting including the New Horizons Forum and Aerospace Exposition*, 2012, p. 26.

[18] S. Armanini, J. Caetano, G. De Croon, C. De Visser, and M. Mulder, "Quasi-steady aerodynamic model of clap-and-fling flapping mav and validation using free-flight data," *Bioinspiration & biomimetics*, vol. 11, no. 4, p. 046002, 2016.

[19] S. F. Armanini, C. C. de Visser, G. C. de Croon, and M. Mulder, "A time-scale separation approach for time-varying model identification of a flapping-wing micro aerial vehicle," in *AIAA Atmospheric Flight Mechanics Conference*, 2016, p. 1529.

[20] J. V. Caetano, C. De Visser, G. De Croon, B. Remes, C. De Wagter, J. Verboom, and M. Mulder, "Linear aerodynamic model identification of a flapping wing mav based on flight test data," *International Journal of Micro Air Vehicles*, vol. 5, no. 4, pp. 273–286, 2013.

[21] S. F. Armanini, C. C. de Visser, and G. de Croon, "Black-box lti modelling of flapping-wing micro aerial vehicle dynamics," in *AIAA Atmospheric Flight Mechanics Conference*, 2015, p. 0234.

[22] G. Taylor, R. Bomphrey, and J. 't Hoen, "Insect flight dynamics and control," in *44th AIAA Aerospace Sciences Meeting and Exhibit*, 2006, p. 32.

[23] M. Sun and Y. Xiong, "Dynamic flight stability of a hovering bumblebee," *Journal of experimental biology*, vol. 208, no. 3, pp. 447–459, 2005.

[24] K. Kajak, "A minimal longitudinal dynamic model of a tailless flapping wing robot (under review)," 2018.

[25] V. Klein and E. A. Morelli, *Aircraft system identification: theory and practice*. American Institute of aeronautics and astronautics Reston, VA, 2006.

[26] L. Ljung, *System Identification: Theory for the User*, ser. Prentice Hall information and system sciences series. Prentice Hall PTR, 1999. [Online]. Available: https://books.google.nl/books?id=nHFoQgAACAAJ

[27] J. V. Caetano, C. C. de Visser, B. D. Remes, C. De Wagter, E.-J. Van Kampen, and M. Mulder, "Controlled flight maneuvers of a flapping wing micro air vehicle: a step towards the delfly ii identification," in *AIAA Atmospheric Flight Mechanics (AFM) Conference*, 2013, p. 4843.

[28] J. V. Caetano, B. D. Remes, C. C. de Visser, and M. Mulder, "Modeling a flapping wing mav: Flight path reconstruction of the delfly ii," in *AIAA Modeling and Simulation Technologies (MST) Conference*, 2013, p. 4597.

[29] J. Caetano, M. Weehuizen, C. De Visser, G. De Croon, and M. Mulder, "Rigid-body kinematics versus flapping kinematics of a flapping wing micro air vehicle," *Journal of Guidance, Control, and Dynamics*, vol. 38, no. 12, pp. 2257–2269, 2015.

[30] G. Gebert, P. Gallmeier, and J. Evers, "Equations of motion for flapping flight," in *AIAA Atmospheric Flight Mechanics Conference and Exhibit*, 2002, p. 4872.

[31] G. K. Taylor and A. L. Thomas, "Dynamic flight stability in the desert locust schistocerca gregaria," *Journal of Experimental Biology*, vol. 206, no. 16, pp. 2803–2829, 2003.

[32] V. Klein and J. G. Batterson, "Determination of airplane model structure from flight data using splines and stepwise regression," 1983.

[33] M. Karásek and A. Preumont, "Flapping flight stability in hover: A comparison of various aerodynamic models," *International Journal of Micro Air Vehicles*, vol. 4, no. 3, pp. 203–226, 2012.

II

Preliminary Studies

1

Introduction

In this part of the report the results of the preliminary research are shown. Before the modelling process of the flight dynamics of the DelFly Nimble took place, many studies on similar FWMAVs were reviewed. This study included the analysis of different types of modelling process performed on FWMAVs such as aerodynamic modelling and dynamic modelling (2). Given the fact that the goal is to model the flight dynamics of the DelFly Nimble using a flight data-driven approach, system identification techniques were reviewed and explained in chapter (3). The next step of the research was to perform a study on models used on existing FWMAVs in chapter (4). Based on this research, information on how to best model the flight dynamics of the DelFly Nimble would be obtained. Parameter estimation techniques were applied to most of the papers studied on modelling FWMAVs and are described in chapter (5). The tailless design of the DelFly Nimble is characterized by inherent instability. This means that the DelFly Nimble must be stabilized by a closed-loop automatic feedback control system in order to maintain controlled flight. In order to apply system identification techniques to inherently unstable systems, a study on closed-loop system identification was conducted and explained in chapter (6). Lastly, chapter (7) highlights the best suitable models and approaches, from previous studies, to model the flight dynamics of the DelFly Nimble using data-driven system identification techniques.

2

Aerodynamic- and Dynamic Modelling of FWMAVs

A complete model of a flapping-wing platform consists of several components. The first step in creating a complete model is performing **aerodynamic modelling** (2.1). Here, the aerodynamic forces- and moments must be modelled. Secondly, a model of the system dynamics must be created. The system dynamics model are also called the Equations of Motion (EOM) model where **dynamic modelling** (2.2) takes place. The system dynamics model describes how the forces and moments act on the body of the FWMAV. Lastly, the wing kinematics must be integrated. Note that this can be neglected depending on the assumption one makes. For example, the assumption can be made to neglect the effects of the kinematics of the wing on the body due to the fact the mass of the wings is much lower than the mass of the body.

2.1. Aerodynamic Modelling

Aerodynamic modelling of FWMAVs is mostly done using quasi-steady modelling. In short, quasi-steady modelling assumes that the instantaneous forces on a flapping wing are equal to the forces that would act on the wing moving steadily at the same free-stream velocity and angle of attack *The aerodynamics of hovering insect flight. I. The quasi-steady analysis* (1984). As seen in the paper by Sanjay P. Sane Sane and Dickinson (2002) the aerodynamics of flapping wings are non-linear. These models are based on blade element theory, whereby the forces on each section of the wing are integrated over the total span of the wing in order to obtain the total forces acting on the wing. In many cases, quasi-steady models provide useful approximations on the aerodynamic forces. On the other hand, models produced using the quasi-steady approach are usually developed and validated in a single flight condition, usually hover Armanini (2018). Note that these quasi-steady models are physical derived models and non-linear with a limitation in their validity. However, quasi-steady models offer good approximation on aerodynamic forces with a low computational effort. More complex and advanced methods on aerodynamic modelling is using computational fluid dynamics (CFD). Note that these models are highly non-linear and computational inefficient Armanini, de Visser and de Croon (2015), since it requires a great deal of computational power.

2.2. Dynamic Modelling

As for the aerodynamics, the body dynamics of flapping-wing platforms are also complex, physically derived and usually non-linear. The model of the dynamics are called the Equations of Motion (EOM) of the flapping-wing platform. Several formulations in order to derive the EOM for flapping-wing vehicles have been applied. Newtonian methods Gebert et al. (2002), Gibbs-Appel equations Sibilski et al. (2004) and d'Alemberts principle of virtual work Caetano et al. (2015). In the formulations of the EOM a difference can be made between single-body and multi-body models. When considering a flapping-wing platform as a multi-body system, a distinction between the body- and the wings of the

platform is made. This means that multi-body models consider the inertial effect of wings on the body, and therefore it is important to involve the kinematic effects of the flapping on the body. Including the kinematic effects of the wing in the model increases its complexity. To reduce the complexity of the dynamic model one often uses a single-body model. When using a single-body approach, one assumes that the wing mass is much smaller compared to the body mass, therefore the the wing inertia effects can be neglected. Single-body models are also widely applied to flapping-wing platforms Dietl and Garcia (2008) Taylor et al. (2006). The non-linear EOM are usually linearised around a certain trim-point to improve calculation efficiency and maintaining accuracy. Linearising the EOM is common when modelling the dynamics of flapping-wing platforms which will become more apparent further in this study.

3

System Identification

A **system identification** approach differs from the two approaches in sections (2.1 and 2.2) described above. Where the aerodynamic- and dynamic modelling approaches are physically derived, the system identification approach is based on obtaining a model from experimental data, for example from flight tests. Moreover the system identification cycle is explained in Appendix B. So, from the experimental data (flight tests data) a model can be extracted. System identification offers a good comprise between computational efficiency, accuracy and model complexity compared to both simplified physical derived models and highly complex numerical models (CFD). This makes system identification an attractive method for producing dynamic models Armanini (2018). For this reason the system identification approach will be studied and applied to the model identification process of the DelFly Nimble. The main working principle of system identification in general, is described by the following: Given are the input **u** and output **y**, the objective of system identification is to find the system **S** (refer to **Figure 3.1**). In order to obtain a mathematical model of a physical system, such as the flight dynamic model of an aircraft or FWMAV in this case, one can apply aircraft system identification to model the dependence of aerodynamic forces and moments on aircraft motion and control variables. This means that one assumes a model structure based on a priori knowledge and hypotheses, and determining the model parameters such that the obtained model represents the actual flight data as accurately as possible Armanini (2018)Klein and Batterson (1983) Klein and Morelli (2006).

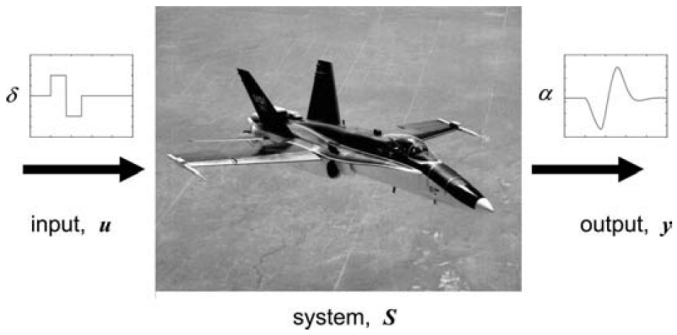

Figure 3.1: System Identification Applied to Aircraft. Source: Klein and Morelli (2006).

Klein Klein and Batterson (1983) Klein and Morelli (2006) describes that the aerodynamic forces and moments can be determined using equation 3.1,

$$y(t) = \theta_0 + \theta_1 x_1 + \ldots + \theta_{g-1} x_{g-1} \tag{3.1}$$

where $y(t)$ is the aerodynamic force or aerodynamic coefficient measured, x_1 to x_{g-1} are the measure responses of the platform (regressors), for example velocity and rotational rates, and θ_1 to θ_{g-1} are

the parameters to be estimated using parameter estimation techniques. Note that the parameter terms can be either linear or non-linear. If the parameters terms are linear, then we speak of a linear-in-the-parameters model. If the parameter terms are non-linear, we speak of a non-linear-in-the-parameters model. It could be the case that for some modelling problems, the relationship between the regressors and the response variable is non-linear in the parameter. In this case, one can make use of a non-linear in the parameter model structure. Mostly used model structures in fixed wing aircraft are linear-in-the-parameter models and are favoured since non-linear parameters increase the complexity of the estimation process Armanini (2018) Armanini, de Visser, de Croon and Mulder (2015) Klein and Morelli (2006) Gim et al. (2016) Chand et al. (2015) Grauer et al. (2011) Caetano, De Visser, De Croon, Remes, De Wagter, Verboom and Mulder (2013). The choice of model structure is usually based on experience or, are selected from a pool of candidate regressors using statistical model structure determination techniques Klein and Morelli (2006). Since this approach uses actual measured data of the platform, the results from the model identification process will most likely closely resemble the actual platform and are therefore more difficult to generalize, compared to the aerodynamic- and dynamic modelling approach where the model was physically derived.
In order to obtain a model that has meaning, it is important that the data should be collected in conditions that are as similar as possible to the real operating conditions.

Model structures used for system identification range from black-box models, where the model is non-physical derived and no distinction can be made between the aerodynamics and the dynamics, to white-box models where the model is completely physical derived and can give better insight into the aerodynamic and dynamic behaviour. It is very common for FWMAVs that a combination between a white-box and a black-box model are used Armanini (2018), called 'grey-box models', due to the fact the physical phenomenons of the flapping platform are very hard to derive. The grey-box model combines the advantages of the black- and grey-box models by means of providing insight into the dynamic and aerodynamic behaviour when little knowledge of the actual physics of the system at hand is available. The parameters to be estimated in these grey-box models also have a physical meaning, for example control- and stability derivatives Armanini (2018)Dietl et al. (2011) Armanini, de Visser and de Croon (2015).
Grey-box models are typically used in order to have some physical connection to the physical behaviour of the system at hand. This requires that the model includes a priori knowledge of the system at hand Armanini (2018) Armanini, de Visser and de Croon (2015) Chand et al. (2015) Armanini, de Visser, de Croon and Mulder (2015). The a priori knowledge of the system comes from the Equations of Motion (EOM) of a conventional rigid-body aircraft. It has been shown that the EOMs from a conventional aircraft give an adequate description of the DelFly for most flight conditions. In order to model the motion of a FWMAV around a certain steady state trimmed condition and simplify the equations, the EOMs are typically linearized around this trim point J.A. Mulder (2013). Flapping-wing dynamics are time-varying and typically non-linear, and therefore linear models are insufficient into fully capturing them. Nonetheless, it can be shown that linearisation provide an acceptable initial approximation within the limited regions of the flight envelope. Simplified models can be useful, for instance to develop basic and computationally efficient simulation frameworks Armanini, de Visser and de Croon (2015).

4

Models of Existing FWMAVs

In the research field of flapping wing MAVs many researchers attempted to model the dynamics of these flying machines. In this section we will provide an overview of the models used in several studies in which researchers attempted to model the dynamics of FWMAVs . The goal is to obtain information on the type of models used, the model structure and the regression model type used, in order to determine the most suitable modelling techniques and model structures for the the DelFy Nimble.

Linear Aerodynamic Model Identification of a Flapping Wing MAV Based on Flight Test Data

Caetano, De Visser, De Croon, Remes, De Wagter, Verboom and Mulder (2013)

The paper by J.V. Caetano, C.C. de Visser, G.C.H.E. de Croon, B. Remes, describes a system identification approach on the DelFly II, which is a passively stable tailed FWMAV, to construct a aerodynamic model that can be used for simulations. Here, a motion capturing system was used to measure the states of the platform. This model captures the flapping-averaged dynamics of the FWMAV and the assumptions are made for a single rigid body (constant inertia properties). In addition, the model structure, describing the aerodynamic- forces and moments, are all linear. Flapping-averaged means that the mean force created by one flapping cycle is used for modelling.
For the dynamic model use was made of the EOM for aircraft obtained from Vladislav Klein, Eugene A. Morelli Klein and Morelli (2006), given in the equations (4.1a-4.1c).

Force equations:

$$\begin{aligned} \dot{u} &= a_x - gsin(\theta) + rv - qw \\ \dot{v} &= a_y + gcos(\theta)sin(\phi) + pw - ru \\ \dot{w} &= a_z + gcos(\theta)sin(\phi) + qu - pv \end{aligned} \tag{4.1a}$$

Moment equations:

$$\begin{aligned} l &= \dot{p}I_{xx} + qr(I_{zz} - I_{yy}) - (pq + \dot{r})I_{xz} \\ m &= \dot{q}I_{yy} + rp(I_{xx} - I_{zz}) - (p^2 + r^2)I_{xz} \\ n &= \dot{r}I_{zz} + pq(I_{yy} - I_{xx}) - (qr + \dot{p})I_{xz} \end{aligned} \tag{4.1b}$$

Kinematic equations:

$$\begin{aligned} \dot{\phi} &= p + qsin(\phi)tan(\theta) + rcos(\phi)tan(\theta) \\ \dot{\theta} &= qcos(\phi) - rsin(\phi) \\ \dot{\psi} &= q\frac{sin(\phi)}{cos(\theta)} + r\frac{sin(\phi)}{cos(\theta)} \end{aligned} \tag{4.1c}$$

where the definitions of all the terms can be found in Klein and Morelli (2006). The measured aerodynamic- forces and moments (Equations 4.1a-4.1c) were then calculated from the experimental data obtained from the flight tests.

For the aerodynamic model structure selection two linear models were used: (1) a full model that incorporates all the state variables reconstructed from the tracking system, and (2) a reduced model that

only includes state variables that may be measured or calculated directly from the existing on-board sensors. The structure of the model is given in equation 4.2 below.

$$F_i = C_{F_0} + \sum_{s=1}^{n} C_{F_S} \cdot S \quad with \;\; S : \{\phi, \theta, \phi, u, v, w, p, q, r, \alpha, \beta, \delta_f, \delta_e, \delta_r\} \tag{4.2}$$

where α and β are measured states and $F : \{X, Y, Z, L, M, N\}$ are the forces and moments calculated using the EOM. $\delta_f, \delta_e, \delta_r$ are the flapping frequency, elevator input angle, and rudder input angle, respectively. The term F_i represents the input for the forces and moments obtained from the EOM. The first term on the right-hand side, C_{F_0}, is the affine coefficient; S represents a state and C_{F_S} is the state's coefficient or parameter for a given force or moment F_i. The full model structure is then defined such that each of the aerodynamic forces and moments is a linear function of all the states.
The reduced model structure only uses states that are measurable using on-board sensors which include much less states than the full model. The reduced model only includes the states: $\{\phi, \theta, \phi, \delta_f, \delta_e, \delta_r\}$ and is represented in the equations (4.3-4.8) below.

$$X = X_0 + X_q q + X_\theta \theta + X_{\delta_e} \delta_e + X_{\delta_f} \delta_f \tag{4.3}$$
$$Y = Y_0 + Y_p p + Y_\phi \phi + Y_{\delta_r} \delta_r + Y_{\delta_f} \delta_f \tag{4.4}$$
$$Z = Z_0 + Z_q q + Z_\theta \theta + Z_{\delta_e} \delta_e + Z_{\delta_f} \delta_f \tag{4.5}$$
$$L = L_0 + L_\theta \theta + L_{\delta_r} \delta_r + L_{\delta_f} \delta_f \tag{4.6}$$
$$M = M_0 + M_\theta \theta + M_{\delta_e} \delta_e + M_{\delta_f} \delta_f \tag{4.7}$$
$$N = N_0 + N_\theta \theta + N_{\delta_r} \delta_r + N_{\delta_f} \delta_f \tag{4.8}$$

The next step in the modelling process is estimating the parameters in the full- and reduced model. For this an ordinary least squares (OLS) estimator was used to estimate the parameters in the linear models. Note that in the next section more information regarding parameter estimation techniques, such as OLS estimation, will be presented. The process of parameters estimation is a fairly simple process in finding the parameters of the full- and reduced linear models. For example, the estimation of the parameters of the aerodynamic force in x-direction (X) is determined using the following matrix operations:

$$\hat{\theta} = \begin{bmatrix} \hat{X}_0 \\ \hat{X}_q \\ \hat{X}_\theta \\ \hat{X}_{\delta_e} \\ \hat{X}_{\delta_f} \end{bmatrix} = (R^T R)^{-1} R^T X$$

with $\hat{\theta}$ the column vector containing the estimated parameters and the regression matrix R;

$$R = \begin{bmatrix} 1 & q(1) & \theta(1) & \delta_e(1) & \delta_f(1) \\ 1 & q(2) & \theta(2) & \delta_e(2) & \delta_f(2) \\ \vdots & \vdots & \vdots & \vdots & \vdots \\ 1 & q(N) & \theta(N) & \delta_e(N) & \delta_f(N) \end{bmatrix} \quad n_{parameters} \times N$$

The estimated parameters of X are indicated by a hat $\hat{X}$, with the regression matrix **R** containing N observations (or regressors) of the states. This means that the size of the **R**-matrix is determined by the number of parameters $n_{parameters}$ and the number of data points N. Finally, by multiplying the estimated parameters $\hat{\theta}$ with the measured states X, the output of the model y is estimated.

The results of the system identification approach where promising. Good predictions from the aerodynamics forces and moments were obtained for both models. However, the reduced model was less accurate in modelling the aerodynamic forces and moments. In addition, the models were also used to predict the new states of the ornithopter in a non-linear dynamic simulator. This simulator used

the real inputs sequence to predict the Delfly's new states, based on a real initial condition. Here the identification coefficients, estimated during the parameter estimation process, were used to calculate the aerodynamic forces and moments that were input in the non-linear equations of motion to compute the new state derivatives, which were then integrated resulting in the new states. The results showed that it was possible to reconstruct its flight path and attitude with considerable accuracy for the initial parts of the simulation. However, the simulation quickly diverged after half a second.

Black-Box LTI Modelling of Flapping-Wing Micro Aerial Vehicle Dynamics

Armanini, de Visser and de Croon (2015)

The paper by Sophie F. Armanini, Coen C. de Visser and Guido C. H. E. de Croon present a development of a black-box linear state-space model for flight dynamics of a FWMAV namely, the DelFly II. Since a black-box model structure was selected, it was therefore impossible to distinguish the aerodynamics and dynamics of the platform. A system identification technique was used in order to obtain a longitudinal- and lateral dynamic models using data recorded from a motion tracking system. Ordinary least squares and maximum likelihood-based estimation approaches were applied in the time domain. Note that theory on maximum likelihood estimation (MLE) will be discussed in the next section. For now, MLE is simply a estimation routine to estimate unknown parameters in a pre-defined model.

The black-box method does not make use of the EOM for describing the trajectory of the DelFly II but uses the measured states only for modelling. Furthermore, the following states and inputs for longitudinal- and lateral dynamic modelling were selected (Equations 4.9 - 4.10),

$$x_{lon} = [q \;\; u \;\; w \;\; \theta], \;\; u_{lon} = \delta_e \tag{4.9}$$

$$x_{lat} = [p \;\; r \;\; v \;\; \phi], \;\; u_{lon} = \delta_r \tag{4.10}$$

The states and inputs from equation (4.9 - 4.10) were used as regressors in the regression matrix. In this particular case, the OLS estimator has the exact same structure as described in the previous paper, namely;

$$\hat{\Theta} = (X^T X)^{-1} X^T z,$$

where **X** is the regression matrix and z the output measurement vector written in vector form;

$$z = X\Theta + \epsilon, \tag{4.11}$$

where ϵ is the measurement error in vector form. **A** and **B** are defined as

$$\mathbf{A} = [a_{ii}], \;\; \mathbf{B} = [b_{ij}], \quad i = 1, 2, ..., n_x, \;\; j = 1, 2, ..., n_u, \tag{4.12}$$

where n_x is the number of states and n_u the number of inputs. The regression matrix **X** is then constructed from the combined states and inputs at all the N measurement points;

$$\mathbf{X} = \begin{bmatrix} x_{1,1} & x_{2,1} & \cdots & x_{n_x,1} & u_{1,1} & u_{2,1} & \cdots & u_{n_u,1} \\ x_{1,1} & \ddots & & \vdots & u_{1,1} & \ddots & & \vdots \\ \vdots & & \ddots & \vdots & \vdots & & \ddots & \vdots \\ x_{1,N} & \cdots & & x_{n_x,N} & u_{1,N} & \cdots & & u_{n_u,N} \end{bmatrix},$$

The estimation process will then be performed per individual state n_x. So, for each output z_i each row in the original state-space system can be formulated as,

$$z_i = \begin{bmatrix} \dot{x}_{i,1} \\ \dot{x}_{i,2} \\ \vdots \\ \dot{x}_{i,N} \end{bmatrix} = X\Theta + \begin{bmatrix} \epsilon_{i,1} \\ \epsilon_{i,2} \\ \vdots \\ \epsilon_{i,N} \end{bmatrix}, \;\; \hat{\Theta} = \begin{bmatrix} a_{i1} \\ a_{i2} \\ \vdots \\ a_{in_x} \\ b_{i1} \\ b_{i2} \\ \vdots \\ b_{in_u} \end{bmatrix}$$

This means that, when using the OLS, the parameters must be estimated for each individual state

$i = 1, 2, ..., n_x$, so each row i in the system matrices **A** and **B** are estimated consecutively. In addition, state derivatives were obtained from numerical differentiation.
A disadvantage of using a OLS is that it assumes the measurements contain no noise. In practical situations measurements always contain noise. In the paper another technique was used to estimate the parameters of the dynamic model of the DelFly II, such as the Total Least Squares or Maximum Likelihood-based estimation. Another method to decrease the amount of noise in the measurements is to pre-process the estimation data by means of state-estimation techniques also known as the two-step method Organization et al. (1994). Still, using the OLS estimator one is able to obtain reasonable accurate results Armanini, de Visser and de Croon (2015).

Another estimation method used in the paper includes the Maximum likelihood (ML) estimation, also known as the output error method (OEM), which deals with measurement errors but not with process noise. The theory regarding the ML estimator will be discussed in the next section. This way of modelling the dynamics of the DelFly II has shown good results. The output response of the estimated dynamic model accurately resemble the measured output of the actual DelFly II. Although accurate results for both the longitudinal- and lateral model were obtained, the only problem is that the black-box model cannot distinguish the aerodynamics- from the dynamic effects.

Insect Flight Dynamics and Control

Taylor et al. (2006)
The paper by Graham K. Taylor, Richard J. Bomphrey and Jochem 't Hoen attempted to model the insect flight dynamics. In addition, empirical data from real insects have been used, measurements obtained from wind tunnel and rotary balance measurement units in order to create a model. Both linear and non-linear EOMs were used during the modelling process.
First the linear dynamic model that is presented in the paper assumes a rigid body and used the linearised equations of motion about a steady state of equilibrium (trim point). The longitudinal dynamics are given by:

$$\begin{bmatrix} \delta\dot{u} \\ \delta\dot{w} \\ \delta\dot{q} \\ \delta\dot{\theta} \end{bmatrix} = \begin{bmatrix} X_u/m & X_w/m & X_q/m - w_0 & X_\theta/m - gcos(\theta_0) \\ Z_u/m & Z_w/m & Z_q/m + u_0 & Z_\theta/m - gsin(\theta_0) \\ M_u/I & M_w/I & M_q/I & M_\theta/I \\ 0 & 0 & 1 & 0 \end{bmatrix} \begin{bmatrix} \delta_u \\ \delta_w \\ \delta_q \\ \delta_\theta \end{bmatrix}$$

where X_i, Z_i and W_i, $i \in \{u, w, q, \theta\}$ are the partial derivatives of the static forces and moments with respect to the state variables, and δ represent the perturbation of the corresponding variable. Note that this is a grey-box model structure.

For the non-linear analysis in the paper, a non-linear framework grey-box is used. The insect in the model is still treated as a rigid body with constant mass distribution. The longitudinal dynamics are then given by equations (4.13-4.16):

$$m\dot{u} = -m(wq + gsin(\theta)) + X_0 + X_u u + X_w w + X_q q + X_\theta \theta \tag{4.13}$$
$$m\dot{w} = m(uq + gcos(\theta)) + Z_0 + Z_u u + Z_w w + Z_q q + Z_\theta \theta \tag{4.14}$$
$$I\dot{q} = M_0 + M_u u + M_w w + M_q q + M_\theta \theta \tag{4.15}$$
$$\dot{\theta} = q \tag{4.16}$$

where, for example, the force X is approximated by the linear expansion (Equation 4.17);

$$X = X_0 + X_u u + X_w w + X_q q + X_\theta \theta \tag{4.17}$$

and the other components Z and M are approximated in a similar fashion. Results from the models show that the non-linear models show better results compared to the linear models.

Dipteran Insect Flight Dynamics. Part1 Longitudinal Motion About Hover

Faruque and Humbert (2010)
The paper of Imraan Faruque and J.SeanHumbert presents a model of the longitudinal hovering dynamics for an dipterous insect. It assumes a rigid body structure where the forces are approximated

by wingstroke-averaged forces. In addition, frequency based system identification tools are used to identify the unknown parameters of the model. The study also includes the identification of the aerodynamic effects of the flapping wing insect, where the aerodynamic effects are physically derived. The system of ordinary differential equations, or the EOM, used in the study of the longitudinal portion are (Equations 4.18);

$$\begin{aligned} X &= m(\dot{u} + qw - rv) + mgsin(\theta) \\ Z &= m(\dot{w} + pv - qu) - mgcos(\theta)cos(\phi) \\ M &= I_{yy}\dot{q} - I_{xz}(\dot{r} + pg) - (I_{yy} - I_{zz})qr \end{aligned} \tag{4.18}$$

where X, Z and M are the aerodynamic forces and moment respectively. For example the linearised equation in x is then (Equation 4.19);

$$\Delta\dot{u} = \frac{\Delta X}{m} - gcos(\theta_0)\Delta\theta \tag{4.19}$$

where ΔX has the physical interpretation of being the perturbation force due to state and/or control perturbations from equilibrium (trim) values. For traditional linearised analysis, a linear control model was developed which separates out the linear effect of each of the longitudinal variables u, v, w, θ, q as (Equation 4.20);

$$\frac{\Delta X}{m} = X_u\Delta u + X_w\Delta w + X_\theta\Delta\theta + X_q\Delta q + \frac{\Delta X_c}{m} \tag{4.20}$$

where X_c is the term that include each of the control inputs (Equation 4.21);

$$\frac{\Delta X_c}{m} = X_f\Delta f + X_\beta\Delta\beta + X_{\theta_{off}}\Delta\theta_{off} \tag{4.21}$$

where the flapping frequency f, ϕ_{off} is the mean position (center) of the wing oscillation (which is the stroke offset of the wing), and the stroke plane angle β are the control inputs which will affect the aerodynamic force X. So, the formula for the state $\Delta\dot{u}$ then becomes (Equation 4.22);

$$\Delta\dot{u} = X_u\Delta u + X_w\Delta w + X_\theta\Delta\theta + X_q\Delta q + X_f\Delta f + X_\beta\Delta\beta + X_{\theta_{off}}\Delta\theta_{off} - gcos(\theta_0)\Delta\theta \tag{4.22}$$

Equation 4.22 is considered to be of great importance when looking at the DelFly Nimble. This method gives a direct link to how the perturbation of the aerodynamic forces change when, for example, the pitch or deflection of a control surface changes or deviates from its trimmed position. So, if one is able to measure, for example, the pitch and deflection of a certain control surface, then these measurements can be used to model the aerodynamics of the DelFly Nimble. The linear model, equation 4.20, is then substituted into equation 4.19 which forms the first term of the state equation $\dot{x} = Ax + Bu$ where $x = [\Delta u, \Delta w, \Delta q, \Delta\theta]^T$ and the control inputs are; $u = [\Delta f, \Delta\Phi, \Delta\beta, \Delta\phi_{off}]^T$. The matrices are defined as;

$$A = \begin{bmatrix} X_u & 0 & 0 & -g \\ Z_u & Z_w & 0 & 0 \\ M_u & M_w & M_q & 0 \\ 0 & 0 & 1 & 0 \end{bmatrix}$$

and

$$B = \begin{bmatrix} 0 & 0 & X_\beta & X_{\phi,off} \\ Z_f & Z_\psi & 0 & 0 \\ 0 & 0 & M_\beta & M_{\phi,off} \\ 0 & 0 & 0 & 0 \end{bmatrix}$$

Note, that the partial derivative of θ, w and q terms (X_θ, X_w and X_q) are not included in the **A**-matrix. This due to the fact that the terms are zero for any flight configuration because the wings lift and drag components are functions of the kinematics, the wing shape, the environment, and not the state variables. Also the **B**-matrix does not include one term, namely X_f. This is due to the fact that the magnitude of the lift vector does not affect the aerodynamic force X.

The perturbation forces are expressed in a time-invariant linear system in state-space form. In addition to the A-matrix, the B-matrix (control matrix) also contains very useful information and provides a direct insight into the physics of how control inputs affect the flight motion of the platform. Although the configuration of the FWMAV in this paper is different compared to the DelFly Nimble, the process of modelling its dynamics is considered to be very useful when applied to the DelFly Nimble given its potential to gain insight in the dynamic behaviour of the platform.

Development of the Nano Hummingbird: A Tailless Flapping Wing Micro Air Vehicle

Keennon et al. (2012)

Matthew Keennon, Karl Klingebiel, Henry Won and Alexander Andriukov describe the use of a simplified aerodynamic model that is backed by extensive experimental data without going into any detail on how the model is actually structured. Using the hummingbird as a biological model, the primary focus of the development program was on designing the flapping wing propulsion system and the associated control mechanisms required for tailless flapping wing flight with the capability of precision hover. The paper does provides information that it has used helicopter performance models. However, one can argue about the usefulness of this information when applied to the DelFly Nimble.

Controlled Flight of a Biologically Inspired, Insect-Scale Robot

Ma et al. (2013)

Kevin Y. Ma, Pakpong Chirarattananon, Sawyer B. Fuller and Robert J. Wood used a similar approach as Imraan Farugues taken over by Cheng et al. (2011). The main difference is that this study includes the use of feedback control derivatives in the state space system to determine the physical effects of the flight motions. This approach does not fit the data driven system identification process that will be applied to the DelFly Nimble due to the use of the feedback control derivatives in the model. The main objective regarding the Nimble is to estimate the aerodynamic control derivatives and not the feedback control derivatives.

A Biomimetic Robotic Platform to Study Flight Specializations of Bats

Ramezani et al. (2017)

The approach in the paper is used to model the dynamics of the platform (a bat) is based on the Lagrange method using kinetic and potential energies. This approach is very different from most of the other researchers studied so far.

COLIBRI: A Hovering Flapping Twin-Wing Robot

Roshanbin et al. (2017)

The work of A. Roshanbin, H. Altartouri, M. Karasek and A. Preumont uses a state-space model to model the longitudinal pitch dynamics where the parameters in the state space model of the longitudinal dynamics are evaluated (which are a function of a damping constant) using pendulum experiments. The basis of the dynamic model is described by linearised Newton-Euler equations (also known as the equations of motion).

Dynamic Flight Stability of a Hovering Bumblebee

Sun and Xiong (2005)

The study of Mao Sun and Yan Xiong focusses on the longitudinal dynamic flight stability of a hovering bumblebee. The longitudinal dynamic flight stability of a hovering bumblebee was studied using the method of computational fluid dynamics to compute the aerodynamic derivatives and the techniques of eigenvalue and eigenvector analysis for solving the equations of motion. Like most of the work done on Ornithopters, Mao Sun also make use of rigid body approximations meaning the body does not change its shape or its size during translational- or rotational manoeuvres. The action of the flapping wing is represented by the cycle-average forces and moments. This means that the average forces and moments produced by the wing are averaged with respect to one complete cycle. Originally the equations of motion are non-linear but are linearised, thereby approximating the motion of the platform

only at small disturbances from its steady, or trimmed, state. The linearised equations used are;

$$\Delta X = m\Delta\dot{u} = X_u\Delta u + X_w\Delta w + X_q\Delta q - mg\Delta\theta \tag{4.23}$$
$$\Delta Z = m\Delta\dot{w} = Z_u\Delta u + Z_w\Delta w + Z_q\Delta q \tag{4.24}$$
$$\Delta M = I_{yy}\Delta\dot{q} = M_u\Delta u + M_w\Delta w + M_q\Delta q \tag{4.25}$$
$$\Delta\dot{\theta} = \Delta q \tag{4.26}$$
$$\Delta\dot{x_E} = \Delta u \tag{4.27}$$
$$\Delta\dot{z_E} = \Delta w \tag{4.28}$$

where $X_u, X_w, X_q, Z_u, Z_w, Z_q, M_u, M_w$ and M_q are the stability derivatives (aerodynamic derivatives) to be estimated. X, Z are the well known aerodynamic forces and M is the aerodynamic pitching moment. The mass is indicated by m and I_{yy} is the pitching moment of inertia around the y-axis. The Δ indicates a small disturbance quantity from the steady-state or trimmed condition. Note that in trimmed hovering flight θ is zero due to the fact the x-axis is aligned with the horizontal frame of reference. As a result X = 0 , Z = -mg and M = 0. In deriving the equations of (4.23-4.28), the aerodynamic forces and moments are described as functions of the disturbed motion variables as discussed earlier. For example X is a function of several perturbations;

$$X = X_u\Delta u + X_w\Delta w + X_q\Delta q \tag{4.29}$$

Finally the EOM (with the substituted stability derivatives) are then represented in a matrix system. To determine the stability derivatives, Mao Sun used CFD (Computational Fluid Dynamics) tools and techniques. Using these techniques, Mao Sun was able to determine the parameters which were required to be estimated in the A-matrix. As a result, from the A-matrix Sun was able to determine the stability of the platform by analysing the eigenvalues at several natural modes of the system.

Longitudinal Flight Dynamics of Hovering MAVs/Insects

Taha et al. (2014)

During the analysis of the dynamic model it became clear that a rigid body assumption was made which neglected the inertial effects of the wing on the body. The same assumptions were made in many other studies and have led to good results. However, this particular study only addresses the longitudinal model. Due to the flapping, a wing-fixed frame is used and is considered to coincide with the body-fixed frame for zero wing kinematic angels. The equations of motion used are similar to those used in a conventional aircraft, namely;

$$\begin{bmatrix}\dot{u}\\ \dot{w}\\ \dot{q}\\ \dot{\theta}\end{bmatrix} = \begin{bmatrix}-gw - gsin(\theta)\\ qu + qcos(\theta)\\ 0\\ q\end{bmatrix} + \begin{bmatrix}\frac{1}{m}X\\ \frac{1}{m}Z\\ \frac{1}{I_{yy}}M\\ 0\end{bmatrix}$$

where g is the gravitational acceleration, m the body mass and I_{yy} the moment of inertia around the body y-axis y_b. The the state variables are; $x = [u, w, q, \theta]^T$ where u and w the velocity of the body center of mass in the x_b and z_b directions and θ and q are the pitching angle and the angular velocity about the y_b axis respectively. The X, Z and M variables are the well know aerodynamic forces and moments in the x_b, z_b directions and about the y_b axis respectively. The aerodynamic modelling process in the paper are physically derived and are considered to be complex, due to the complex flow field that occurs during the flapping process such as the leading edge vortices and the rotational effect of the wings. These processes are very hard to model analytically. However, as many others, Haithem E. Taha also uses a analytical approach instead of an empirical approach that is more focused on making models based on data from flight tests. As a result, the aerodynamic coefficients used in the state space model are estimated analytically, describing the physical nature of the derivatives mathematically. However, the state-space system remains similar to most of the work studied so far and is displayed below;

$$\begin{bmatrix}\dot{u}\\ \dot{w}\\ \dot{q}\\ \dot{\theta}\end{bmatrix}=\begin{bmatrix}-gw-gsin(\theta)\\ qu+qcos(\theta)\\ 0\\ q\end{bmatrix}+\begin{bmatrix}\frac{1}{m}X\\ \frac{1}{m}Z\\ \frac{1}{I_{yy}}M\\ 0\end{bmatrix}+\begin{bmatrix}X_u(t) & X_w(t) & X_q(t) & 0\\ Z_u(t) & Z_w(t) & Z_q(t) & 0\\ M_u(t) & M_w(t) & M_q(t) & 0\\ 0 & 0 & 0 & 0\end{bmatrix}$$

where $X_{u/v/w}$, $Z_{u/v/w}$ and $M_{u/v/w}$ are the stability derivatives and are time-varying. In other words, the time-varying stability derivatives (or aerodynamic derivatives) are written directly in terms of the system parameters, where the parameters are the flapping angle (back and forth), wing pitch angle, mass and other parameters of the platform. Since these stability derivatives are non-linear (the parameters vary non-linearly), the non-linear system is linearised to perform the stability analysis.

A Hovering Flapping-Wing Microrobot with Altitude Control and Passive Upright Stability

Teoh et al. (2012)

The study of Z. E. Teoh, S. B. Fuller, P. Chirarattananon, N. O. Pérez-Arancibia, J. D. Greenberg and R. J. Wood focusses on the stability analysis of the Flapping-Wing Microrobot uses passive air dampers for stabilisation. The aerodynamic damping coefficients are determined using wind tunnel tests and measurements. From these wind tunnel measurements a simplified linear model was used. The study also shows how the drag of the flapping wings is proportional to v (the free stream velocity) for a constant w (the velocity of the wing relative to the body) using wing tunnel tests. Based on the wind tunnel measurements the model that approximates the aerodynamic force can be written as (Equation 4.30);

$$f_d = -bv \tag{4.30}$$

where b is estimated using a least squares linear regression on the force data (force data obtained from wind tunnel measurements f_d) and the airspeed v. The primary task goal of this particular study is stabilization in pitch θ. The aerodynamic dampers are placed below and under the center of mass (COM) of the body. As the RoboBee flies, a drag force caused by the forward (lateral) movement causes a torque around the COM. The sum of all lateral forces are then equated (see Figure 4.1a-4.1b) in order to produce an equation that describes the non-linear lateral dynamics (Equation 4.31);

$$\begin{aligned} m\dot{v_x} &= F_1 + F_2 + F_w + F_{t,l} \\ &= -b_1(v_x - d_1\omega cos(\theta)) - b_2(v_x + d_2\omega cos(\theta)) \end{aligned} \tag{4.31}$$

where ω is the angular velocity. Then the non-linear equation for the torque to rotational acceleration is described (Equation 4.32);

$$\begin{aligned} J\dot{\omega} &= T_1 + T_w + T_2 \\ &= d_1b_1(v_x - d_1\omega cos(\theta)) - d_2b_2(v_x + d_2\omega cos(\theta)) + d_wb_w(v_x - d_w\omega cos(\theta)) \end{aligned} \tag{4.32}$$

where further definitions of the parameters, indicated in the equations, can be found in the paper. To simplify the equations and computations, the equations 4.31 and 4.32 are linearised around $\theta = 0$ which is the steady state hover condition. Furthermore, when $d_1 = d_2 = d$ and linearising the equations the states can be represented by the following linear dynamic equations;

$$\dot{v_x} = \frac{1}{m}[(-2b - b_w)v_x - F_t\theta + b_wd_w\omega] \tag{4.33}$$

$$\dot{\theta} = \omega \tag{4.34}$$

$$\dot{v_x} = \frac{1}{J}[b_wd_wv_x + (-2bd^2 - b_wd_w^2)\omega] \tag{4.35}$$

where J is the total moment of inertia about the COM. These equations are then put into a state-transition matrix (state-space system) where the state vector is defined as $x = [v_x, \theta, \omega]^T$, where the

assumption is made that $F_t = mg$;

$$A = \begin{bmatrix} \frac{1}{m}(-2b - b_w) & -g & \frac{1}{m}b_w d_w \\ 0 & 0 & 1 \\ \frac{1}{J}b_w d_w & 0 & \frac{1}{J}(-2bd^2 - b_w d_w^2) \end{bmatrix}$$

The Routh-Hurwits criterion was then used to determine the stability of the system. Using this approach the goal was to determine the parameters for which the platform was stable using the passive air dampers.

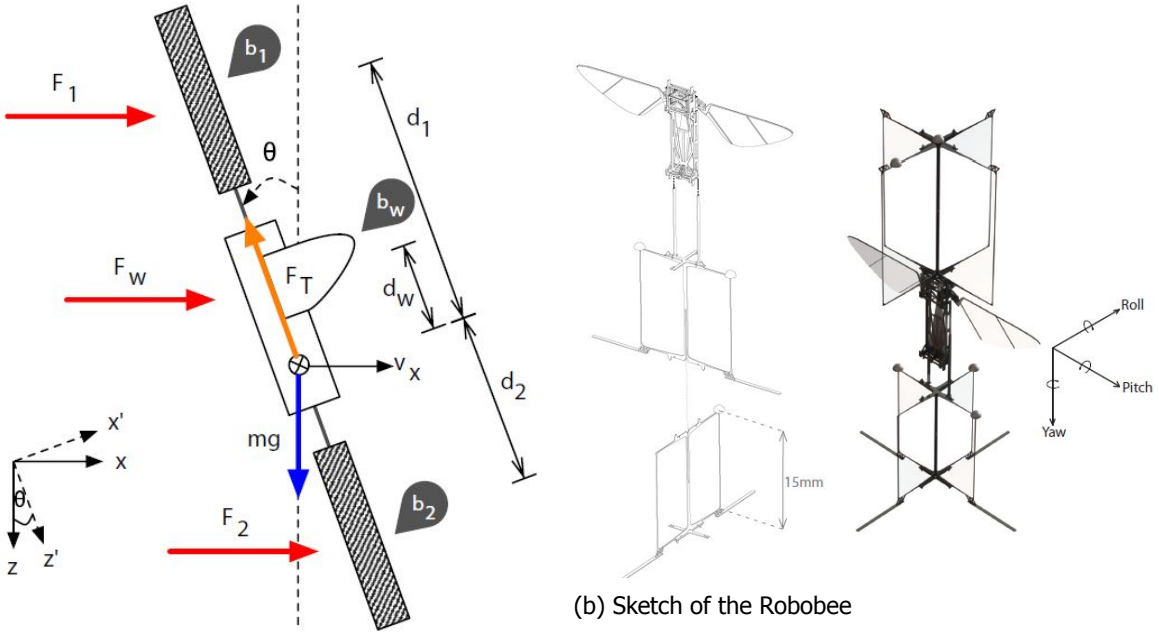

(a) Free body diagram of the Robobee.

(b) Sketch of the Robobee

Figure 4.1: A hovering flapping-wing microrobot called the Robobee.

In addition to the scope of the model, it is clear that the study only includes the longitudinal model which means that the platform only has control authority over the axis defined in the model.

A Minimal Longitudinal Dynamic Model of a Tailless Flapping Wing Robot

Kajak (2018)

Previous study performed on the DelFly Nibmle at the faculty of Aerospace Engineering in Delft also gives valuable information regarding the selection of a dynamic model and the obtained data from flight tests done by K.M. Kajak. The derivation of the model has a more analytic origin in combination with some empirical experiments done in the wind tunnel and using optical tracking measurements. During the research K.M. Kajak adopted formulas for calculating the velocity of the wings when flapping;

$$U = 2\Phi f \frac{b}{4} \tag{4.36}$$

where Φ is the flapping amplitude in radians, f the flapping frequency [Hz] and b the wingspan. In order to determine the drag force of the wings during flapping, K.M. Kajak used an approach similar to the one used by Z. E. Teoh Teoh et al. (2012), where the the average drag-force (during one cycle) can be approximated using;

$$\bar{f_d} = \frac{1}{2}\beta[(U-u)^2 - (U+u)^2] = -2\beta U u \tag{4.37}$$

where the assumption is made that the flapping velocity of the wings is much higher than the free stream velocity (U >> u). Here β is a forces coefficient. Also note that f_d is the drag force for *both* of the flapping wings. Due to the fact the drag force is linear with respect to the free stream velocity, one can formulate a linear behaviour between the two;

$$\bar{f_d} = -2\beta u \tag{4.38}$$

The *dynamic model* used to model the flight dynamics of the DelFly Nimble is based on the standard equations of motions also used by previous work. Note that Karl only modelled the longitudinal dynamics and thus, a lateral dynamic model is not included in the thesis. The longitudinal equations are;

$$X = m(\dot{u} + qw) + mg_0 sin(\theta_0) \tag{4.39}$$
$$Z = m(\dot{w} - qu) - mg_0 cos(\theta_0) \tag{4.40}$$
$$M = \ddot{\theta} I_{yy} \tag{4.41}$$

where X, Z and M are the aerodynamic forces in X, Z direction and M the aerodynamic moment (or pitching moment) around the y-axis, respectively. Included in the model are the dihedral actuator states, which can potentially be valuable in future research. The states of the dihedral actuator can be used in the model to determine the effect on the aerodynamic forces during manoeuvres in flight. Dihedral actuator states are indicated by l_d and $\dot{l_d}$. Referring to Figure 4.2, the derived equations in the body axis are;

$$u_{COP} = u - l_z\dot{\theta} - \dot{l_d} \tag{4.42}$$
$$w_{COP} = w + (l_d + l_x)\dot{\theta} \tag{4.43}$$
$$X = -2b_x u_{COP} \tag{4.44}$$
$$Z = -2T - 2b_z w_{COP} \tag{4.45}$$
$$M = -Xl_z + Z(l_d + l_x) \tag{4.46}$$

where in equations of X and Z the factor 2 is incorporated to model the two wings. The terms b_x and b_z in the equations of X and Z are the aerodynamic force coefficients with respect to the air velocity component along the body axis x and z, respectively. The force coefficients are then obtained either from damped pendulum tests Teoh et al. (2012) or a wind tunnel tests. In this particular case, wind tunnel tests were performed to determine the coefficients b_x and b_z. Assuming zero accelerations in equations (4.39-4.40) and that in trimmed flight the term $qw = 0$, the value of X can be easily calculated (Equation 4.47);

$$X = mg_0 sin(\theta_0) \tag{4.47}$$

where the trimmed value of θ is the measured pitch angle. By substituting the values of X and Z form the equations of motion into equation 4.44 and 4.45, one can substitute the measured values of velocity and pitch angle to obtain the force coefficients in trimmed flight (b_x and b_z). In addition to the dynamic model of the body, further study includes models estimating the actuator dynamics, such as the flapping dynamics and dihedral dynamics represented in transfer functions. These transfer functions can be seen as individual tools to model the dynamics of the actuators of the DelFly Nimble. The models showed reasonable accurate results during the simulation phase. The full non-linear longitudinal model can be found in the thesis. In addition to K.M. Kajak's work, M. Karakeseks work (currently under review) Karasek (2018) gives a good overview on the performance of the DelFly Nimble based on aerodynamic models.
Additionally, the non-linear state derivatives used for the non-linear simulation were presented in the work of K.M. Kajak. By summing all the forces and moments (displayed in the free body diagram), using;

$$+\swarrow \sum F_{x,body} = m\dot{u} \tag{4.48}$$
$$+\nearrow \sum F_{z,body} = m\dot{w} \tag{4.49}$$
$$+(clockwise) \sum M_{y,body} = I_{yy}\ddot{\theta}. \tag{4.50}$$

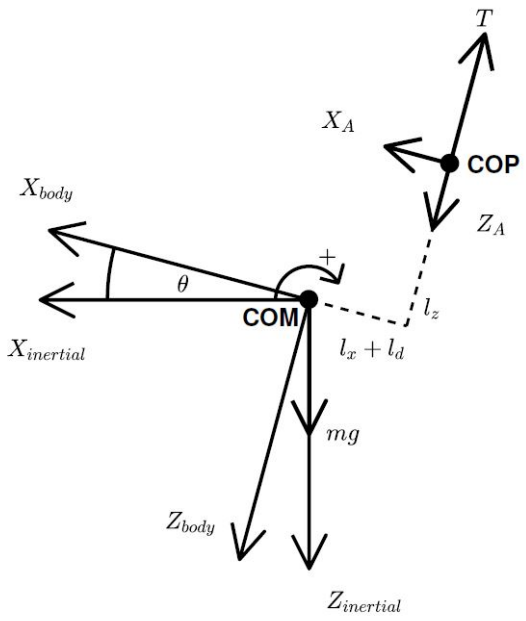

Figure 4.2: DelFly Nimble longitudinal free body diagram

From the free body diagram and using equations (4.48-4.50), the non-linear state derivatives can be derived (Equations 4.51-4.53);

$$\dot{u} = -gsin(\theta) - \frac{2b_x u}{m} + \frac{2l_z b_x \dot{\theta}}{m} + \frac{2b_x \dot{l}_p}{m} \tag{4.51}$$

$$\dot{w} = gcos(\theta) - \frac{2c_1 f}{m} - \frac{2c_2}{m} - \frac{2b_z w}{m} - \frac{2b_z(l_p + l_x)\dot{\theta}}{m} \tag{4.52}$$

$$\ddot{\theta} = [2b_x l_z u - 2b_x l_z^2 \dot{\theta} - 2b_x l_z \dot{l}_p - 2c_1 f(l_p + l_x) - 2c_2(l_p + l_x) - 2b_z w(l_p + l_x) - 2b_z(l_p + l_x)^2 \dot{\theta}]/I_{yy} \tag{4.53}$$

Identification of Time-Varying Models for Flapping-Wing Micro Aerial Vehicles

Armanini (2018)

Sophie Armanini makes use of cycle-averaged dynamics to model the flight dynamics of the DelFly II. Cycle-averaged means that, for example, the force produced by the flapping wings are averaged before being used in the model. First the EOM from a standard aircraft were used (linearised around a trim point). In addition to the EOM, a linear model structure was defined for each of the aerodynamic forces and moments that, based on previous work, suggest that linear models describe a significant part of the DelFly aerodynamics in slow forward flight Caetano, Remes, de Visser and Mulder (2013). In the linear model only measurable and physically plausible states were included resulting in the following equations (4.54-4.59);

$$X = X_q \Delta q + X_u \Delta u + X_w \Delta w + X_{\delta_e} \Delta \delta_e + mgsin(\theta_0) \tag{4.54}$$

$$Y = Y_p \Delta p + Y_r \Delta r + Y_v \Delta v + Y_{\delta_r} \Delta \delta_r \tag{4.55}$$

$$Z = Z_q \Delta q + Z_u \Delta u + Z_w \Delta w + Z_{\delta_e} \Delta \delta_e - mgcos(\theta_0) \tag{4.56}$$

$$L = L_p \Delta p + L_r \Delta r + L_v \Delta v + L_{\delta_r} \Delta \delta_r \tag{4.57}$$

$$M = M_q \Delta q + M_u \Delta u + M_w \Delta w + M_{\delta_e} \Delta \delta_e \tag{4.58}$$

$$N = N_p \Delta p + N_r \Delta r + N_v \Delta v + N_{\delta_r} \Delta \delta_r \tag{4.59}$$

The equations (4.54-4.59) are then substituted into the linearised EOM. Note, the $\Delta\delta_e$ and $\Delta\delta_r$ terms used indicates the use of an elevator and rudder for the DelFly II. However, the DelFly Nimble does not have a tail, as discussed earlier. So, instead of using the parameters of the horizontal control

surfaces, one could restructure the linear model such that it includes the dihedral deflections. This will be studied during this project. Returning to the model in this paper. To produce a state-space model structure, the EOM were linearised around a certain trim point followed by the substitution of equations (4.54-4.59) into the linearised EOM. The result of this process is a grey-box state-space model structure that describes the longitudinal and lateral cycle-averaged dynamics of the DelFly II. The longitudinal dynamics are;

$$\begin{bmatrix}\Delta\dot{q}\\ \Delta\dot{u}\\ \Delta\dot{w}\\ \Delta\dot{\theta}\end{bmatrix}=\begin{bmatrix}\frac{M_q}{I_{yy}} & \frac{M_u}{I_{yy}} & \frac{M_w}{I_{yy}} & 0\\ \frac{X_q}{m}-w_0 & \frac{X_u}{m} & \frac{X_w}{m} & -gcos(\theta_0)\\ \frac{Z_q}{m}-u_0 & \frac{Z_u}{m} & \frac{Z_w}{m} & -gsin(\theta_0)\\ 1 & 0 & 0 & 0\end{bmatrix}\begin{bmatrix}\Delta q\\ \Delta u\\ \Delta w\\ \Delta\theta\end{bmatrix}+\begin{bmatrix}\frac{M_{\delta_e}}{I_{yy}} & b_{\dot{q}}\\ \frac{X_{\delta_e}}{m} & b_{\dot{u}}\\ \frac{Z_{\delta_e}}{m} & b_{\dot{q}}\\ 0 & b_{\dot{\theta}}\end{bmatrix}\begin{bmatrix}\Delta\delta_e\\ 1\end{bmatrix}$$

and the lateral dynamics;

$$\begin{bmatrix}\Delta\dot{p}\\ \Delta\dot{r}\\ \Delta\dot{v}\\ \Delta\dot{\Phi}\end{bmatrix}=\begin{bmatrix}\frac{I_{zz}}{I_c}L_p+\frac{I_{xz}}{I_c}N_p & \frac{I_{zz}}{I_c}L_r+\frac{I_{xz}}{I_c}N_r & \frac{I_{zz}}{I_c}L_v+\frac{I_{xz}}{I_c}N_v & 0\\ \frac{I_{xz}}{I_c}L_p+\frac{I_{xx}}{I_c}N_p & \frac{I_{xz}}{I_c}L_r+\frac{I_{xx}}{I_c}N_r & \frac{I_{xz}}{I_c}L_v+\frac{I_{xx}}{I_c}N_v & 0\\ \frac{Y_p}{m}+w_0 & \frac{Y_r}{m}-u_0 & \frac{Y_v}{m} & gcos(\theta_0)\\ 1 & 0 & 0 & 0\end{bmatrix}\begin{bmatrix}\Delta p\\ \Delta r\\ \Delta v\\ \Delta\Phi\end{bmatrix}+\begin{bmatrix}\frac{I_{zz}}{I_c}L_{\delta_r}+\frac{I_{xz}}{I_c}N_{\delta_r} & b_{\dot{p}}\\ \frac{I_{xz}}{I_c}L_{\delta_r}+\frac{I_{xx}}{I_c}N_{\delta_r} & b_{\dot{r}}\\ \frac{Y_{\delta_r}}{m} & b_{\dot{v}}\\ 0 & b_{\dot{\Phi}}\end{bmatrix}\begin{bmatrix}\Delta\delta_r\\ 1\end{bmatrix}$$

where, $I_c = I_{xx}Izz - I_{xz}^2$. Note that the model also included the bias terms b subscript, to increase the precision of the model and filtering out dynamics not captured by the rest of the model. Measurements were performed using an optical tracking system called the OptiTrack Motion Capture System. Now the grey-box models are defined, the logical next step is to estimate the parameters, which are the unknown parameters in the state-space model. In this particular case, a maximum likelihood estimator (MLE) (using an output error approach) algorithm was used to estimate the unknown parameters in both the longitudinal- and lateral dynamic models. A study on parameter estimation techniques, such as the MLE, will be presented in the next section of this report.

5

Parameter Estimation Techniques

Another essential part of the system identification process is the estimation theory where the parameters, used in the state-space models or other model structures, need to be estimated. Klein Klein and Morelli (2006) and Ljung (1998) outline several theories that can be applied when dealing with parameter estimation problems. In this chapter we will discuss the most commonly applied optimization algorithms for system identification. The filter-error optimization algorithm allows for process noise (turbulence) to be present in the system. However, in this study, the assumption is made that the system to be identified is not subjected to process noise, or turbulence during free-flight tests. In the first four sections we will discuss output-errors methods such as the ordinary least squares (OLS) 5.1-, the weighted least squares (WLS) 5.2-, the generalized least squares (GLS) 5.3-, and the non-linear least squares (NLS) 5.3 methods. Finally, the working principles of the maximum likelihood estimation routine will be explained in section 5.5.
In general the parameter estimation process consists of the following steps:

1. Obtain state and measurement data.
2. Formulate the linear model structure, for example the general expression for a linear model structure (Equation 3.1).
3. By applying the theory on parameter estimation one is able to obtain the least squares estimator, in which the unknown parameters are estimated.
4. Evaluate and validate the results by comparing the output of the model with the actual measurements of the platform.

A model is linear in the parameter if the output y is given by;

$$y = H\theta \tag{5.1}$$

where H is the regression matrix which needs to be formulated during the process, θ the unknown parameters to be estimated and y the output from the model. The regression matrix contains the pre-assumed model structure defined in equation 3.1, is linear, has low computational complexity and is easy to implement as already mentioned in the sections above. The measurement equation is defined as (Equation 5.2);

$$z = H\theta + v \tag{5.2}$$

where z are the measurements and v the measurement noise or residual. Rearranging the the equation of z and solving for the residual v leads to equation 5.3;

$$v = z - H\theta \tag{5.3}$$

In order to estimate the parameter one needs a cost function in order to optimize for various estimators. Using the estimator for the Least-Squares Model the estimates for θ are realized by minimizing the

weighted sum of squared differences between the measured outputs and the model outputs (Equation 5.4),

$$J(\theta) = \frac{1}{2}(z - H\theta)^T R^{-1}(z - H\theta) \tag{5.4}$$

where R^{-1} is a weighting matrix, chosen by judgment. This means that one is able to change the weights in the matrix when one is under the assumption that certain measurements are unreliable and must not carry much weight during calculations. Equation 5.4 is also know as the weighted least-squares estimator (WLS) containing the matrix R. However, in the absence of the matrix R one obtains the ordinary least-squares (OLS) estimator (Equation 5.5), with cost function;

$$J(\theta) = \frac{1}{2}(z - H\theta)^T (z - H\theta) \tag{5.5}$$

When considering a set of measured data $z(i), i = 1, 2, ..., N$, the OLS estimator for a scalar measurement is obtained by minimizing equation 5.5 leading to;

$$J = \frac{1}{2}\sum_{n=1}^{N}[z(i) - H(i)\theta]^2 \tag{5.6}$$

which in matrix notation becomes (Equation 5.7);

$$J = v^T v = (z - H\theta)^T (z - H\theta) \tag{5.7}$$

Applying this method will be discussed later. In addition to the least-squares model, there are additional models available such as the Bayesian model and the Fisher model. However, since the least-squares model is an adequate estimator, the other models are not considered to be valuable to be studied any further.

Regression is a statistical technique for modelling and examining the relation between measured variables. An example for a linear in the parameter regression model is given here (Equation 5.8);

$$C_m = C_{m_0} + C_{m_\alpha}\alpha + C_{m_M}M + C_{m_{\alpha M}}\alpha M + v_m \tag{5.8}$$

In the equation α and M are the variables (or independent variables) that are measured where for each test point measurements of α, M and C_m are used as input into the linear model. In this particular model, the moment coefficient C_m depends on the variables α and M, where C_{m_0}, C_{m_α}, C_{m_M} and $C_{m_{\alpha M}}$ are constant model parameters to be estimated. It is assumed that the measurement errors of α and M are zero. However, the dependent variable C_m is subjected to random measurement error and thus the v_m term in the equation is included, which describes the random effects of measurement errors in the depended variable. Measurements on the dependent variable C_m can be obtained either by direct measurements from wind-tunnel experiments, or from other measurements using equation 5.9;

$$C_m = \frac{1}{\frac{1}{2}\rho V^2 Sb}[\dot{p}I_{xx} + qr(I_{zz} - I_{yy}) - (pq + \dot{r})I_{xz}] \tag{5.9}$$

where the measured variables are V, $\dot{p}$, $\dot{r}$, p, q and r which are obtained from air-data sensors, IMU sensor and/or other sensors. In addition to the linear parameter regression model, one can also include control surface deflections in the model since the moment coefficient is affected by elevator deflections. The general expression for the linear model structure (Equation 3.1) can be generalized into the following model form for relating the independent variables (Equation 5.10);

$$y = \theta_0 + \sum_{j=1}^{n}\theta_j\xi_j \tag{5.10}$$

where y is the dependent variable, ξ_j are linear or non-linear functions of the independent variables x_1, x_2,..., x_m, and the model parameters θ_0, θ_1, θ_2,..., θ_n quantify the influence of each term on the dependent variable y. Note that the terms ξ_j are functions of the independent variables $\xi_j \equiv$

$\xi_j(x_1, x_2, ..., x_m)$, where the independent variables are state measurements of the aircraft, such as α and the Mach number M for example. Most of the time the parameter constant θ_0 can be assumed to have a magnitude of 1, which will then model the bias in the dependent variable. Unfortunately the measured values of the dependent variable include random measurement noise such that;

$$z(i) = \theta_0 + \sum_{j=1}^{n} \theta_j \xi_j(i) + v(i) \quad i = 1, 2, ..., N \tag{5.11}$$

where $z(i)$ are the output measurements and N the number of data points obtained during flight, and where $\xi_j(i)$ depends on the the m-number of independent variables x_1, x_2,..., x_m at the i^{th} data point. Equation 5.11 is called the regression equation, similar to the one in equation 3.1. In equation 5.11 v is defined as the equation error. When applying the parameter estimation theory described above, and using the least-squares model, one can obtain the unknown parameter model parameters θ. The objective is to find and estimate $\hat{\theta}$ of the parameter vector $\theta^T = [\theta_0 \quad \theta_1 \quad ... \quad \theta_n]$ using the parameter estimation theory. However, choosing a appropriate or adequate model structure is a different problem and will therefore be discussed later. In general an adequate model is not always know beforehand and therefore must be identified from the measured data and applying a model structure determination process.

5.1. Ordinary Least Squares

Moving on to the process of determining the vector $\theta^T = [\theta_0 \quad \theta_1 \quad ... \quad \theta_n]$. In matrix form the equation from the section above (Equation 5.10), can be written as;

$$y = X\theta \tag{5.12}$$

,and the equation of the measurements as;

$$z = X\theta + v \tag{5.13}$$

where

$$z = [z(1) \quad z(2) \quad ... \quad z(N)]^T = N \times 1 \quad vector \quad N \quad measurements$$
$$\theta = [\theta_0 \quad \theta_1 \quad ... \quad \theta_n]^T = n_p \times 1 \quad vector \quad of \quad unknown \quad parameters, \quad n_p = n + 1$$
$$X = [1 \quad \xi_1 \quad ... \quad \xi_n] = N \times n_p \quad matrix \quad of \quad vectors \quad of \quad ones \quad and \quad regressors$$
$$v = [v(1) \quad v(2) \quad ... \quad v(N)]^T = N \times 1 \quad vector \quad of \quad measurement \quad errors$$

Note that in the equations (5.1-5.7) the H matrix contain the regressors. However, from now the regression matrices will be denoted by X. The best estimator for θ, using the least-squares principle, is obtained by minimizing the sum of squared differences between the measurements and the model, hence, Least-Squares Parameter Estimation. Here the best estimator can be obtained by minimizing the well know cost function;

$$J(\theta) = \frac{1}{2}(\mathbf{z} - \mathbf{X}\theta)^T(\mathbf{z} - \mathbf{X}\theta) \tag{5.14}$$

wherein the function is subsequently minimized using the following equation;

$$\frac{\partial J}{\partial \theta} = 0 \tag{5.15}$$

The parameter estimate $\hat{\theta}$ that minimizes the cost function must satisfy;

$$\frac{\partial J}{\partial \theta} = -\mathbf{X}^T\mathbf{z} + \mathbf{X}^T\mathbf{X}\hat{\theta} = \mathbf{0} \tag{5.16}$$

rewriting the equation leads to;

$$\mathbf{X}^T\mathbf{X}\hat{\theta} = \mathbf{X}^T\mathbf{z} \tag{5.17}$$

Further rewriting the equation results in the least-squares estimator;

$$\hat{\theta} = (\mathbf{X}^T\mathbf{X})^{-1}\mathbf{X}^T\mathbf{z} \tag{5.18}$$

Not only the parameter estimation can be obtained using this equation, but the equation itself also includes valuable information regarding the variances of the estimated parameters, which is called the covariance matrix of the parameter estimate θ.

$$Cov(\hat{\theta}) = \sigma^2(\mathbf{X}^T\mathbf{X})^{-1} \tag{5.19}$$

where σ^2 is the constant variance, which basically is a scaling factor which scales the covariance matrix. Due to the fact it is a scaling factor, excluding the constant σ^2 from the calculations will not affect the information regarding the variance of the corresponding parameters in the covariance matrix.

5.2. Weighted Least Squares

If the information regarding the sensor noise is available then one is able to construct the Weighted Least-Squares (WLS) Estimator, which takes the standard deviations of the sensor noise into account. The main advantage of the WLS Estimator is that it is possible to assign a lower value to the measurements which show less variance, meaning that the estimator will base the model more on the measurements containing less variance then the measurements containing much variance. Focusing on the matrix R in equation 5.4;

$$R = diag(\sigma_1^2 \quad \sigma_2^2 \quad ... \quad \sigma_N^2) \tag{5.20}$$

which is a diagonal matrix. Applying the same procedure as with the OLS, then after some substitutions and rearranging the Weighted Least-Squares Estimator can be formulated as;

$$\hat{\theta}_{WLS} = (\mathbf{X}^T\mathbf{W}^{-1}\mathbf{X})^{-1}\mathbf{X}^T\mathbf{z} \tag{5.21}$$

The WLS Estimator is very useful when the measurements of the real system output show high variance and one is in the possession of the sensor noise.

5.3. Generalized Least Squares

For the OLS Estimator case the assumption is made that the measurements errors have zero mean, and are uncorrelated with equal variance. If this does not hold one is forced to use the Generalized Least-Squares (GLS) Estimator which takes the correlation among the measurements into account.

5.4. Non-Linear Least Squares

Note that the least squares estimator, described in the sections above, only is useful when the model structure is linear. However, in some case it could be that the relationship between the regressors and the response variable (for example the aerodynamic force X) is non-linear in the parameter Klein and Morelli (2006). For this particular case the least squares model must be formulated as;

$$\mathbf{z} = \mathbf{h}(\theta) + \mathbf{v} \tag{5.22}$$

which is equivalent to a non-linear regression model;

$$z(i) = f[\mathbf{x}(\mathbf{i}), \theta] + \mathbf{v}(i) \quad i = 1, 2, ..., N \tag{5.23}$$

where $\mathbf{x}^T(i)$ is a row vector of regressors computed from measured data at the i^{th} data point, f is a non-linear function of $\mathbf{x}(i)$, and the parameters in the vector are denoted by θ. Now in order to to obtain the least squares estimator one must minimize the sum of squared errors by applying the well-known cost function (Equation 5.24);

$$J(\theta) = \frac{1}{2}\sum_{i=1}^{N}(\mathbf{z}(i) - f[\mathbf{x}(i), \theta])^2 \tag{5.24}$$

The minimum of the cost function is then found by satisfying the normal equations (Equation 5.25);

$$\left.\frac{\partial J}{\partial \theta}\right|_{\theta=\hat{\theta}} = -\sum_{i=1}^{N}(\mathbf{z}(i) - f[\mathbf{x}(i), \hat{\theta}])\left.\frac{\partial f[\mathbf{x}(i), \hat{\theta}]}{\partial \theta}\right|_{\theta=\hat{\theta}} = 0 \tag{5.25}$$

where $\partial J/\partial\theta$ is a row vector containing the partial derivatives of the non-linear scalar function $J(\theta)$ with respect to the elements of θ, and $\frac{\partial f[\mathbf{x}(i),\hat{\theta}]}{\partial\theta}$ is a row vector of output sensitivities to changes in the model parameters. Note that $\hat{\theta}$ can only be obtained by an iterative non-linear optimization technique such as the maximum likelihood estimation technique Klein and Morelli (2006). This technique will be discussed in greater detail in the next section.

5.5. Maximum Likelihood Estimation

From the study on existing FWMAVs it is clear that both the OLS estimator and the Maximum Likelihood Estimator are good tools to determine the unknown parameters of a system. In the case where the measurements are a non-linear function of the parameters, a maximum likelihood estimator is typically used. In general, model parameter estimates are found by maximizing a likelihood function, which involves minimizing the weighted least-squares difference between measured outputs and model outputs. This non-linear estimator is required because of the non-linear connection between model parameters and model outputs. The maximum likelihood usually includes the use of a state estimator, or Kalman Filter, which purpose is to estimates the states as accurately as possible. The state estimator is necessary because of the presence of process noise in the dynamic equations, which means that the states are random variables. If however, measurements contain little to no process noise, a MLE can be used without the use of a state estimator Klein and Morelli (2006).

Maximum Likelihood estimation is based on probabilistic principles. The cost function relating the inputs and the outputs is an expression for the probability of an observation occurring given particular values of the system parameters, and the aim is thus to determine the parameter values that maximize the probability of the measured input having led to the measured output. This results in a non-linear optimization problem involving an iterative adjustment of the model parameters to minimize the difference between measured and model-predicted system outputs Armanini, de Visser and de Croon (2015). The MLE used in the papers studied so far is also known as the output error method (OEM), which takes the measurement errors into account but not the process noise. Therefore, if process noise is present, the measured states must be pre-processed using a Kalman Filter to remove this process noise first. When pre-processing is performed the first step of the estimation process is to set-up the cost function. The cost function for this problem can be defined as the negative logarithm of the likelihood function expressing the probability p of an observation $\mathbf{z}$ occurring at a particular time point k, given the parameter vector Θ;

$$J(\Theta, R) = -lnp(\mathbf{z}|\Theta) = \frac{1}{2}\sum_{k=1}^{n_k}[\mathbf{z}(k) - \mathbf{y}(k)]^T\mathbf{R}^{-1}[\mathbf{z}(k) - \mathbf{y}(k)] + \frac{n_k}{2}ln[det(\mathbf{R})] + \frac{n_k n_y}{2}ln(2\pi) \tag{5.26}$$

where $\mathbf{R}$ is the measurement noise covariance matrix, n_k the number of data samples, n_y the number of output variables measured, and $\mathbf{z}(k)$ and $\mathbf{y}(k)$ are the measured and model-predicted outputs, respectively at time point k. The schematic of the output-error method is displayed in Figure 5.1.
The error covariance matrix $\mathbf{R}$ needs to estimated separately from the measurements and initial parameters guess at the start of each iteration step. After the first iteration step, the next iteration will contain the parameters from the previous estimation step. $\mathbf{R}$ is obtained by partial differentiation of equation (5.26) with respect to $\mathbf{R}$ and setting it equal to zero, where the calculated $\mathbf{R}$ is given by;

$$\hat{\mathbf{R}} = \frac{1}{N}\sum_{k=1}^{N}[\mathbf{z}(k) - \mathbf{y}(k)][\mathbf{z}(k) - \mathbf{y}(k)]^T \tag{5.27}$$

The next step is to substitute equation (5.27) into equation (5.26) when having obtained a maximum likelihood estimate of $\mathbf{R}$;

$$J(\Theta) = \frac{1}{2} n_y N + \frac{N}{2} ln[det(\mathbf{R})] + \frac{N n_y}{2} ln(2\pi) \tag{5.28}$$

Since the first and last term of equation (5.28) are constants, they can be neglected without affecting the minimization result. Thus, the cost function is reduced to;

$$J(\Theta) = det(\mathbf{R}) \tag{5.29}$$

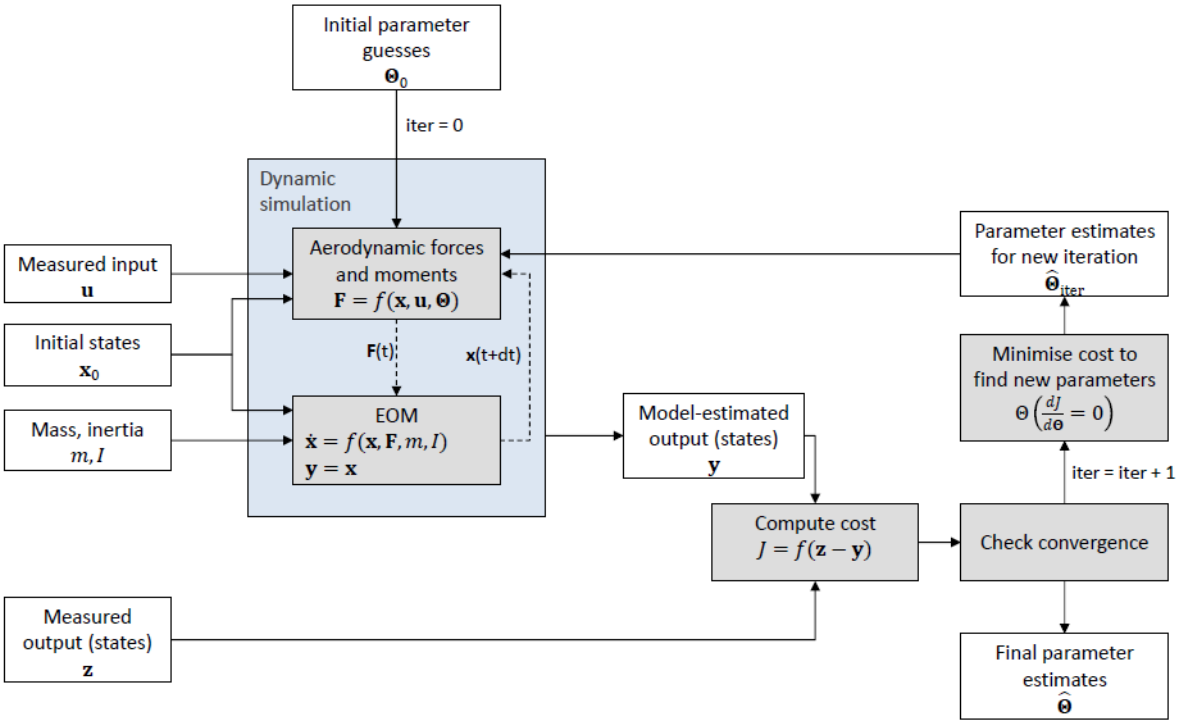

Figure 5.1: Schematic Parameter Estimation: Output-Error Approach. *Source: Armanini (2018)*

The last step is to to estimate a new set of parameters for the next iteration (iter = iter + 1) step. For this step equation (5.26) must be considered again. Note that now the last two terms of this equation are constants. When minimizing this equation with respect to the parameter vector (partial derivative with respect to Θ) leads to the following cost function;

$$J(\Theta) = \frac{1}{2} \sum_{k=1}^{N} [\mathbf{z}(k) - \mathbf{y}(k)]^T \mathbf{R}^{-1} [\mathbf{z}(k) - \mathbf{y}(k)] \tag{5.30}$$

In order to determine a new set of parameters, equation (5.30) is minimized by applying the Gauss-Newton technique Jategaonkar (2015), where the parameter estimates for the new iteration is calculated by;

$$\Delta\Theta = -[(\frac{\partial^2 J}{\partial \Theta^2})_i]^{-1} (\frac{\partial J}{\partial \Theta})_i \tag{5.31}$$

and then finally the parameter estimates for the new iteration becomes;

$$\Theta_{i+1} = \Theta_i + \Delta\Theta \tag{5.32}$$

6

Close-Loop System Identification

Some platforms are designed to be open-loop unstable without using any form of feedback control, such as the DelFly Nimble. These platforms are inherently unstable and are stabilized using automatic closed-loop feedback control. Due to the automatic feedback control any input given to the system (reference input) by the pilot, or directly at the control surface actuator by a computerized system, will be distorted by the feedback control which greatly influences the possibility to perform system identification on the platform. During dynamic modelling the objective is to excite the natural motions of the system at hand as much as possible which is done by performing specially designed manoeuvres during the flight test. If the platform is inherently stable, then the system does not require any automatic feedback control, which means the state response of the system is not affected by any feedback control and, as a result, outputs it natural motion. The problem with system identification on closed-loop automatic feedback systems is that excitation of the platform is seen by the feedback system as a disturbance that should be damped out. But the rejection of response of the system is undesirable, since it destroys, or damps out, the natural motion of the system. Measurements of the natural motion are of great importance during the identification phase, because the natural motion contain informative data. In order to still obtain informative one can do two things:

1. Reduce the feedback gains of the control system as much as possible such that the natural motions of the platform are excited as much as possible.

2. Perform aggressive manoeuvres on the platform that excite the system as much as possible. The selection of the most effective manoeuvre will be the result of trail and error flight testing, or based on theoretical analysis. Some aggressive manoeuvres are directly damped, while other manoeuvres are not aggressively damped by the system.

As Vladislav Klein and Eugene A. Morelli explain, system identification and parameter estimation can be perfectly performed using the theory described above (Parameter estimation- and Ordinary least-squares method) Klein and Morelli (2006). This means that closed-loop system identification is perfectly possible when applied to the DelFly Nimble. The main challenges are exciting the platform properly enough, or aggressively, by manoeuvres in order to obtain informative data fit for system identification. These manoeuvres will be selected based on flight tests performed during this project and other projects.

Note that there are two ways to perform system identification on closed-loop systems:

- Using the theory and steps of Vladislav Klein and Eugene A. Morelli and include the actuator deflections and other states, such as the pitch rate, in the linear regression model. Doing so, the effects of the actuator deflections and pitch rate on the aerodynamic forces and moments can be modelled. Vladislav Klein and Eugene A. Morelli use an example of an inherently unstable fighter aircraft, which is made stable using automatic feedback control. The deflections from the control surfaces were measured and are included in the linear regression model. However, it is worthy to note that this approach only works when the control deflections of the control

surfaces can be measured (in degrees or radians). Luckily this is possible since K.M. Kajak Kajak (2018) was already successful in measuring the control deflections of the dihedral actuator. In **Block-Diagram 1** a system in closed-loop is indicated which resembles a simplified version of the DelFly Nimble's closed-loop automatic feedback control system. Using Vladislav Klein and Eugene A. Morelli approach one is only interested in the output y and the input δ of the system. When these two are know, then it is possible to apply Vladislav Klein's approach in order to perform system identification.

- The problem will get a lot more complicated when the control surface deflections are not measurable. If this is the case one is forced to consult the theory and methods of Lennart Ljung Ljung (1998) which focusses on system identification when δ is unknown, but only u and e are known, seen in **diagram 1**. Due to to the fact the actuator deflections of the DelFly Nimble are considered to be measurable, it will be unnecessary to study Lennart Ljung methods any further.

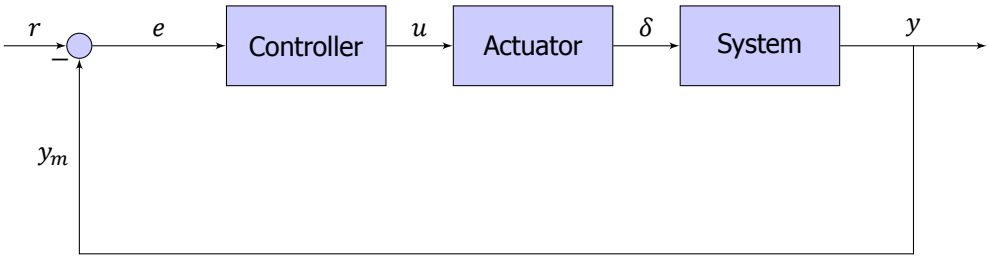

Block-Diagram 1: Closed-loop automatic feedback system

7

Conclusions and Limitations

In this section the goal is to highlight the advantages and disadvantages of the models and approaches used in previous studies when reflecting them to the DelFly Nimble.

In the paper by J.V. Caetano, C.C. de Visser Caetano, De Visser, De Croon, Remes, De Wagter, Verboom and Mulder (2013), use was made of non-linear EOM in order to describe the dynamics of the platform. From the EOM the aerodynamic forces and moments acting on the platform are then computed. The computed aerodynamic- forces and moments are then used as input for the left side of equations (4.3-4.8) together with the pre-processed states on the right side of the equation. Since the aerodynamic model structure is linear, it is relatively easy to compute the unknown parameters using an ordinary least squares (OLS) estimator. A major disadvantage of this modelling process, is that the aerodynamic model of the moments is not accurately enough for non-linear simulation. This modelling technique can be of great use when applied to the DelFly Nimble. However, problems may arise when applying non-linear simulation to the estimated models. It should be noted that data was gathered at 0.25 [m/s] forward speed, which could mean that the estimated models are only applicable for this particular flight regime.

The paper by Sophie F. Armanini and Coen C. de Visser Armanini, de Visser and de Croon (2015) uses a same approach as described in the previous paper. The 'black-box' modelling process will not give any insight into the physics of the platform. This particular modelling process however mainly differs in the fact that no aerodynamic model structure (no a priori knowledge of the systems physics) is used, where usually the parameters in the aerodynamic model are estimated. The 'black-box' modelling process will not give any insight into the physics of the platform. Since it is desirable to somehow retain a physical connection in the model structure, this black-box modelling process is considered to be insufficient when applied to the DelFly Nimble.

Other modelling approaches, like the ones from Z.E. Teoh Teoh et al. (2012) and K.M. Kajak Kajak (2018) make use of theoretical derived models, also called 'white-box', where the unknown parameter are estimated using experimental data. Note that the parameters of these non-linear models are, in general, difficult to estimate. Z.E. Teoh for example used the Routh-Hurwits criterion to determine the region of the parameters for which the system is stable.

The modelling method described by Sophie Armanini Armanini (2018) is a so-called 'grey-box' modelling method. The grey-box model combines best of both worlds, which means that less knowledge of the system dynamics is required compared to the white-box modelling method, which requires full knowledge of the system dynamics, in order to produce accurate results. Sophie Armanini used a linear aerodynamic model structure containing states that are measurable and physically plausible. The linear aerodynamic equations used are then substituted into the linearised EOM (linearised around a particular trim point) and then represented in a state-space model. This model is linear, therefore making it simple and computationally efficient for simulation, controller design and stability analysis. All the unknown parameters in the state-space model are then estimated using a maximum likelihood

estimator. The result is a local grey-box time-averaged model. Given the fact that this modelling process produces accurate results, it is computational efficient, gives insight into the physical behaviour of the platform and can be applied to inherently unstable platforms, it is considered to be one of the best approaches to produce models of the DelFly Nimble that describe its flight dynamics, while still maintaining a meaningful physical connection.

The unknown parameters in the models are estimated using several parameters estimation techniques. If the models structure is linear, then an ordinary least squared (OLS) estimation procedure is usually selected. A disadvantage of using a linear model structure is that in some cases the relationship between the regressors and the response variable is non-linear in the parameter. In that case a non-linear model must be used. When the model structure is non-linear, a non-linear least squares algorithm must be used in order to determine the parameters. The optimal estimate of the parameters can then be only obtained using a maximum likelihood estimation (MLE) algorithm. This process is more computational complex compared to the OLS estimation technique Klein and Morelli (2006).

In addition, before starting the system identification process of the DelFly Nimble, it is important to map out the limitations and challenges that could be encountered during this project. In the first place, due to the small size of the DelFly Nimble the accommodation of sensors is very limited. Integration of accurate GPS-receivers are Air-data sensors, that can measure the states of the platform, is difficult. On the other hand, other sensors are available that are able to accurately measure the states required for system identification. Examples of the available sensors are on-board IMU sensors and Opti-Track sensors. However, there are some limitations when using these sensors:

1. When using the IMU in combination with the OptiTrack system the available measurement space is very limited due to the measuring area of the OptiTrack system (around a maximum of 10 x 10 x 3 meters). This means that the limited space will probably cause some difficulties when performing flights tests.
2. When using only the IMU, the measurements are subjected to drift errors which can influence the accuracy of the measured states Armanini (2018).
3. Due to the fact the DelFly Nimble is a fragile platform, aggressive manoeuvres required for identification could potentially damage the platform and/or decrease the accuracy of the measurements.

Bibliography

Armanini, S. (2018), 'Identification of time-varying models for flapping-wing micro aerial vehicles'.

Armanini, S., de Visser, C., de Croon, G. and Mulder, M. (2015), 'Time-varying model identification of flapping-wing vehicle dynamics using flight data', *Journal of Guidance, Control, and Dynamics* **38**(12), 526–541.

Armanini, S. F., de Visser, C. C. and de Croon, G. (2015), Black-box lti modelling of flapping-wing micro aerial vehicle dynamics, *in* 'AIAA Atmospheric Flight Mechanics Conference', p. 0234.

Caetano, J., Armanini, S., de Visser, C., de Croon, G. and Mulder, M. (2015), Data-informed quasi-steady aerodynamic model of a clap-and-fling flapping wing mav, *in* 'Bali, Indonesia), International Conference on Unmanned Intelligent Systems (ICIUS)'.

Caetano, J. V., De Visser, C., De Croon, G., Remes, B., De Wagter, C., Verboom, J. and Mulder, M. (2013), 'Linear aerodynamic model identification of a flapping wing mav based on flight test data', *International Journal of Micro Air Vehicles* **5**(4), 273–286.

Caetano, J. V., Remes, B. D., de Visser, C. C. and Mulder, M. (2013), Modeling a flapping wing mav: Flight path reconstruction of the delfly ii, *in* 'AIAA Modeling and Simulation Technologies (MST) Conference', p. 4597.

Chand, A. N., Kawanishi, M. and Narikiyo, T. (2015), Parameter estimation for the pitching dynamics of a flapping-wing flying robot, *in* 'Advanced Intelligent Mechatronics (AIM), 2015 IEEE International Conference on', IEEE, pp. 1552–1558.

Cheng, B., Deng, X. and Hedrick, T. L. (2011), 'The mechanics and control of pitching manoeuvres in a freely flying hawkmoth (manduca sexta)', *Journal of Experimental Biology* **214**(24), 4092–4106.

Dietl, J., Herrmann, T., Reich, G. and Garcia, E. (2011), 'Dynamic modeling, testing, and stability analysis of an ornithoptic blimp', *Journal of Bionic Engineering* **8**(4), 375–386.

Dietl, J. M. and Garcia, E. (2008), 'Stability in ornithopter longitudinal flight dynamics', *Journal of Guidance, Control, and Dynamics* **31**(4), 1157–1163.

Faruque, I. and Humbert, J. S. (2010), 'Dipteran insect flight dynamics. part 1 longitudinal motion about hover', *Journal of theoretical biology* **264**(2), 538–552.

Gebert, G., Gallmeier, P. and Evers, J. (2002), Equations of motion for flapping flight, *in* 'AIAA Atmospheric Flight Mechanics Conference and Exhibit', p. 4872.

Gim, H., Kim, S., Suk, J. and Cho, S. (2016), 'Longitudinal system identification of ornithopter with automated flight tests', *IFAC-PapersOnLine* **49**(17), 194–199.

Grauer, J., Ulrich, E., Hubbard, J. E., Pines, D. and Humbert, J. S. (2011), 'Testing and system identification of an ornithopter in longitudinal flight', *Journal of Aircraft* **48**(2), 660–667.

J.A. Mulder, W.H.J.J. van Staveren, J. v. d. V. C. d. V. (2013), *Flight Dynamics*, Delft University of Technology, Delft.

Jategaonkar, R. V. (2015), *Flight vehicle system identification: a time-domain methodology*, American Institute of Aeronautics and Astronautics, Inc.

Kajak, K. (2018), 'A minimal longitudinal dynamic modelof a tailless flapping wing robot'.

Karasek, M. (2018), 'A bio-inspired free-flying robot reveals that flies use torque coupling in rapid banked turns'.

Keennon, M., Klingebiel, K. and Won, H. (2012), Development of the nano hummingbird: A tailless flapping wing micro air vehicle, *in* '50th AIAA aerospace sciences meeting including the new horizons forum and aerospace exposition', p. 588.

Klein, V. and Batterson, J. G. (1983), 'Determination of airplane model structure from flight data using splines and stepwise regression'.

Klein, V. and Morelli, E. A. (2006), *Aircraft system identification: theory and practice*, American Institute of aeronautics and astronautics Reston, VA.

Ljung, L. (1998), System identification, *in* 'Signal analysis and prediction', Springer, pp. 163–173.

Ma, K. Y., Chirarattananon, P., Fuller, S. B. and Wood, R. J. (2013), 'Controlled flight of a biologically inspired, insect-scale robot', *Science* **340**(6132), 603–607.

Organization, N. A. T., Mulder, J., Sridhar, J. and Breeman, J. (1994), *Identification of Dynamic Systems: Applications to Aircraft, Part 2, Nonlinear Analysis and Manoeuvre Design*.

Ramezani, A., Chung, S.-J. and Hutchinson, S. (2017), 'A biomimetic robotic platform to study flight specializations of bats', *Science Robotics* **2**(3), Art–No.

Roshanbin, A., Altartouri, H., Karásek, M. and Preumont, A. (2017), 'Colibri: A hovering flapping twin-wing robot', *International Journal of Micro Air Vehicles* **9**(4), 270–282.

Sane, S. P. and Dickinson, M. H. (2002), 'The aerodynamic effects of wing rotation and a revised quasi-steady model of flapping flight', *Journal of experimental biology* **205**(8), 1087–1096.

Sibilski, K., Loroch, L., Buler, W. and Zyluk, A. (2004), Modeling and simulation of the nonlinear dynamic behavior of a flapping wings micro-aerial-vehicle, *in* '42nd AIAA Aerospace Sciences Meeting and Exhibit', p. 541.

Sun, M. and Xiong, Y. (2005), 'Dynamic flight stability of a hovering bumblebee', *Journal of experimental biology* **208**(3), 447–459.

Taha, H. E., Hajj, M. R. and Nayfeh, A. H. (2014), 'Longitudinal flight dynamics of hovering mavs/insects', *Journal of Guidance, Control, and Dynamics* **37**(3), 970–979.

Taylor, G., Bomphrey, R. and 't Hoen, J. (2006), Insect flight dynamics and control, *in* '44th AIAA Aerospace Sciences Meeting and Exhibit', p. 32.

Teoh, Z. E., Fuller, S. B., Chirarattananon, P., Prez-Arancibia, N., Greenberg, J. D. and Wood, R. J. (2012), A hovering flapping-wing microrobot with altitude control and passive upright stability, *in* 'Intelligent Robots and Systems (IROS), 2012 IEEE/RSJ International Conference on', IEEE, pp. 3209–3216.

The aerodynamics of hovering insect flight. I. The quasi-steady analysis (1984), *Philosophical Transactions of the Royal Society of London B: Biological Sciences* **305**(1122), 1–15.
URL: *http://rstb.royalsocietypublishing.org/content/305/1122/1*

A

Estimated Parameters

All the estimated parameter from the time-average linear longitudinal grey-box models are reported in this section including the mean error of the markers from the OptiTrack system. The datasets are organized in numbers and steady-state flight condition, ranging from 1 to 18, and are displayed in table A.1.

Datasets #1-#4	0.0 m/s (hover condition)
Datasets #5-#9	0.5 ±0.05 m/s
Datasets #10-#13	0.75 ±0.05 m/s
Datasets #14-#18	1.0 ±0.05 m/s

Table A.1: Datasets with corresponding steady-state condition.

Table A.2: Dataset #1. Mean markers error: 1.1363e-03[m]

$$\begin{pmatrix} X_q \\ X_u \\ X_w \\ X_{\delta_D} \\ Z_q \\ Z_u \\ Z_w \\ Z_{\delta_D} \\ M_q \\ M_u \\ M_w \\ M_{\delta_D} \end{pmatrix} = \begin{pmatrix} 0.0041 \\ -0.1011 \\ 0.008852 \\ 0.7218 \\ -0.005641 \\ 0.01959 \\ -0.00586 \\ 0.2982 \\ -0.001907 \\ 0.01943 \\ -0.001928 \\ 0.2782 \end{pmatrix}$$

Table A.3: Dataset #2. Mean markers error: 8.9819e-04[m]

$$\begin{pmatrix} X_q \\ X_u \\ X_w \\ X_{\delta_D} \\ Z_q \\ Z_u \\ Z_w \\ Z_{\delta_D} \\ M_q \\ M_u \\ M_w \\ M_{\delta_D} \end{pmatrix} = \begin{pmatrix} 0.01422 \\ -0.1184 \\ 0.007849 \\ 0.4572 \\ -0.002814 \\ 0.02107 \\ -0.003448 \\ 0.2033 \\ -0.001482 \\ 0.01796 \\ -0.001316 \\ 0.1997 \end{pmatrix}$$

Table A.4: Dataset #3. Mean markers error: 1.1123e-03[m]

$$\begin{pmatrix} X_q \\ X_u \\ X_w \\ X_{\delta_D} \\ Z_q \\ Z_u \\ Z_w \\ Z_{\delta_D} \\ M_q \\ M_u \\ M_w \\ M_{\delta_D} \end{pmatrix} = \begin{pmatrix} 0.008405 \\ -0.1038 \\ 0.02339 \\ 0.5167 \\ 0.01114 \\ -0.007934 \\ -0.003772 \\ 0.09665 \\ -0.001727 \\ 0.01788 \\ -0.001561 \\ 0.2034 \end{pmatrix}$$

Table A.5: Dataset #4. Mean markers error: 1.2645e-03[m]

$$\begin{pmatrix} X_q \\ X_u \\ X_w \\ X_{\delta_D} \\ Z_q \\ Z_u \\ Z_w \\ Z_{\delta_D} \\ M_q \\ M_u \\ M_w \\ M_{\delta_D} \end{pmatrix} = \begin{pmatrix} 0.001202 \\ -0.1086 \\ 0.01738 \\ 0.5276 \\ 0.001187 \\ 0.003337 \\ -0.005413 \\ 0.1887 \\ -0.001791 \\ 0.01772 \\ -1.035\,10^{-5} \\ 0.2171 \end{pmatrix}$$

Table A.6: Dataset #5. Mean markers error: 8.3496e-04[m]

$$\begin{pmatrix} X_q \\ X_u \\ X_w \\ X_{\delta_D} \\ Z_q \\ Z_u \\ Z_w \\ Z_{\delta_D} \\ M_q \\ M_u \\ M_w \\ M_{\delta_D} \end{pmatrix} = \begin{pmatrix} 0.003343 \\ -0.0752 \\ 0.03232 \\ 0.5591 \\ -0.002398 \\ 0.04696 \\ -0.009413 \\ 0.1817 \\ -0.001967 \\ 0.02373 \\ -0.0009669 \\ 0.2017 \end{pmatrix}$$

Table A.7: Dataset #6. Mean markers error: 8.4546e-04[m]

$$\begin{pmatrix} X_q \\ X_u \\ X_w \\ X_{\delta_D} \\ Z_q \\ Z_u \\ Z_w \\ Z_{\delta_D} \\ M_q \\ M_u \\ M_w \\ M_{\delta_D} \end{pmatrix} = \begin{pmatrix} 0.01184 \\ -0.08243 \\ 0.0303 \\ 0.6005 \\ 0.005465 \\ 0.02141 \\ -0.003029 \\ 0.1055 \\ -0.001883 \\ 0.02583 \\ -0.002138 \\ 0.2277 \end{pmatrix}$$

Table A.8: Dataset #7. Mean markers error: 5.3589e-04[m]

$$\begin{pmatrix} X_q \\ X_u \\ X_w \\ X_{\delta_D} \\ Z_q \\ Z_u \\ Z_w \\ Z_{\delta_D} \\ M_q \\ M_u \\ M_w \\ M_{\delta_D} \end{pmatrix} = \begin{pmatrix} 0.001109 \\ -0.08488 \\ 0.02876 \\ 0.5539 \\ -0.007355 \\ 0.04097 \\ -0.01274 \\ 0.181 \\ -0.002179 \\ 0.02182 \\ -0.003911 \\ 0.2022 \end{pmatrix}$$

Table A.9: Dataset #8. Mean markers error: 5.8097e-04[m]

$$\begin{pmatrix} X_q \\ X_u \\ X_w \\ X_{\delta_D} \\ Z_q \\ Z_u \\ Z_w \\ Z_{\delta_D} \\ M_q \\ M_u \\ M_w \\ M_{\delta_D} \end{pmatrix} = \begin{pmatrix} 0.008314 \\ -0.06851 \\ 0.02875 \\ 0.6968 \\ -0.002372 \\ 0.03343 \\ -0.01162 \\ 0.2302 \\ -0.002247 \\ 0.02705 \\ -0.001448 \\ 0.2609 \end{pmatrix}$$

Table A.10: Dataset #9. Mean markers error: 6.0081e-04[m]

$$\begin{pmatrix} X_q \\ X_u \\ X_w \\ X_{\delta_D} \\ Z_q \\ Z_u \\ Z_w \\ Z_{\delta_D} \\ M_q \\ M_u \\ M_w \\ M_{\delta_D} \end{pmatrix} = \begin{pmatrix} 0.007877 \\ -0.07165 \\ 0.02537 \\ 0.7725 \\ -0.0106 \\ 0.04753 \\ -0.01563 \\ 0.2764 \\ -0.00215 \\ 0.02674 \\ -0.00306 \\ 0.2762 \end{pmatrix}$$

Table A.11: Dataset #10. Mean markers error: 5.7269e-04[m]

$$\begin{pmatrix} X_q \\ X_u \\ X_w \\ X_{\delta_D} \\ Z_q \\ Z_u \\ Z_w \\ Z_{\delta_D} \\ M_q \\ M_u \\ M_w \\ M_{\delta_D} \end{pmatrix} = \begin{pmatrix} 0.01018 \\ -0.08534 \\ 0.02167 \\ 0.5346 \\ -0.004967 \\ 0.03995 \\ -0.0114 \\ 0.1552 \\ -0.001388 \\ 0.02312 \\ -0.003551 \\ 0.2013 \end{pmatrix}$$

Table A.12: Dataset #11. Mean markers error: 5.6801e-04[m]

$$\begin{pmatrix} X_q \\ X_u \\ X_w \\ X_{\delta_D} \\ Z_q \\ Z_u \\ Z_w \\ Z_{\delta_D} \\ M_q \\ M_u \\ M_w \\ M_{\delta_D} \end{pmatrix} = \begin{pmatrix} 0.0114 \\ -0.0593 \\ 0.02108 \\ 0.6044 \\ -0.01281 \\ 0.06121 \\ -0.01442 \\ 0.2281 \\ -0.001589 \\ 0.02838 \\ -0.004016 \\ 0.2256 \end{pmatrix}$$

Table A.13: Dataset #12. Mean markers error: 6.1194e-04[m]

$$\begin{pmatrix} X_q \\ X_u \\ X_w \\ X_{\delta_D} \\ Z_q \\ Z_u \\ Z_w \\ Z_{\delta_D} \\ M_q \\ M_u \\ M_w \\ M_{\delta_D} \end{pmatrix} = \begin{pmatrix} 0.01418 \\ -0.07767 \\ 0.02251 \\ 0.5489 \\ -0.008099 \\ 0.04002 \\ -0.01434 \\ 0.1672 \\ -0.001505 \\ 0.02583 \\ -0.003653 \\ 0.215 \end{pmatrix}$$

Table A.14: Dataset #13. Mean markers error: 6.1194e-04[m]

$$\begin{pmatrix} X_q \\ X_u \\ X_w \\ X_{\delta_D} \\ Z_q \\ Z_u \\ Z_w \\ Z_{\delta_D} \\ M_q \\ M_u \\ M_w \\ M_{\delta_D} \end{pmatrix} = \begin{pmatrix} 0.004679 \\ -0.06158 \\ 0.02584 \\ 0.5672 \\ -0.01101 \\ 0.05019 \\ -0.01085 \\ 0.1527 \\ -0.001356 \\ 0.02558 \\ -0.003451 \\ 0.2098 \end{pmatrix}$$

Table A.15: Dataset #14. Mean markers error: 7.6065e-04[m]

$$\begin{pmatrix} X_q \\ X_u \\ X_w \\ X_{\delta_D} \\ Z_q \\ Z_u \\ Z_w \\ Z_{\delta_D} \\ M_q \\ M_u \\ M_w \\ M_{\delta_D} \end{pmatrix} = \begin{pmatrix} 0.01635 \\ -0.04036 \\ 0.033 \\ 0.5248 \\ -0.01819 \\ 0.06518 \\ -0.01387 \\ 0.1763 \\ -0.003138 \\ 0.02813 \\ -0.0019 \\ 0.1635 \end{pmatrix}$$

Table A.16: Dataset #15. Mean markers error: 7.4305e-04[m]

$$\begin{pmatrix} X_q \\ X_u \\ X_w \\ X_{\delta_D} \\ Z_q \\ Z_u \\ Z_w \\ Z_{\delta_D} \\ M_q \\ M_u \\ M_w \\ M_{\delta_D} \end{pmatrix} = \begin{pmatrix} 0.01616 \\ -0.05131 \\ 0.033 \\ 0.5234 \\ -0.01494 \\ 0.0547 \\ -0.01549 \\ 0.1653 \\ -0.002558 \\ 0.02557 \\ -0.002138 \\ 0.1638 \end{pmatrix}$$

Table A.17: Dataset #16. Mean markers error: 7.7979e-04[m]

$$\begin{pmatrix} X_q \\ X_u \\ X_w \\ X_{\delta_D} \\ Z_q \\ Z_u \\ Z_w \\ Z_{\delta_D} \\ M_q \\ M_u \\ M_w \\ M_{\delta_D} \end{pmatrix} = \begin{pmatrix} 0.018 \\ -0.05373 \\ 0.03354 \\ 0.4622 \\ -0.01541 \\ 0.05497 \\ -0.01394 \\ 0.1306 \\ -0.002724 \\ 0.02538 \\ -0.002347 \\ 0.1496 \end{pmatrix}$$

Table A.18: Dataset #17. Mean markers error: 1.4777e-03[m]

$$\begin{pmatrix} X_q \\ X_u \\ X_w \\ X_{\delta_D} \\ Z_q \\ Z_u \\ Z_w \\ Z_{\delta_D} \\ M_q \\ M_u \\ M_w \\ M_{\delta_D} \end{pmatrix} = \begin{pmatrix} 0.008208 \\ -0.03027 \\ 0.02034 \\ 0.6608 \\ -0.01312 \\ 0.1036 \\ -0.01634 \\ 0.3162 \\ -0.002163 \\ 0.0231 \\ -0.002474 \\ 0.1722 \end{pmatrix}$$

Table A.19: Dataset #18. Mean markers error: 7.9841e-04[m]

$$\begin{pmatrix} X_q \\ X_u \\ X_w \\ X_{\delta_D} \\ Z_q \\ Z_u \\ Z_w \\ Z_{\delta_D} \\ M_q \\ M_u \\ M_w \\ M_{\delta_D} \end{pmatrix} = \begin{pmatrix} 0.004695 \\ -0.04663 \\ 0.01672 \\ 0.8694 \\ -0.009382 \\ 0.08477 \\ -0.02561 \\ 0.4368 \\ -0.001899 \\ 0.02871 \\ -0.004963 \\ 0.2628 \end{pmatrix}$$

B

The system identification cycle

The system identification process consists of several steps with the ultimate goal of producing data-driven flight dynamic models. The steps that form the system identification process consists of seven steps to be exact, which can be run through as many times as required. Hence the term system identification 'cycle'. The system identification cycle is displayed in **Figure B.1** below. Klein and Morelli (2006)

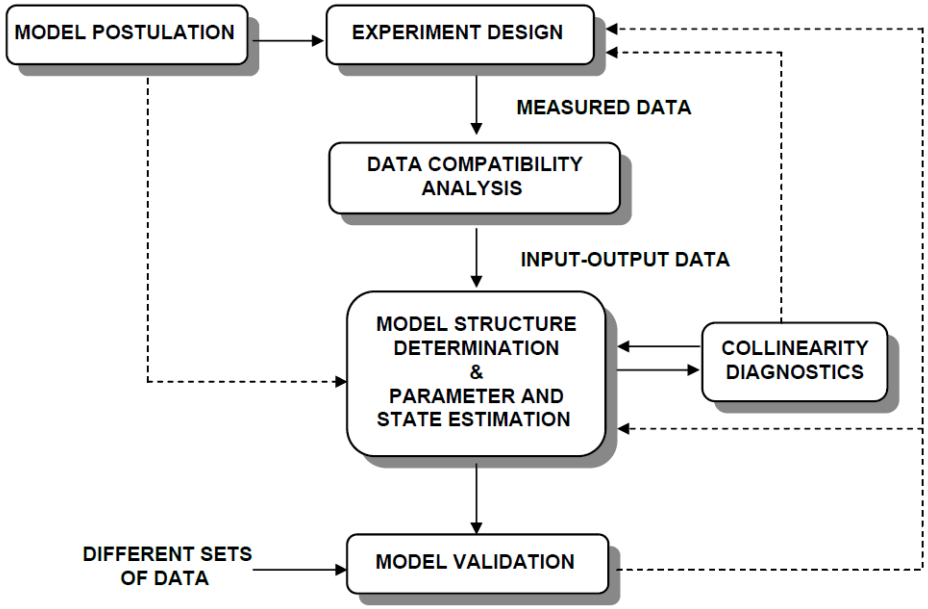

Figure B.1: The System Identification Cycle Klein and Morelli (2006)

Aircraft system identification includes model postulation, experiment design, data compatibility analysis, model structure determination, parameter and state estimation, collinearity diagnostics, and model validation. Performing each of the steps is required in order to identify a mathematical formulation of the functional dependence of the applied aerodynamic forces and moments on aircraft motion and control variables. Starting with the first step in the System Identification Cycle; model postulation.

1. Model postulation

Model postulation is based on a priori knowledge about the aircraft dynamics and aerodynamics. The postulated model influences the type of flight-test manoeuvre used for system identification. It is common practice to express the aerodynamic forces and moments in terms of linear expansions, polynomials, or polynomial spline functions in the states and controls, with time-invariant parameters quantifying the contribution of each to the total aerodynamic force or moment. In recent years, this formulation

has been extended to cases with unsteady aerodynamic effects modelled by indicial functions or additional state equations.Klein and Morelli (2006)

2. Experiment design
Experiment design includes selection of an instrumentation system, and specification of the aircraft configuration, flight conditions, and manoeuvres for system identification. The instrumentation system is primarily required to measure input and output variables at regular sampling intervals during the manoeuvre. Input variables are throttle position and control surface deflections for open-loop or bare-airframe modelling. The output variables include quantities specifying the magnitude and direction of the air-relative velocity (airspeed, angle of attack, and sideslip angle), angular velocities, translational and angular accelerations, and Euler attitude angles. In addition to these variables, quantities defining flight conditions and configuration are also recorded. An important aspect of the experiment design is the selection of input forms for the flight maneuvers. The input influences aircraft response, which in turn influences the accuracy of the system identification from flight measurements. Attempts to obtain parameter estimates with high accuracy in the most efficient manner has led researchers to the development of optimized inputs for aircraft parameter estimation.Klein and Morelli (2006)

3. Data compatibility analysis
In practice, measured aircraft response data can contain systematic errors, even after careful instrumentation and experimental procedure. To verify data accuracy, data compatibility analysis can be applied to measured aircraft responses. Data compatibility analysis includes aircraft state estimation based on known rigid-body kinematics and available sensor measurements, estimation of systematic instrumentation errors, and a comparison of reconstructed responses with measured responses. The state equations for the data compatibility analysis are kinematic relationships among the measured aircraft responses, and the model parameters are constant biases and scale factor errors for the sensors.Klein and Morelli (2006)

4. Model structure determination
Model structure determination in aircraft system identification means selecting a specific form for the model from a class of models, based on measured data. For example, this might involve choosing an appropriate polynomial expansion in the aircraft motion and control variables to model a component of aerodynamic force acting on the aircraft, from the class of all possible polynomial models of order two or less. The model should be parsimonious to retain good prediction capability, while still adequately representing the physical phenomena. An adequate model is a model that fits the data well, facilitates the successful estimation of unknown parameters associated with model terms whose existence can be substantiated, and has good prediction capabilities. One of the techniques, stepwise regression, has been used extensively in practice. In this technique, the determination of a model proceeds in three steps: postulation of terms that might enter the model, selection of an adequate model based on statistical metrics, and validation of the selected model. The other technique generates multivariate orthogonal modelling functions from the data to facilitate model structure determination. The orthogonality of the modelling functions make it possible to automate the first two of the three steps listed earlier for model structure determination. Retained orthogonal functions can be decomposed without error into ordinary polynomial terms for the final model form.Klein and Morelli (2006)

5. Parameter and state estimation
Four items are needed for implementation of aircraft system identification: an informative experiment, measured input-output data, a mathematical model of the aircraft being tested, and an estimation technique. Parameter and state estimation constitute a principal part of the aircraft system identification procedure. Currently, two methods—equation-error and output-error—are used for most aircraft parameter estimation. The equation-error method is based on linear regression using the ordinary least-squares principle. The unknown aerodynamic parameters are estimated by minimizing the sum of squared differences between measured and modelled aerodynamic forces and moments. Linear regression constitutes a linear estimation problem, meaning that the model output is linearly dependent on the model parameters. This simplifies the optimization required to find parameter estimates to the solution of an overdetermined set of linear equations, which can be found using well-known techniques from linear algebra. In the output-error method, the unknown parameters are obtained by minimizing

the sum of weighted square differences between the measured aircraft outputs and model outputs. The estimation problem is nonlinear because the unknown parameters appear in the equations of motion, which are integrated to compute the states. Outputs are computed from the states, controls, and parameters, using the output equations. Iterative nonlinear optimization techniques are required to solve this nonlinear estimation problem. Theoretically, either the equation-error or the output-error method can be a maximum likelihood estimator, which means that the cost function optimization used for computing the unknown parameters is equivalent to maximizing the probability density of the outcome from the experiment.Klein and Morelli (2006)

6. Collinearity diagnostics

In almost all practical applications of linear regression, the model terms are correlated to some extent. Usually, the levels of correlation are low, and therefore not problematic. However, in some situations, the model terms are almost linearly related. When this happens, the problem of data collinearity exists, and inferences about the model based on the data can be misleading, or completely wrong. The ability to diagnose data collinearity is important to users of linear regression or other parameter estimation techniques. Such a diagnostic consists of two basic steps: 1) detecting the presence of collinearity among the model terms, and 2) assessing the extent to which these relationships have adversely affected estimated parameters. Then, diagnostic information can aid in deciding what corrective actions are necessary and worthwhile.Klein and Morelli (2006)

7. Model validation

Model validation is the last step in the identification process, and should be applied regardless of how the model was found. The identified model must demonstrate that its parameters have physically reasonable values and acceptable accuracy, and that the model has good prediction capability on comparable maneuvers. Flight-determined parameter estimates should be compared with any available information about the aircraft aerodynamics, which can include theoretical predictions, wind-tunnel measurements, or estimates from previous flight measurements using different maneuvers and/or different estimation techniques. During these comparisons, the limitations and accuracy of theoretical calculations, wind-tunnel measurements, and the flight results must be taken into consideration. Prediction capability of an identified model is checked on data not used in the identification process. The measured input for the prediction data is applied to the identified model to compute predicted responses, which are then compared with measured values. The differences between predicted values from the model and measured values should be random in nature, indicating that all deterministic components in the measured output have been represented by the identified model.Klein and Morelli (2006)

C

Validation Forward Flight Models

In this section the validation results are presented for the forward speed models, from 0.5 m/s up to 1.0 m/s. As shown in the validation metrics and plots, we can see that the models are accurate. Except for the model in 1.0 m/s forward flight condition. This offset is probably caused by a different trim condition between the estimation dataset and the validation dataset.

Validation of the model in 0.5 m/s forward flight condition:

Match *validation* data with measured data			
Output Variable	Output Correlation	R2	RMSE (% of measurement range)
X	0.97	0.90	7.15%
Z	0.64	0.32	11.49%
M	0.95	0.85	7.38%
$\dot{q}$	0.96	0.85	7.38%
$\dot{u}$	0.94	0.84	7.21%
$\dot{w}$	0.90	0.68	8.54%
$\dot{\theta}$	0.99	0.99	0.66%

Table C.1: Validation metrics of the longitudinal model in 0.5 m/s forward flight condition (Figures C.1a-C.1b).

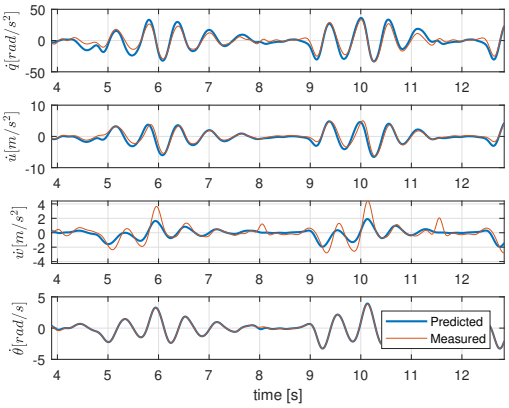

(a) Validation of the states. Measured- and model predicted output of the states in 0.5 m/s forward flight condition

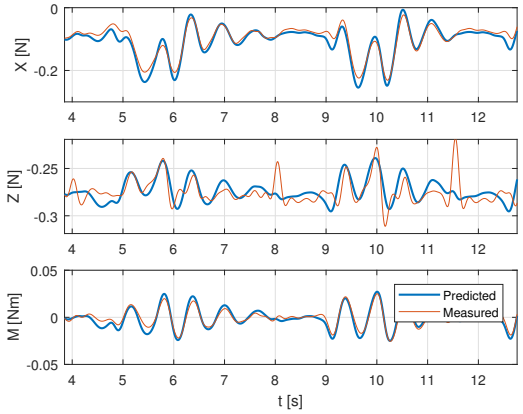

(b) Validation of the aerodynamic- forces and moment. Measured- and model predicted output of the aerodynamic- forces and moment in 0.5 m/s forward flight condition.

Figure C.1: Predicted output of the estimated time-averaged longitudinal 0.5 m/s forward flight model.

Validation of the model in 0.75 m/s forward flight condition:

Match *validation* data with measured data			
Output Variable	Output Correlation	R2	RMSE (% of measurement range)
X	0.93	0.70	11.01%
Z	0.41	0.10	8.44%
M	0.94	0.83	7.45%
$\dot{q}$	0.93	0.83	7.45%
$\dot{u}$	0.96	0.57	11.44%
$\dot{w}$	0.83	0.52	8.55%
$\dot{\theta}$	0.99	0.98	2.43%

Table C.2: Validation metrics of the longitudinal model in 0.75 m/s forward flight condition (Figures C.2a-C.2b).

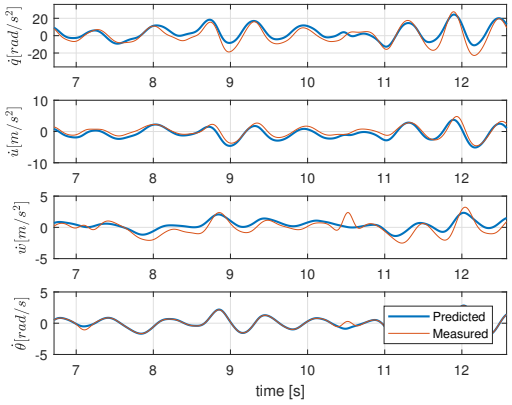

(a) Validation of the states. Measured- and model predicted output of the states in 0.75 m/s forward flight condition

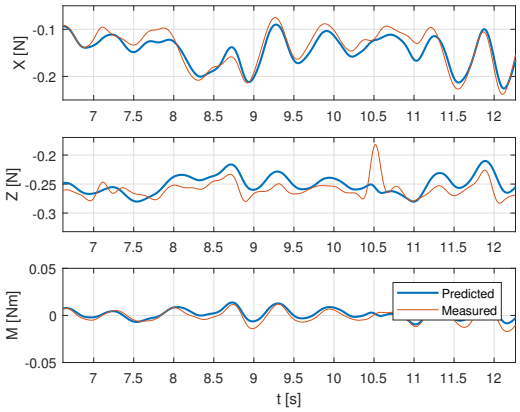

(b) Validation of the aerodynamic- forces and moment. Measured- and model predicted output of the aerodynamic- forces and moment in 0.75 m/s forward flight condition.

Figure C.2: Predicted output of the estimated time-averaged longitudinal 0.75 m/s forward flight model.

Validation of the model in 1.0 m/s forward flight condition:

Match *validation* data with measured data			
Output Variable	Output Correlation	R2	RMSE (% of measurement range)
X	0.89	-0.23	24.46%
Z	0.56	-0.04	11.14%
M	0.96	0.35	17.24%
$\dot{q}$	0.96	0.35	17.24%
$\dot{u}$	0.96	-0.03	21.26%
$\dot{w}$	0.90	0.58	10.83%
$\dot{\theta}$	0.98	0.96	4.31%

Table C.3: Validation metrics of the longitudinal model in 1.0 m/s forward flight condition (Figures C.3a-C.3b).

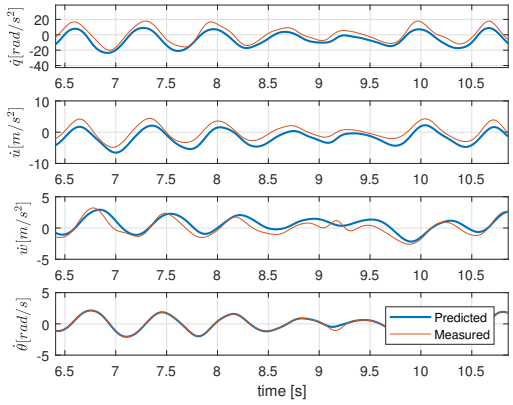

(a) Validation of the states. Measured- and model predicted output of the states in 1.0 m/s forward flight condition

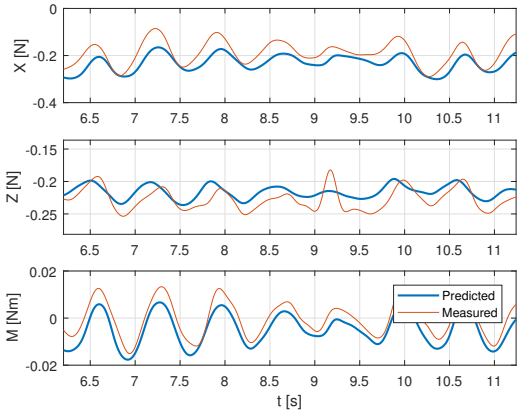

(b) Validation of the aerodynamic- forces and moment. Measured- and model predicted output of the aerodynamic- forces and moment in 1.0 m/s forward flight condition.

Figure C.3: Predicted output of the estimated time-averaged longitudinal 1.0 m/s forward flight model.

D

Validation of the Improved Linear Models in Hover Condition

In this section validation results are provided of the improved/adjusted linear models for the aerodynamic force Z in hover condition, including the corresponding metrics, such as the output correlation and goodness of fit (R^2) (Table D.1 and Figure D.1).

Match *validation* data with measured data			
Output Variable	Output Correlation	R2	RMSE (% of measurement range)
Z_{model1}	0.88	0.78	6.94%
Z_{model2}	0.84	0.71	7.87%
Z_{model3}	0.56	0.32	12.14%

Table D.1: Validation metrics of the adjusted linear models in hover flight.

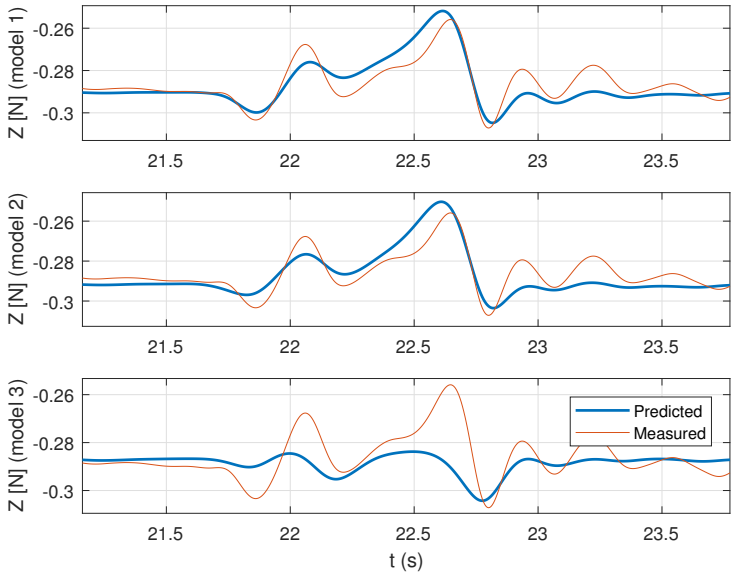

Figure D.1: Validation of the aerodynamic force Z for all the adjusted linear models.